FG

NUSC Technical Report 5335

AD A025408

Time Delay Estimation

G. CLIFFORD CARTER

Office of the Director for Science and Technology

COPY AVAILABLE TO DDC DOES NOT PERMIT FULLY LEGIBLE PRODUCTION

9 April 1976

DDC
RECEIVED
JUN 14 1976
D

NAVAL UNDERWATER SYSTEMS CENTER
New London Laboratory

Approved for public release; distribution unlimited.

PREFACE

This study was prepared as a dissertation in partial fulfillment of the requirements for the degree Doctor of Philosophy in Electrical Engineering and Computer Science at the University of Connecticut. The work was done under NUSC Project No. A75225, "Estimation of the Smoothed Coherence Transform"; Principal Investigator, G. C. Carter (Code TF); Navy Subproject No. ZR000 01; Program Manager, T. A. Kleback, Naval Material Command (MAT 03521).

The author acknowledges the contributions of those individuals who supported the completion of this research. Specifically, he acknowledges the assistance of the following groups and individuals:

From the University of Connecticut — the members of the control and communications section of the Department of Electrical Engineering and Computer Science for their constructive comments throughout the course of this work; Drs. H. M. Lucal and R. J. Kochenburger for reviewing portions of the manuscript and serving on his advisory committee; Dr. C. H. Knapp for the significant assistance, time, and effort devoted to this entire research project.

From the Naval Underwater Systems Center — the art department and print shop for the professional preparation of this dissertation: Drs. W. A. Von Winkle and E. S. Eby and Messrs. D. L. Nichols, C. R. DeVoe, and R. H. Prager for actively contributing to the financial and administrative atmosphere necessary to complete this work; Mr. J. C. Sikorski for his contributions to appendix C; Mr. E. L. McLaughlin for his contributions to appendix D; Dr. A. H. Nuttall for his general interest and many informative, discussions especially on the material in section B of chapter 5 and section 2 of appendix B; Mr. A. H. Lotring for editing the entire manuscripts; Ms. N. K. Impellitteri and Mrs. A. Zimmerman for typing the rough and final drafts, respectively.

REVIEWED AND APPROVED 9 April 1976

W. A. Von Winkle
Director, Science & Technology

The author of this report is located at the New London Laboratory, Naval Underwater Systems Center, New London, Connecticut 06320.

UNCLASSIFIED

SECURITY CLASSIFICATION OF THIS PAGE (When Data Entered)

REPORT DOCUMENTATION PAGE	READ INSTRUCTIONS BEFORE COMPLETING FORM
1. REPORT NUMBER: NUSC-TR-5335	2. GOVT ACCESSION NO. / 3. RECIPIENT'S CATALOG NUMBER
4. TITLE (and Subtitle): TIME DELAY ESTIMATION	5. TYPE OF REPORT & PERIOD COVERED: Technical rept.
	6. PERFORMING ORG. REPORT NUMBER
7. AUTHOR(s): G. Clifford Carter	8. CONTRACT OR GRANT NUMBER(s)
9. PERFORMING ORGANIZATION NAME AND ADDRESS: Naval Underwater Systems Center, New London Laboratory, New London, Connecticut 06320	10. PROGRAM ELEMENT, PROJECT, TASK AREA & WORK UNIT NUMBERS: NUSC-A75225, ZR000-01
11. CONTROLLING OFFICE NAME AND ADDRESS: Chief of Naval Material (MAT 03521), Washington, D. C. 20310	12. REPORT DATE: 9 April 1976
	13. NUMBER OF PAGES: 241
14. MONITORING AGENCY NAME & ADDRESS (if different from Controlling Office): 245 p.	15. SECURITY CLASS. (of this report): UNCLASSIFIED
	15a. DECLASSIFICATION/DOWNGRADING SCHEDULE

16. DISTRIBUTION STATEMENT (of this Report)

Approved for public release; distribution unlimited.

17. DISTRIBUTION STATEMENT (of the abstract entered in Block 20, if different from Report)

18. SUPPLEMENTARY NOTES

19. KEY WORDS (Continue on reverse side if necessary and identify by block number)

FORTRAN	Digital signal processing	Group delay
Computer programs	Delay	Magniture-squared coherence
Coherence	Fast Fourier transform	Spectral estimation
Coherence estimation	FFT	Time delay estimation

20. ABSTRACT (Continue on reverse side if necessary and identify by block number)

This study investigates methodologies for passive estimation of the bearing to a slowly moving acoustically radiating source. The mathematics for the solution to such a problem is analogous to estimating the time delay (or group delay) between two time series. The estimation of time delay is intimately related to the coherence between two time series. New results on using coherence to provide information about linear and nonlinear systems are presented.

(over)

DD FORM 1 JAN 73 1473 EDITION OF 1 NOV 65 IS OBSOLETE S/N 0102-014-6601

UNCLASSIFIED

SECURITY CLASSIFICATION OF THIS PAGE (When Data Entered)

405 718

19. KEY WORDS (Cont'd)

Generalized crosscorrelation
Information content
Nonlinear systems
Linear systems

20. ABSTRACT (Cont'd)

The maximum likelihood (ML) estimate of time delay is derived; the explicit dependence of the estimate on coherence is evident in the realization in which the two time series are prefiltered (to accentuate frequency bands of high coherence) and subsequently crosscorrelated. The hypothesized delay at which the generalized crosscorrelation (GCC) function peaks is the time delay estimate. The variance of the time delay estimate is obtained. Other realizations are considered. The estimation formulation is extended to multiple sources, moving source, and multiple sensors.

Also included are statistics of the estimates of the magnitude-squared coherence (MSC), including the probability density function, the cumulative distribution function, and the m-th moment of the MSC estimate. A complete discussion of the bias and the variance of the MSC estimates is presented. The receiver operating characteristics of a linearly thresholded coherence estimation detector are also presented. A general FORTRAN IV computer program using the fast Fourier transform to estimate time delay is given.

ACCESSION for
NTIS White Section
DDC Buff Section
UNANNOUNCED
JUSTIFICATION
BY
DISTRIBUTION/AVAILABILITY CODES
Dist. AVAIL. and/or SPECIAL
A

DDC
RECEIVED
JUN 14 1976
D

TABLE OF CONTENTS

LIST OF TABLES

LIST OF ILLUSTRATIONS

LIST OF SYMBOLS AND ABBREVIATIONS

Symbols

$B(\ )$	bias of
$C_{x_1x_2}(\ )$	magnitude-squared coherence
d	distance (meters) between two sensors
d_f	deflection criterion
D	true but unknown time delay (sec)
$E(\ )$	mathematical expectation
f	frequency (Hz)
${}_2F_1$	hypergeometric function
$G_{x_1x_1}(\ )$	auto-power spectrum of $x_1(t)$
$G_{x_1x_2}(\ )$	cross-power spectrum of $x_1(t)$ with $x_2(t)$
$H_{e_n}(\ )$	Hermite polynomial
H	linear time invariant filter
$Im(\ )$	imaginary part of
I_{xy}	information between x(t) and y(t)
j	$\sqrt{-1}$
J_i	cost (award) functions
$n(t)$	noise waveform
N	number of independent FFT's
$p(\ )$	first order probability density function
P	number of data points per FFT
$Prob(\ )$	probability

Q_x	power spectral density matrix of x
$R_{x_1x_2}(\ )$	crosscorrelation function of $x_1(t)$ with $x_2(t)$
$\mathbf{R}_x(\ )$	crosscorrelation matrix
Re( )	real part of
s(t)	signal waveform
t	time (sec)
T	observation time (sec)
$\underline{V}$	steering vector
$Var(\hat{v})$	variance of random variable $\hat{V}$
$Var^{R1}(\hat{v})$	variance of random variable $\hat{V}$ which has been estimated according to rule R1
$X_n(k)$	DFT of n-th weighted data segment of x(t) at k-th frequency
W( )	weighting function
α	attenuation
β	time compression
$\tilde{\beta}$	β/β_a
$\gamma_{x_1x_2}(f)$	complex coherence of $x_1(t)$ with $x_2(t)$
$\Gamma(\ )$	Gamma function
$\phi_{x_1x_2}(\ )$	phase of cross-power spectrum of $x_1(t)$ with $x_2(t)$
Θ	bearing angle
$\eta(\ )$	no memory nonlinearity
$\rho(\ )$	normalized crosscorrelation
σ_v^2	variance of random variable v
σ_v	standard deviation of random variable v

τ	hypothesized time delay (sec)
ω	$2\pi f$ (rad/sec)
ω_Δ	$2\pi/T$
ξ	nominal speed of sound in the nondispersive medium (water)
$\hat{}$	estimate; for example, $\hat{D}$ is the estimate of D
$\forall$	for all
$\circledast$	convolution
$(z)_k$	Pochhammer's symbol
*	complex conjugate

Abbreviations

AML	approximate maximum likelihood
CC	complex coherence
cdf	cumulative distribution function
CZT	Chirp Z-transform
DFT	discrete Fourier transform
FFT	fast Fourier transform
FIR	finite impulse response
LOP	line of position
MAD	multiplication and addition
MC	magnitude coherence
MCZT	modified Chirp Z-transform
ML	maximum likelihood
MMSE	minimum MSE
MSC	magnitude-squared coherence
MSE	mean square error
PAM-CZT	partitioned and modified CZT

pdf	probability density function
PHAT	phase transform
ROC	receiver operating characteristics
SCOT	smoothed coherence transform
SNR	signal-to-noise ratio

CHAPTER 1

INTRODUCTION

This research investigates methods for estimating the position of a moving source by the processing of an acoustically radiated signal received at two or more physically separated sensors. If the source signal is received at two geographical positions in the presence of uncorrelated noise, then, depending on the signal strength and duration, it is possible to estimate the bearing to the source relative to the sensor baseline. When the source signal is received at three sensors, range, as well as bearing to the source, can be estimated by using the intersection of two bearing lines of position (LOPs). The mathematics for the solution to the problem of finding the "best" estimate of bearing is analogous to the more general problem of estimating the time delay (or group delay) between two time series. Therefore, this dissertation derives the maximum likelihood (ML) estimate time delay.

Techniques for estimation of time delay can be applied to a variety of practical problems, in addition to those motivating this research. For example, if we consider a signal which probes a linear time invariant

system, then the problem of estimating time delay can be viewed as attempting to identify a parameter of the probed system, based on time-limited, noise-corrupted observations of the system input and output. The delay is a particularly valuable characterization of the system (and interrelationship between two processes) when the system output is an attenuated and delayed version of the input. Physical plants in which delays occur can also be visualized in terms of the bearing estimation problem.

For example, consider two geographically separated sensors that receive a signal from an acoustically radiating point source, as shown in Figure 1-1. If the properties of the medium are such that the signal from the source propagates at a constant velocity, then the travel time from the source to either sensor is directly proportional to the distance traveled. Thus, the difference between the travel time (from the source to each sensor) or time delay is given by the difference in path lengths divided by the propagation velocity. There exists a well defined locus of points (relative to the sensors) for which the time delay is constant. Hence, knowledge of the time delay is sufficient to dictate that the source is located somewhere on that locus of points. In particular, the acoustic source must be located on the locus of points that satisfies the constant time delay constraint, namely, the hyperbola in Figure 1-2. The bearing angle, θ, that the hyperbolic asymptote makes with the baseline is a good approximation

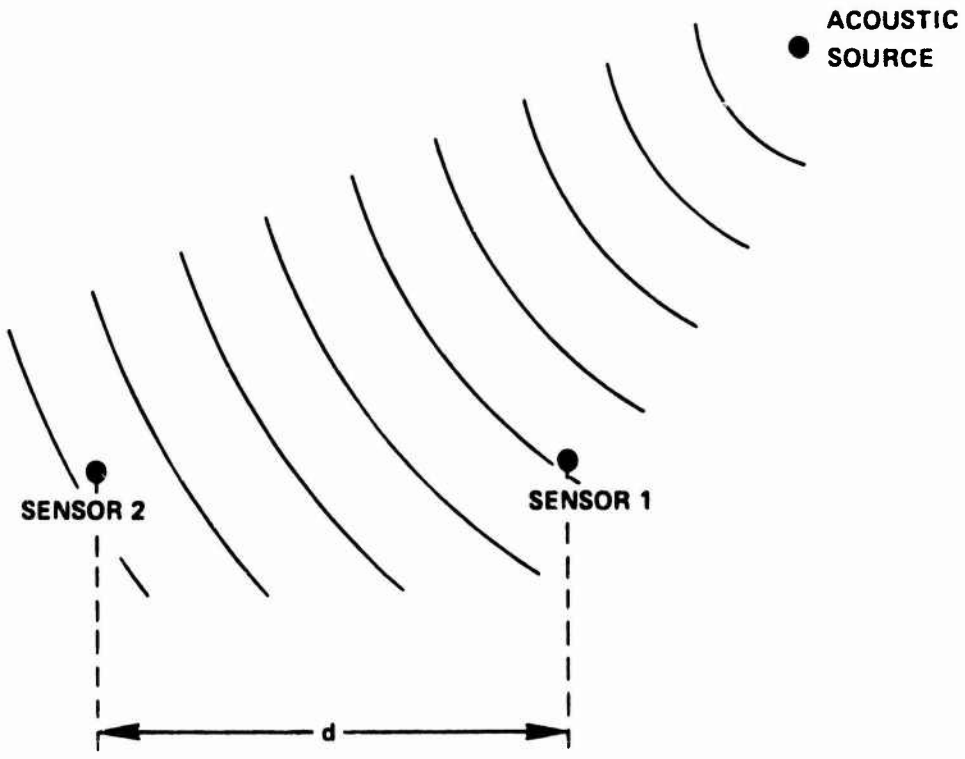

Figure 1-1 Acoustic Source and Sensors

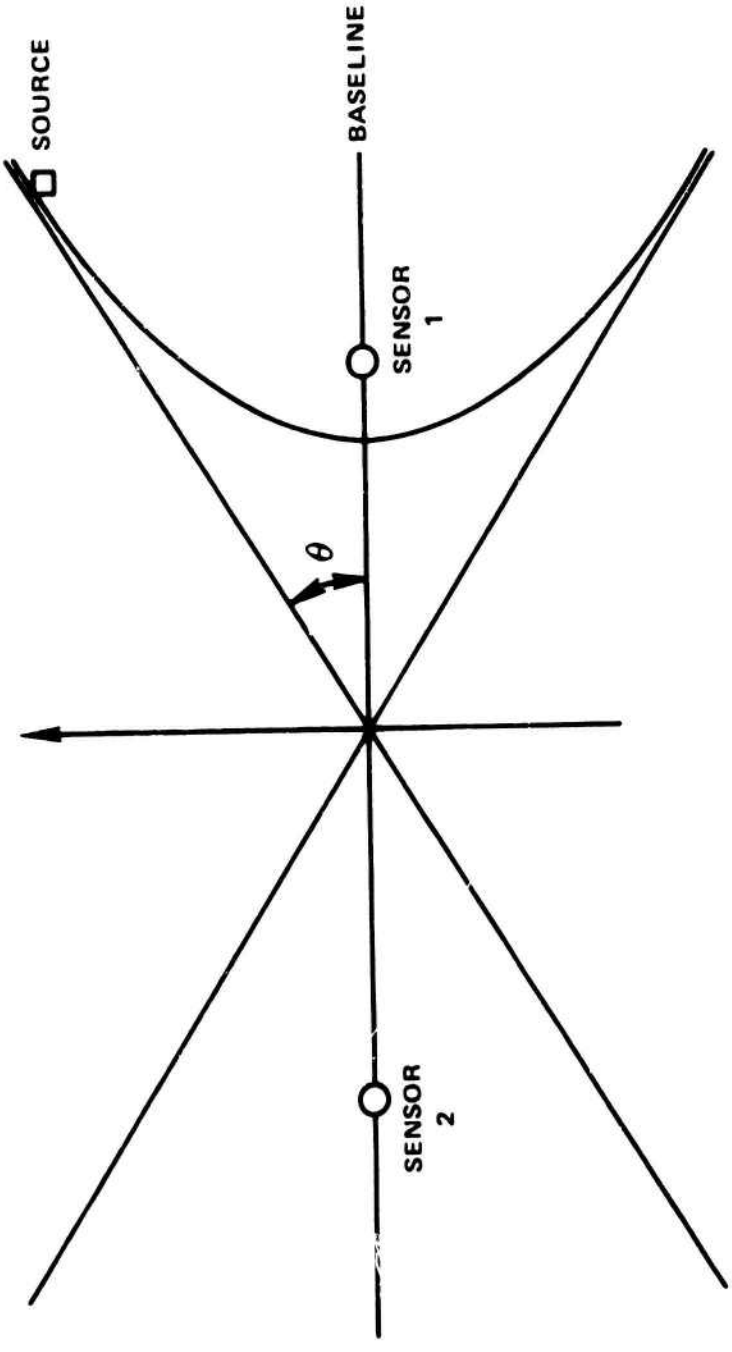

Figure 1-2 Bearing Angle Interpretation

to the true bearing to the source (relative to the midpoint of the baseline) especially for distant sources. Thus, by making a distant point source (or equivalently a plane wave) assumption and solving for the bearing angle θ, one is equivalently finding the angle that the hyperbolic asymptote (or line of position (LOP)) makes with the baseline. Familiarity with hyperbola suggests that the source need not be very distant (relative to the sensor separation d) in order for the arrival angle to be a good estimator of true source angle. In the estimation problem, the receivers are attempting to estimate bearing (or position) of a source that is radiating a signal either intentionally or unintentionally. During intentional radiation (for example, a communications system) signal statistics are selectable within certain practical and regulatory limitations. In other applications, the signal characteristics are unknown and the output of the sensors must be processed without this a priori knowledge in order to estimate time delay or equivalently source bearing. In this thesis it is assumed that the source characteristics are not under the control of the designer and at best the spectral characteristics of the signal are known or estimated.

The time delay estimation research presented in this text is arranged in six chapters and four appendices. Because the estimation of time delay and bearing is intimately related to the coherence between two received

waveforms, an extensive investigation of coherence is given (in Chapter 2). New results on using coherence to provide information about linear and nonlinear system identification are presented and proved. Among other results, Chapter 2 explicitly shows how the signal-to-noise ratio (SNR) is a function of coherence.

In Chapter 3, the ML estimate of time delay between two signals is derived under jointly stationary Gaussian assumptions. The explicit dependence of the time delay estimate on coherence is evident in the estimator realization in which the two time series are prefiltered (to accentuate frequency bands according to the strength of the coherence) and subsequently crosscorrelated. The time argument at which the generalized crosscorrelation (GCC) function peaks is the time delay estimate (Carter and Knapp (1976a)). The method of derivation is akin to the ML bearing estimate derived by MacDonald and Schultheiss (1969) with two exceptions: (1) the technique here requires no plane wave assumption but finds the ML estimate of the more general time delay parameter, from which one can estimate both the hyperbolic LOP and source bearing, and, (2) the derivation here does not constrain the additive noise waveforms at different sensors to have the same spectral characteristics. These conditions allow for widely spaced sensors since the spectral characteristics of the noise can be different and the

signal wavefront is not constrained to be planar.

Having derived the ML estimate of time delay, we show that it is equivalent to the GCC function with prefiltering suggested by Hannan and Thomson (1973). Although the ML estimator is the same as the method suggested by Hannan and Thomson (1973), this could not have been accurately predicted ahead of time. The Hannan Thomson (HT) processor was obtained as a GCC function with optimally determined weighting. In related work, Clay, Hinich, and Shaman (1973) arrived at a less general ML estimate for bearing, due to the assumption that the signal spectral characteristics were flat in the frequency band of interest. The results of this thesis are also more general than those of MacDonald and Schultheiss (1969) because there is no signal plane wave assumption and the noise spectral characteristics can differ from sensor to sensor.

When the received signal and noise waveforms are stationary and Gaussian with known spectral characteristics, it is shown that the ML estimate of time delay achieves the Cramér-Rao bound. Thus, the ML estimate, in this case, achieves a variance less than or equal to that attained by any other means. Two realizations of the time delay estimate are given: the first, uses the GCC function with appropriate prefilters; the second appropriately filters, sums, squares, and averages as

suggested by Carter and Knapp (1976a). Further, when the spectral characteristics are known the variance of the delay estimates is derived for all GCC processors. When the signal and noise spectral characteristics are unknown, as is often the case in the passive bearing estimation problem, it is suggested that an approximate technique be used, whereby estimates of the ML weighting are inserted in the place of the correct weighting. This heuristic procedure will converge to the ML estimate provided the weighting is properly estimated. The appendices summarize work in this area by Carter, Knapp, and Nuttall (1973a) to estimate the spectral densities including coherence. (Details of the appendices are discussed later in the introduction.)

In Chapter 4, the variances of six proposed time delay estimates, including ones suggested by Roth (1971) and Carter, Nuttall, and Cable (1973), are compared for an example case where the signal and noise have rectangular spectra with different bandwidths. The results confirm the advantages of ML time delay estimation.

The estimation formulation is extended, in Chapter 5, to three important generalizations: multiple sources, moving source, and multiple sensors. The multiple source problem introduces a new term in the award function which was maximized in Chapter 3 to obtain a single time delay estimate. This additional term is the

information between two processes. Nettheim (1966), using results of Gelfand and Yaglom (1959), has shown the Shannon (1949) definition of information to be directly related to the coherence between two processes. Thus, as with the single time delay estimation problem, coherence plays an important role. Source motion significantly complicates the bearing estimation problem as indicated in section B of Chapter 5. Indeed, unless some preprocessing is done, the received waveforms appear uncorrelated despite the presence of a common but time compressed (or less generally, Doppler shifted) signal. A method based on the ideas of Chapter 3 is suggested for preprocessing the received waveforms to remove the effect of source motion. The last section of Chapter 5 extends the filter and sum realization for time delay estimation to a multiple sensor environment. Finally, Chapter 6 is a brief discussion and summary of applications for the methods of time delay estimation and suggestions for future work.

The appendices of this dissertation are provided to implement and corroborate the theory developed in Chapter 3. Appendix A summarizes two methods of spectral estimation given in Carter, Knapp, and Nuttall (1973a) and Carter and Knapp (1975). Appendix B gives important results of the statistical behavior of the estimates of the magnitude-squared coherence (MSC), including the probability density function (pdf), the cumulative

distribution function (cdf),and the m-th moment of the MSC estimate. A complete discussion of the bias and the variance of the MSC estimates is presented, including a simulation (done by Nuttall and Carter (1976b)) that supports theoretical results of Haubrich (1965) and Carter, Knapp, and Nuttall (1973a) and refutes past simulation results of Benignus (1969a). Using a method suggested by Benignus (1969a), a reduced bias method of MSC estimation is verified; however, it is discovered that for many practical estimation situations the reduced bias MSC estimator will have increased mean square error (MSE) when compared with the MSC estimator given in Appendix A. An example is given of erroneous simulation results (in particular, unexpectedly large bias) when the assumptions of the theory have been violated.

In the process of detecting a coherent source it is desirable to establish a threshold above which a source is considered detected. Rules for establishing such a threshold are given (Carter (1976)) in order to achieve a specified probability of false alarm. Having established such a threshold, it is possible to determine the probability of detecting a coherent source; the probability of detection will depend both on the observation time and the underlying strength of the coherent source. Example receiver operating characteristics are plotted for different observation times and coherent source levels.

Appendix C gives a complete FORTRAN IV computer listing of a program to estimate time delay. The program was successfully compiled and run on both a Univac and an IBM computer. Appendix D presents an example case to validate both the theory and the computer program.

The text, then, is arranged as follows: Chapter 3 contains the derivation for the ML time delay estimator; because these results depend on the coherence between two random processes, we first demonstrate in Chapter 2 what characteristics the coherence possesses. Chapter 4 compares the ML estimator derived in Chapter 3 with other proposed methods for estimating time delay. Chapter 5 extends the results of Chapter 3 to three important generalizations: multiple sources, moving source, and multiple sensors. Applications and a general discussion are presented in Chapter 6. The four appendices are all concerned with experimental verification of approximate methods for estimating time delay presented in Chapter 3.

CHAPTER 2

THEORY AND APPLICATIONS OF COHERENCE

The solution to the physical problem of estimating source bearing is intimately tied to the coherence between spatially separated passive sensors.

This chapter presents the definition and properties of the coherence and several new results on its use. These results bear both directly and indirectly on the solution to the optimum delay estimation problem.

2A. Definition, Relationship to Crosscorrelation, and Properties

2A1. Definition

The coefficient of coherency (CC) between two wide sense stationary random processes is the normalized cross power spectral density function defined by Weiner (1930) as

$$\gamma_{x_1x_2}(f) = \frac{G_{x_1x_2}(f)}{\sqrt{G_{x_1x_1}(f)\, G_{x_2x_2}(f)}}, \qquad (2\text{-}1)$$

where f denotes the frequency (Hz), $G_{x_1x_2}(f)$ is the cross-power spectrum between $x_1(t)$ and $x_2(t)$, and $G_{x_1x_1}(f)$, $G_{x_2x_2}(f)$ denote the auto powe. spectra of $x_1(t)$, $x_2(t)$, respectively. Despite some confusion in the literature, Weiner intended for the CC to be complex. This is

apparent since he discusses (p. 194, Weiner (1930)) both the modulus and the argument of the CC. Moreover, in suggesting how one might compute the CC, the modulus of the complex numerator is not indicated. The CC is also referred to as the complex coherence (Carter, Knapp, and Nuttall (1973a)). Many of the results which follow depend on the magnitude-squared of the CC (MSC). The MSC is also referred to as the squared coherency (Jenkins and Watts (1968)).

In order to simplify the notation throughout the thesis, we define

$$C_{x_1x_2}(f) \equiv \left|\gamma_{x_1x_2}(f)\right|^2 . \qquad (2\text{-}2)$$

When the two processes under consideration are apparent, we further simplify the notation by letting

$C(f) \equiv C_{x_1x_2}(f) \equiv C_{12}(f)$.

The magnitude of the CC (MC) is denoted by

$$\left|\gamma_{x_1x_2}(f)\right| = \sqrt{C_{x_1x_2}(f)} . \qquad (2\text{-}3)$$

The term "coherence" can imply CC, MC or MSC. Indeed, variables that are a function of the MSC (or MC) alone are also functions of the CC alone, but not necessarily vice versa. While it seems most natural mathematically to refer to the CC as the coherence, the majority of the literature refers to the MSC as coherence.

Since $G_{x_1x_1}(f)$ and $G_{x_2x_2}(f)$ are real, the phase of the CC denoted by

$$\phi_{x_1x_2}(f) = \mathrm{Arg}\left[\gamma_{x_1x_2}(f)\right] \qquad (2\text{-}4a)$$

$$= \text{Arg}\left[G_{x_1x_2}(f)\right] \qquad (2\text{-}4b)$$

$$= \text{Arg}\left[G_{x_1x_2}(f)/G_{x_1x_1}(f)\right]; \qquad (2\text{-}4c)$$

that is, the phase of the CC is the same as the phase of the cross spectrum. Later we will interpret (2-4c) as the phase of the optimum linear filter that maps $x_1(t)$ to $x_2(t)$.

2A2. Relation to Crosscorrelation

The CC between x(t) and y(t) can be confused with the crosscorrelation coefficient or normalized cross-correlation function defined for zero mean processes by

$$\rho_{xy}(\tau) = \frac{R_{xy}(\tau)}{\left[R_{xx}(0)\ R_{yy}(0)\right]^{\frac{1}{2}}} . \qquad (2\text{-}5)$$

The normalized crosscorrelation is a function of lag and not frequency. Further note that the normalizing factor is the scalar $\left[R_{xx}(0)\ R_{yy}(0)\right]^{\frac{1}{2}}$, independent of τ. It is not a lag dependent normalization. The CC has an abscissa dependent type of normalization (2-1). However, there are two models of filtering that aid in interpreting the CC as a type of crosscorrelation.

In the first model, we are given x(t) and y(t) as depicted in Figure 2-1, and we want to find the CC between x(t) and y(t). If we prefilter x(t) by the linear filter $H_1(f)$ and y(t) by the linear $H_2(f)$, then (from p. 399, Davenport (1970)) the cross spectrum between the filter outputs is

$$G_{x_1y_1}(f) = G_{xy}(f)\ H_1(f)H_2^{*}(f) \quad . \qquad (2\text{-}6)$$

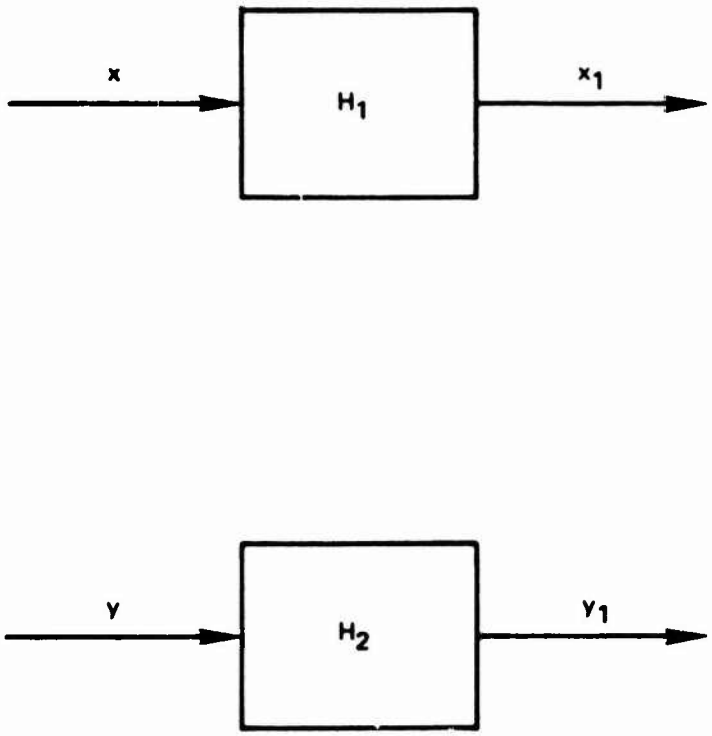

Figure 2-1 Distinct Linear Filters H_1 H_2 with Inputs x,y and Outputs x_1, y_1

Thus, if we select

$$H_1(f)H_2^*(f) = \frac{1}{\sqrt{G_{xx}(f)G_{yy}(f)}} \quad , \tag{2-7}$$

it follows that

$$G_{x_1y_1}(f) = \gamma_{xy}(f).$$

Thus, the CC between x(t) and y(t) can be obtained by first prefiltering x(t) by the realizable whitening filter

$$H_1(f) = \frac{1}{\sqrt{G_{xx}(f)}} e^{j\phi(f)} \tag{2-8}$$

and prefiltering y(t) with a realizable whitening filter with the same phase as (2-8). Namely, we select

$$H_2(f) = \frac{1}{\sqrt{G_{yy}(f)}} e^{j\phi(f)} \quad . \tag{2-9}$$

Such filtering ensures

$$\phi_{x_1y_1}(f) = \phi_{xy}(f) \quad . \tag{2-10}$$

That is, the phase between input processes is invariant to equiphase filtering. Then, to compute the CC between x(t) and y(t), we compute the cross spectrum between $x_1(t)$ and $y_1(t)$. This could be accomplished by cross-correlating $x_1(t)$ and $y_1(t)$ and taking the inverse Fourier transform (or see Appendix A).

In the second model used to understand the CC we observe that for $x_1(t)$ and $y_1(t)$ (in Figure 2-1) zero mean

$$\rho_{x_1y_1}(\tau) = \frac{\int_{-\infty}^{\infty} G_{xy}(f)H_1(f)H_2^*(f)e^{j2\pi f\tau}\,df}{\left[\int_{-\infty}^{\infty} G_{xx}(f)\left|H_1(f)\right|^2 df \int_{-\infty}^{\infty} G_{yy}(f)\left|H_2(f)\right|^2 df\right]^{\frac{1}{2}}} \quad (2\text{-}11)$$

Thus if

$$H_1(f)=H_2(f) = \begin{cases} e^{j\phi(f_c)}, & f_c - \frac{\Delta f}{2} < |f| < f_c + \frac{\Delta f}{2} \\ 0, & \text{elsewhere} \end{cases}, \quad (2\text{-}12)$$

(2-11) becomes (for small Δf)

$$\rho_{x_1y_1}(\tau) \cong \frac{\left[G_{xy}(f_c)e^{j2\pi f_c\tau}+G_{xy}(-f_c)e^{-j2\pi f_c\tau}\right]\Delta f}{\left[G_{xx}(f_c)2\Delta f \cdot G_{yy}(f_c)2\Delta f\right]^{\frac{1}{2}}} \quad (2\text{-}13a)$$

$$\cong \frac{\mathrm{Re}\left[G_{xy}(f_c)e^{j2\pi f_c\tau}\right]}{G_{xx}(f_c)G_{yy}(f_c)} \quad (2\text{-}13b)$$

$$\cong \mathrm{Re}\left[\gamma_{xy}(f_c)e^{j2\pi f_c\tau}\right] \quad (2\text{-}13c)$$

$$\cong \left|\gamma_{xy}(f_c)\right|\left[\cos 2\pi f_c(\tau - D)\right] . \quad (2\text{-}13d)$$

The crosscorrelation coefficient at zero argument is given by

$$\rho_{x_1y_1}(0) = \mathrm{Re}\left[\gamma_{xy}(f_c)\right] . \quad (2\text{-}14)$$

Thus we see from (2-14) and (2-13d) how the CC is related to the crosscorrelation coefficient.

2A3. Properties

The power spectral density matrix is positive semidefinite (Jenkins and Watts (1968)). Therefore,

for two random processes, we see that

$$|Q_x(f)| = \begin{vmatrix} G_{x_1x_1}(f) & G_{x_1x_2}(f) \\ G_{x_2x_1}(f) & G_{x_2x_2}(f) \end{vmatrix} \geq 0 \quad . \qquad (2\text{-}15a)$$

For real processes, $G_{x_2x_1}(f) = G^*_{x_1x_2}(f)$ and thus

$$G_{x_1x_1}(f)G_{x_2x_2}(f) - |G_{x_1x_2}(f)|^2 \geq 0 \ , \qquad (2\text{-}15b)$$

and

$$G_{x_1x_1}(f)G_{x_2x_2}(f) \geq |G_{x_1x_2}(f)|^2 . \qquad (2\text{-}15c)$$

Further, $G_{x_1x_1}(f)$ and $G_{x_2x_2}(f)$ are nonnegative, real functions of f. When $G_{x_1x_1}(f)$, $G_{x_2x_2}(f)$ are strictly positive definite (that is, when $G_{x_1x_1}(f)G_{x_2x_2}(f)>0$), (2-15c) can be divided through by $G_{x_1x_1}(f)G_{x_2x_2}(f)$ without changing the sense of the inequality thereby yielding

$$C_{x_1x_2}(f) \leq 1, \ \forall f . \qquad (2\text{-}16a)$$

Further, the magnitude-squared of any complex number is greater than or equal to zero. Thus,

$$0 \leq C_{x_1x_2}(f) \leq 1 \quad . \qquad (2\text{-}16b)$$

The MSC always falls between zero and one. Further, as will be shown, it is zero if the processes $x_1(t)$ and $x_2(t)$ are uncorrelated; and, it is equal to unity if there exists a linear relation between $x_1(t)$ and $x_2(t)$. The cross-power spectrum is then defined by

Hannan and Thomson (1973) as

$$G_{x_1x_2}(f) = \sqrt{G_{x_1x_1}(f)G_{x_2x_2}(f)}\ \gamma_{x_1x_2}(f) \quad . \qquad (2\text{-}17)$$

This definition is interesting since it points out the importance of the coherence. It should be noted that if $\gamma_{x_1x_2}(f)$ is undefined, $G_{x_1x_2}(f)$ cannot be computed from (2-17) (as, for example, when $G_{x_1x_2}(f)$ and $G_{x_1x_1}(f)$ are zero). Here we note that the statement $C_{x_1x_2}(f) = 0$ provides more information than the statement $|G_{x_1x_2}(f)|^2 = 0$, since in the former case, both autospectra must be nonzero. However, it may be more exact to say $|G_{x_1x_2}(f)|^2$ is undefined when no measurement is made.

In order to define the MSC, it is necessary that the numerator and denominator of that ratio not be simultaneously zero. Moreover the MSC will be undefined if either autospectra is zero. For example, if $G_{x_1x_1}(f) = 0$ or $G_{x_2x_2}(f) = 0$ it must be true from (2-15c) that $|G_{x_1x_2}|^2 = 0$. Hence, it can be concluded that if either $G_{x_1x_1}(f)$ or $G_{x_2x_2}(f)$ is zero over some frequency range then the MSC is undefined over that same frequency range. Further, if this is the case, the power spectral density matrix is singular. Another property of the MSC is that the MSC is invariant under linear transformations. If $x(t)$ is filtered by $H_1(f)$ and $y(t)$ is filtered by $H_2(f)$ as depicted in Figure 2-1, then

$$C_{x_1y_1}(f) = \frac{|G_{xy}(f)|^2}{G_{xx}(f)G_{yy}(f)} \quad , \tag{2-18a}$$

$$= \frac{|G_{xy}(f)|^2|H_1(f)|^2|H_2(f)|^2}{G_{xx}(f)|H_1(f)|^2\, G_{yy}(f)|H_2(f)|^2} = C_{xy}(f) \tag{2-18b}$$

Thus provided $|H_1(f)|^2|H_2(f)|^2 \neq 0$

$$C_{x_1y_1}(f) = C_{xy}(f) \quad . \tag{2-19}$$

That is, the MSC is the same between x and y as between the filtered versions x_1 and y_1.

2B. Uses of Coherence Function

The MSC function for the zero-mean, wide-sense stationary processes x(t) and y(t) is useful in several ways, which will be proved in the following sections. First, for two independent processes, the MSC function is zero. Second, the MSC measures the degree of system linearity. Third, under the assumptions to be presented, the MSC function serves as a SNR measure.

2B1. Measure of Correlation

THEOREM 2-1: If two zero-mean stationary processes x(t) and y(t) are independent, they are also uncorrelated and orthogonal;

$$R_{xy}(\tau) = E[x(t)y(t-\tau)] = E[x(t)]\,E[y(t-\tau)] = 0, \tag{2-20a}$$

$$G_{xy}(f) = \int_{-\infty}^{\infty} R_{xy}(\tau)e^{-j2\pi f\tau}d\tau = 0 \quad , \tag{2-20b}$$

and the MSC

$$C_{xy}(f) = 0 \quad , \forall f \tag{2-20c}$$

provided $G_{xx}(f)G_{yy}(f) \neq 0$.

Hence, if the two processes are independent (or uncorrelated) with zero mean, the MSC between them is zero.

DISCUSSION OF THEOREM 2-1: Note that jointly Gaussian random processes that are uncorrelated (incoherent) are also independent. However, it is possible for two processes to be highly dependent yet uncorrelated (incoherent), even if one of the two processes is Gaussian. Although one may be led by physical considerations to presume processes are independent and hence uncorrelated, in practice, it is easier to show processes are uncorrelated than independent. Note that if $C_{xy}(f) = 0$, $\forall f$, it follows that $Re[\gamma_{xy}(f)] = Im[\gamma_{xy}(f)] = 0 = G_{xy}(f)$, $\forall f$ and thence it follows that $R_{xy}(\tau) = 0$, $\forall \tau$. Hence, we see that if two processes are incoherent, then they are also uncorrelated. However, as stated earlier, being incoherent does <u>not</u> necessarily imply being independent. For example, suppose $y(t) = \eta(x)$ and $x(t)$ is a zero mean stationary random Gaussian process with variance σ^2 and first order probability density function (pdf),

$$p(x) = \frac{1}{\sqrt{2\pi\sigma^2}} e^{-x^2/2\sigma^2} \quad ; \tag{2-21}$$

then from Nuttall (1958) and Carter and Knapp (1975)

$$R_{xy}(\tau) = K\, R_{xx}(\tau), \tag{2-22}$$

where

$$K \quad \frac{1}{\sigma^2} \int_{-\infty}^{\infty} \eta(x) x \frac{1}{\sqrt{2\pi\sigma^2}} e^{-x^2/2\sigma^2} \, dx \, . \qquad (2\text{-}23)$$

Therefore, for even nonlinearities, $K=0$ and $R_{xy}(\tau)=0$. Hence $G_{xy}(f)=0$ and $C_{xy}(f)=0$. Thus, it is simple to derive a process $y(t)$ which is completely dependent on $x(t)$ but which is uncorrelated with it. Hence, the converse of theorem (2-1) does not hold and coherence does not provide information on dependence or independence but only on second order measures like correlation.

2B2. Measure of System Linearity

The MSC function can be used to measure system linearity. In Figure 2-2 consider the linear system with input $x(t)$, impulse response $h(\tau)$, and output $y(t)$. The output $y(t)$ is expressed by the convolution integral

$$y(t) = \int_{-\infty}^{\infty} h(\tau)x(t-\tau) \, d\tau \, , \qquad (2\text{-}24a)$$

or

$$y(t) = h(t) \bullet x(t) \, , \qquad (2\text{-}24b)$$

where $\bullet$ denotes convolution.

In the Fourier domain the convolution is the multiplication (Oppenheim and Schafer (1975))

$$Y(f) = H(f)X(f) \, , \qquad (2\text{-}25)$$

where X, H, and Y are Fourier transforms of x, h and y, respectively.

Figure 2-2 Linear System with Impulse Respone h(τ)

THEOREM 2-2:

If a system is linear then

$$\gamma_{xy}(f) = e^{j\phi_{xy}(f)} \quad , \quad \forall f \tag{2-26}$$

and hence

$$C_{xy}(f) = 1, \quad \forall f. \tag{2-27}$$

PROOF OF THEOREM 2-2:

For linear systems,

$$G_{yy}(f)=H_{xy}(f)H^*_{xy}(f)G_{xx}(f), G_{xy}(f)=H^*_{xy}(f)G_{xx}(f) \tag{2-28}$$

or when $G_{xx}(f) \neq 0$

$$G_{yy}(f) = \frac{G_{xy}(f)G^*_{xy}(f)}{G^2_{xx}(f)} \; G_{xx}(f). \tag{2-29}$$

Substituting $G_{yy}(f)$ into the basic definition of CC,

$$\gamma_{xy}(f) = \frac{G_{xy}(f)}{\sqrt{G_{xy}(f)G^*_{xy}(f)}} = \frac{|G_{xy}(f)|\, e^{j\phi_{xy}(f)}}{\sqrt{|G_{xy}(f)|^2}} \tag{2-30a}$$

$$= e^{j\phi_{xy}(f)}. \tag{2-30b}$$

Further,

$$C_{xy}(f) \equiv |\gamma_{xy}(f)|^2 = \cos^2[\phi_{xy}(f)]+\sin^2[\phi_{xy}(f)] = 1. \tag{2-31}$$

DISCUSSION OF THEOREM 2-2: This theorem is related to work of Koopmans (1964), Jenkins and Watts (1968), Otnes and Enochson (1972), Carter, Knapp and Nuttall (1973a), Koopmans (1974), Brillinger (1975), and Halvorsen and Bendat (1975). This theorem, experience, and certain intuition lead one to believe the converse of the theorem should also be true. To date no proof has been presented for the converse. Notably, it is

the converse which would play a most important role in the applications area. This is because one is seldom given a linear system and asked to measure MSC. Rather, one is given an unidentified system and asked: "Is it linear?". In the past, if the MSC was unity, one had a "hunch" that this was true but no rigorous proof existed to assert this truth. The following theorem acts to clarify this dilemma and indeed show what can and what cannot be said about linearity when the MSC is unity.

The strongest theorem which can be proved in this regard is as follows:

THEOREM 2-3: If $C_{xy}(f)=1, \forall f$, then with probability one there exists an optimum filter with unique transfer function $H_o(f)$ that can act on the input, $x(t)$, to an unidentified system to achieve output $y_o(t)$ exactly equal in every detail to the output $y(t)$ of the unidentified system, (that is, $y_o(t)=y(t)$, with probability one). Moreover, the phase of the filter

$$\text{Arg } H_o(f) = \phi_{yx}(f) = \text{Arg } \gamma_{yx}(f) .$$

In order to prove theorem 2-3, it is necessary to introduce and prove a lemma.

LEMMA 2-1: If $G_{ee}(f)$ is the power spectrum of an ergodic random process with member function $e(t)$ and if $G_{ee}(f)=0$, $\forall f$, then $e(t)$ equals zero with probability one for all t.

PROOF OF LEMMA 2-1: From p. 150, Papoulis (1965), the Chebycheff (or Tchebycheff) inequality is

$$\text{Prob}\{|e(t)-E[e(t)]|<\varepsilon\} \geq 1 - \frac{\sigma^2}{\varepsilon^2} \quad , \tag{2-32}$$

where $\varepsilon>0$ can be made arbitrarily small and σ^2 is the variance or power of $e(t)$. The autocorrelation function of $e(t)$ is

$$R_{ee}(\tau) = \int_{-\infty}^{\infty} G_{ee}(f) e^{j2\pi f\tau}\, df, \tag{2-33}$$

but $G_{ee}(f)=0$, $\forall f$ so that $R_{ee}(\tau)=0$, $\forall \tau$. In particular

$$R_{ee}(0) = F\left[e^2(t)\right]=0 = \sigma^2 + E^2[e(t)]. \tag{2-34}$$

Hence $\sigma^2=0$ and $E[e(t)]=0$. Alternatively note that the value of the tails of the autocorrelation is related to the mean value of the function. Specifically, (p. 333, Papoulis (1965))

$$\lim_{\tau\to\infty} R_{ee}(\tau) = E^2[e(t)] \quad . \tag{2-35}$$

So since $R_{ee}(\tau)=0$, $\forall \tau$

$$\lim_{\tau\to\infty} R_{ee}(\tau) = 0 \quad , \tag{2-36}$$

it follows that

$$E^2[e(t)] = 0, \tag{2-37}$$

and thus that

$$E[e(t)] = 0 \quad . \tag{2-38}$$

Therefore, the Chebycheff inequality with $\sigma^2=0$ and $E[e(t)]= 0$ is

$$\text{Prob}\left[|e(t)|<\varepsilon\right] \geq 1 \quad , \tag{2-39a}$$

but $0 \leq \text{Prob}[\ ] \leq 1$ so that

$$\text{Prob}\left[|e(t)|<\varepsilon\right] = 1 \ ; \tag{2-39b}$$

that is, the probability that $|e(t)|$ is less than some arbitrarily small value is one. Statistically, we say that this event happens "with probability one" or we say that it happens "almost surely." So when the power spectrum $G_{ee}(f)$ of this random process is zero for all frequencies, then $e(t)=0$ with probability one.

DISCUSSION OF LEMMA 2-1:

The interpretation of the results can be misleading for transients (nonstationary processes). For example, consider (see, for example, p. 93 of Lee (1960)),

$$\lim_{T\to\infty} \frac{1}{2T} \int_{-T}^{T} e^2(t)dt = R_{ee}(0) = \int_{-\infty}^{\infty} G_{ee}(f)\, df. \tag{2-40}$$

Now clearly there exists $e(t)\neq 0$ such that

$$\lim_{T\to\infty} \frac{1}{2T} \int_{-T}^{T} e^2(t)dt = 0 \ . \tag{2-41}$$

For example, if a finite energy pulse lasts only a few seconds, then the power (or "average" energy) in such a nonrepetitive pulse is zero. This is because

$$\lim_{T\to\infty} \int_{-T}^{T} e^2(t)\, dt$$

equals some nonzero constant energy but

$$\lim_{T\to\infty} \frac{1}{2T} \int_{-T}^{T} e^2(t)dt$$

equals zero; hence, the power is zero. Transient situations of this type are disallowed by the ergodicity constraint which requires stationarity. (Ergodic processes are stationary but not necessarily vice versa.) The essence of the proof then is that for ergodic random processes almost surely e(t)=0 in that frequency band where $G_{ee}(f)=0$. This is a reasonable practical assumption; however, it should not be overlooked that there exists a nonstationary class of processes for which the proof of LEMMA 2-1 does not apply. We now proceed with the proof of theorem 2-3.

PROOF OF THEOREM 2-3: It is instructive to visualize the proof as attempting to select an optimum filter such that the minimum mean squared error (MMSE) is achieved, where the error e(t) is defined as $e(t)=y(t)-y_o(t)$, as shown in Figure 2-3.

The solution will make no presumptions on the origin (source) of y(t). It is useful, however, to envision y(t) as the stationary output of an unidentified system as depicted in Figure 2-4; such a model is a special case of Figure 2-3, but is perhaps a more common system identification problem. Whether the error signal e(t) is generated from Figure 2-3 or Figure 2-4, it follows that the total power is given by

$$\lim_{T\to\infty} \frac{1}{T} \int_{-T/2}^{T/2} e^2(t)dt = \int_{-\infty}^{\infty} G_{ee}(f)\, df \quad . \qquad (2\text{-}42)$$

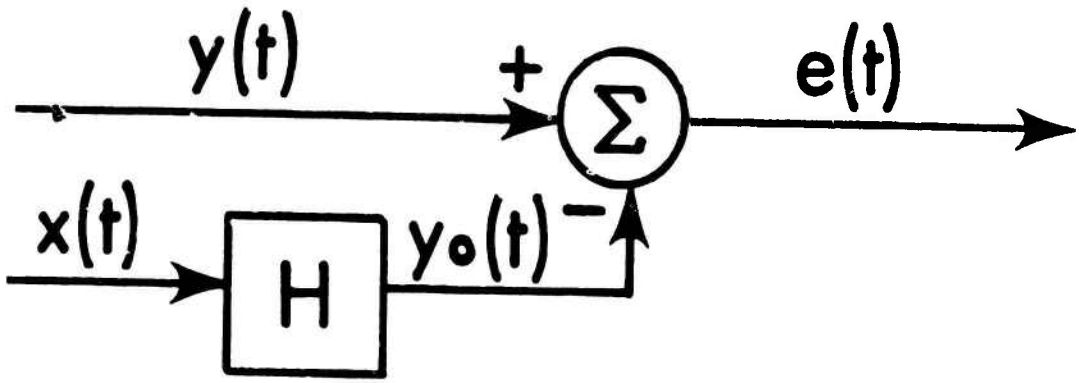

Figure 2-3 Model of Error Resulting from Linearly Filtering x(t) to Match Any Desired Signal y(t)

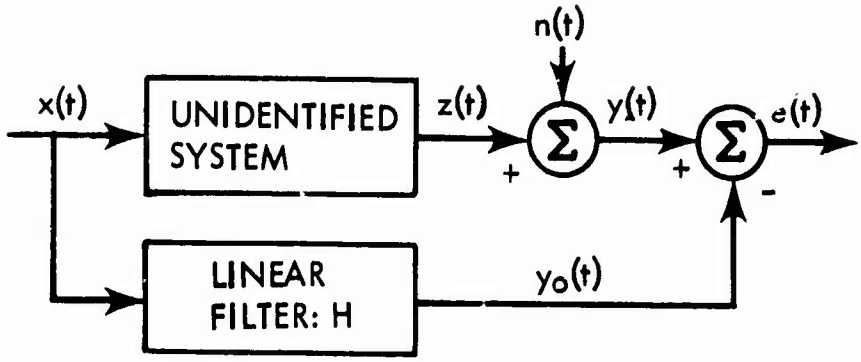

Figure 2-4 Model of Error Resulting from Linear Approximation of Nonlinearity

All power spectra have the property that they are non-negative. The implication is that in integrating over the interval $(-\infty,\infty)$, there will be no portions of $G_{ee}(f)$ that will "cancel" other portions. Solving for $G_{ee}(f)$, it can be shown that

$$G_{ee}(f)=G_{yy}(f) + G_{xx}(f)|H(f)|^2-H(f)G_{xy}(f) -H^*(f)G^*_{xy}(f), \tag{2-43}$$

which can be written, as done by Carter and Knapp (1975), as

$$G_{ee}(f)=G_{xx}(f)\left|H(f)- \frac{G_{yx}(f)}{G_{xx}(f)}\right|^2+G_{yy}(f)\left[1-C_{xy}(f)\right]. \tag{2-44}$$

Since

$$G_{xx}(f) \geq 0,\ G_{yy}(f) \geq 0,\ \text{and}\ 0 \leq C_{xy}(f) \leq 1\ ,$$

it is necessary to minimize

$$\left|H(f) - \frac{G_{yx}(f)}{G_{xx}(f)}\right|^2 \quad ,$$

which is done by selecting the optimum linear filter

$$H_o(f) = \frac{G_{yx}(f)}{G_{xx}(f)} = \frac{\left|G_{yx}(f)\right|}{G_{xx}(f)}e^{j\phi_{yx}(f)} \quad . \tag{2-45}$$

The optimum filter is a Wiener filter and is discussed in texts by Lee (1960) and Van Trees (1968). The Fourier transform of (2-45) is the impulse response

$$h_o(\tau) = \int_{-\infty}^{\infty} H_o(f)e^{j2\pi f\tau}df \quad . \tag{2-46}$$

In general, $h_o(\tau)$ will be a nonzero for $\tau<0$; hence, the system will be nonrealizable. Various methods can be applied to obtain the optimum realizable linear filter; although they are beyond the scope of this thesis, they

are discussed in standard texts such as Lee (1960) or Van Trees (1968).

From (2-45) the cross spectrum between x(t) and y(t),

$$G_{yx}(f) = H_o(f)G_{xx}(f), \tag{2-47}$$

but since x(t) excites a linear filter $H_o(f)$ to produce output $y_o(t)$, it also follows that

$$G_{y_o x}(f) = H_o(f)G_{xx}(f) \quad . \tag{2-48}$$

Substituting (2-48) into (2-47) yields

$$G_{yx}(f) = G_{y_o x}(f) \quad . \tag{2-49}$$

Since $y(t)=e(t) + y_o(t)$,

$$R_{yx}(\tau) = E\{[e(t)+y_o(t)]x(t-\tau)\} \tag{2-50a}$$

$$= R_{ex}(\tau) + R_{y_o x}(\tau) \quad . \tag{2-50b}$$

But by taking the Fourier transform of both sides of (2-49)

$$R_{yx}(\tau) = R_{y_o x}(\tau) \quad . \tag{2-51}$$

Hence, from (2-51) and (2-50)

$$R_{ex}(\tau) = 0, G_{ex}(f)=0; \tag{2-52}$$

that is, the error is uncorrelated with the input x(t). This is an interesting property of the error signal in it's own right. When $x_i(t)$ is linearly filtered by $H_i(f)$ to yield $y_i(t)$ for i=1,2, the cross-power spectrum of the filter outputs is given by Davenport (1970) as

$$G_{y_1y_2}(f) = H_1(f)H_2^*(f)G_{x_1x_2}(f) \quad . \tag{2-53}$$

Hence in the special case where $x_1(t)=x(t)$, $x_2(t)=e(t)$, $H_1(f)=H_o(f)$ and $H_2(f)=1$, it follows that

$$G_{y_oe}(f) = H_o(f)G_{xe}(f) \quad . \tag{2-54}$$

So if the error is uncorrelated with x(t) (that is, if $G_{xe}(f)=0$), then it must be true that $G_{y_oe}(f)=0$ (that is, the error is uncorrelated with the output of the optimum filter). The waveform x(t) being uncorrelated with e(t) implies that e(t) is also uncorrelated with $y_o(t)$. Further,

$$R_{ey}(\tau) = E[e(t)y(t-\tau)], \tag{2-55a}$$

but $y(t)=e(t)+y_o(t)$ so that

$$R_{ey}(\tau) = E\{e(t)\left[e(t-\tau) + y_o(t-\tau)\right]\} \tag{2-55b}$$

$$= R_{ee}(\tau) + R_{ey_o}(\tau) \quad . \tag{2-55c}$$

Recognizing that $R_{ey_o}(\tau)=0$ and taking the Fourier transform of both sides of (2-55) yields

$$G_{ey}(f) = G_{ee}(f) \quad . \tag{2-56}$$

The selection of the optimum H(f) forces (2-44) to become

$$G_{ee}(f) = G_{yy}(f)\left[1 - C_{xy}(f)\right] \quad . \tag{2-57}$$

When $C_{xy}(f)=1$, clearly (from 2-57) $G_{ee}(f)=0$, and thus (from LEMMA 2-1) e(t)=0 with probability one, but

$$y(t) = y_o(t) + e(t), \tag{2-58}$$

so that almost surely,

$$y(t) = y_o(t) \quad . \tag{2-59}$$

Thus, with probability one, the linear filter

$$H_o(f) = H_{y_o x}(f) = \frac{G_{yx}(f)}{G_{xx}(f)} e^{j\phi_{yx}(f)} \qquad (2\text{-}60)$$

will operate on x(t) to achieve $y_o(t)=y(t)$. If the optimum output $y_o(t)=x(t) \circledast h_o(t)$ then by the Fourier transform relation

$$Y_o(f) = X(f)H_o(f) \quad . \qquad (2\text{-}61)$$

The Fourier transform is a one for one reversible transformation so that a unique x(t), y(t) implies a unique X(f), Y(f), but then

$$H_o(f) = \frac{Y_o(f)}{X(f)} \qquad (2\text{-}62)$$

must be unique. This completes the proof of theorem 2-3.

DISCUSSION OF THEOREM 2-3:

Unique transfer functions do not identify unique systems. Indeed, nothing is known about the internal structure of the unidentified system. Further, the fact that the system can be modeled by a linear system $H_o(f)$ such that when both (system and model) are stimulated by an excitation x(t) they yield identical output y(t) does not prove that the system is linear over all inputs. There may indeed be unobservable nonlinearities in the unidentified system. For example, suppose the excitation x(t) is stationary but with first order pdf such that $-A \leq |x(t)| \leq A$. This implies that x(t) never excites the unidentified system for amplitudes greater than A; hence, no conclusions can be drawn about the linearity of the system over all inputs.

Many "real world" systems are linear over a certain range of amplitudes and then saturate above that amplitude as in the case of analog computers (Kochenburger (1972)). As another example, consider any stationary x(t). The stationary excitation has only one invariant power spectrum $G_{xx}(f)$. Systems which appear linear for some $G_{xx}(f)$ but which are clearly nonlinear for different input statistics are simple to envision. If a system is nonlinear but the nonlinearity is not excited (or more generally, not observed), then the system will appear linear and the measurement of the MSC will equal unity. In essence then, the class of nonlinear functions is so large that based on a single excitation (even white Gaussian noise) it is impossible to claim, without qualification, that a system is "linear" simply because the MSC is unity, for all probed frequencies. Another type of nonlinear system is one in which the MSC is observed to be unity in some frequency bands and not unity in other bands. Thus $y_o(t) \neq y(t)$, unless those frequency bands which cannot be accounted for by linear processing are removed. More precisely, if $C_{xy}(f) = 1$ in the frequency band (f_1, f_2) then with probability one there exists an optimum linear filter with unique transfer function $H_o(f)$ that can act on x(t) to achieve optimum output $y_o(t)$ where $y_o(t)=y(t) \bullet h_I(t)$ and $h_I(t)$ is the impulse response of an ideal zero phase, unity gain "box car" filter that

passes only those frequencies in the (f_1, f_2) band. The whole problem of nonlinear systems can be treated by considering what proportion of a system output can be attributed to a linear operation and what proportion is due to a residual or nonlinear operation. In general, the power spectrum of the optimum output

$$G_{y_o y_o}(f) = |H_o(f)|^2 G_{xx}(f) \tag{2-63}$$

or substituting (2-1), (2-2) and (2-45) into (2-63) yields

$$G_{y_o y_o}(f) = G_{yy}(f) C_{xy}(f) \quad . \tag{2-64}$$

This important result (Carter and Knapp (1975)) can be rewritten as

$$C_{xy}(f) = \frac{G_{y_o y_o}(f)}{G_{yy}(f)} \quad . \tag{2-65}$$

The implication is that the MSC measures the portion or amount of power ($G_{yy}(f)$) which can be obtained through optimal linear filtering (in the MMSE sense) of x(t). Moreover, it is always true (provided $C_{xy}(f)$ is defined) that

$$G_{yy}(f) = C_{xy}(f) G_{yy}(f) + \left[1 - C_{xy}(f)\right] G_{yy}(f) \quad . \tag{2-66}$$

Substituting from (2-64) and (2-57) into (2-66) yields

$$G_{yy}(f) = G_{y_o y_o}(f) + G_{ee}(f) \quad , \tag{2-67}$$

which implies the power spectrum of the output of a system is comprised only of the sum of an error spectrum and an optimum spectrum. This same result can be noticed from

$$R_{yy}(\cdot) = R_{ee}(\tau) + R_{y_o e}(\tau) + R_{e y_o}(\tau) + R_{y_o y_o}(\tau) \quad , \qquad (2\text{-}68)$$

but $R_{y_o e}(\tau) = R_{e y_o}(-\tau) = 0, \forall\tau$ so that

$$R_{yy}(\tau) = R_{ee}(\tau) + R_{y_o y_o}(\tau) \quad . \qquad (2\text{-}69)$$

Computing the Fourier transform of (2-69) verifies (2-67).

Just as the MSC measured what portion of $G_{yy}(f)$ could be obtained by (optimal) linear filtering, one minus MSC is a measure of the portion of output power due to an uncorrelated error component; that is,

$$\frac{G_{ee}(f)}{G_{yy}(f)} = 1 - C_{xy}(f) \quad . \qquad (2\text{-}70)$$

Thus, it follows that the ratio of the optimum linear power to the nonlinear or error power is

$$\frac{G_{y_o y_o}(f)}{G_{ee}(f)} = \frac{C_{xy}(f)}{1 - C_{xy}(f)} \quad . \qquad (2\text{-}71)$$

(This ratio will be important in the estimation of time delay.)

For practical nonlinear systems, the identification of the optimum linear component is not always obvious. For example, in the system without noise described by $y(t)=x^3(t)+b\,x(t)$, the optimal linear part is <u>not</u> $bx(t)$. To clarify this point, it will be demonstrated that for a limited class of inputs and a limited class of nonlinearities, analytic expressions for the optimal linear part can be obtained. This offers interesting insight

into both the general system identification problem and the coherence interpretation problem. First, the nonlinearity is constrained to have no memory and no noise, that is, $y=\eta(x)$. Second, the input processes are constrained to be separable in the sense defined by Nuttall (1958). A separable process with second-order pdf $p(x_1,x_2;\tau)$ and mean μ is defined as one for which the integral $\int_{-\infty}^{\infty}(x_1-\mu)p(x_1,x_2;\tau)dx_1$ separates into the product of a function of x_2 alone and a function of τ alone. For example, it can be shown that a Gaussian process possesses these properties and, hence, is a separable process.

Under the no-memory nonlinearity and separable process constraints, it has been proved by Nuttall (1958) the crosscorrelation between x(t) and y(t) at delay τ is given by

$$R_{yx}(\tau) = K \cdot R_{xx}(\tau) \ , \qquad (2\text{-}72a)$$

where

$$K = \frac{1}{\sigma^2} \int_{-\infty}^{\infty} \eta(x)(x-\mu)p(x)dx \ , \qquad (2\text{-}72b)$$

p(x) is the first-order pdf of x(t), $\eta(x)$ is a complete description of the no-memory nonlinear function, and σ^2 is the variance of x(t). Notice that the constant K does not depend on frequency or delay but only on the first-order pdf and the nonlinearity. It follows directly from (2-72a) that, for no-memory nonlinearities excited by separable processes,

$$\gamma_{yx}(f) = \gamma_{xy}(f) = K\sqrt{\frac{G_{xx}(f)}{G_{yy}(f)}} \quad . \tag{2-73}$$

Comparison of (2-73) with (2-45) and (2-1) shows that the constant K is the optimum linear filter in the MMSE sense.

As an example, suppose x(t) has a Gaussian zero-mean, σ^2 variance pdf; then

$$K = \frac{1}{\sigma^2}\int_{-\infty}^{\infty} \eta(x)x \frac{1}{\sqrt{2\pi\sigma^2}} e^{-x^2/2\sigma^2} dx. \tag{2-74}$$

Whenever the pdf is even and $\eta(x)$ is an even function, K=0 so that the coherence is zero. However, when $\eta(x)$ is an odd function, K does not necessarily equal zero even though the unidentified system is nonlinear. For example, when $\eta(x)=x^3(t)+b\,x(t)$, application of (2-74) yields $K=3\sigma^2+b$. Therefore, the optimal linear part of $x^3(t)+bx(t)$ is not bx(t) but rather $y_o(t)=(b+3\sigma^2)x(t)$ for a zero mean Gaussian process with variance of σ^2. For b=0, it follows that $K \neq 0$ and $C_{xy}(f) \neq 0$ provided $G_{xx}(f) \neq 0$. However, if $b=-3\sigma^2$, then K=0 and $C_{xy}(f)=0$. Thus, the MSC may still be zero even though the nonlinearity is not even. A computer simulation of the example with $\sigma^2 = 1/2$ and $b=-3/2$ was conducted, and the results verified the theory (Carter and Knapp (1975)). This result can be independently verified by calculating $R_{xy}(\tau) = E\{x(t)\left[x^3(t-\tau)+bx(t-\tau)\right]\}$, which for Gaussian processes is $3\sigma^2 R_{xx}(\tau)+bR_{xx}(\tau)$. Therefore, $C_{xy}(f)=0$ if $b=-3\sigma^2$, and there is no power in the optimum linear part

of the nonlinearity $\eta(x) = x^3(t) - 3\sigma^2 x(t)$.

Parenthetically, we note that another approach to this problem is to expand the no-memory nonlinearity η as an infinite series of orthogonal polynomials, specifically,

$$y(t) = \eta[x(t)] = \sum_{n=0}^{\infty} a_n H_{e_n}[x(t)] \quad , \tag{2-75a}$$

where the $H_{e_n}(x)$ are e_n Hermite polynomials (see, for example, p. xxxv, Gradshteyn and Ryzhik (1965))

$$H_{e_o}(x)=1, \; H_{e_1}(x)=x, \; H_{e_2}(x)=x^2-1, \; H_{e_3}(x)=x^3-3x$$

and in general

$$H_{e_{n+1}}(x)=xH_{e_n}(x)-nH_{e_{n-1}}(x) \quad . \tag{2-75b}$$

Then, the crosscorrelation between x and y is given by

$$R_{xy}(\tau) = \sum_{n=0}^{\infty} a_n E\{x(t)H_{e_n}[x(t-\tau)]\} \quad . \tag{2-76}$$

The advantage to this method is that, if the family of correlations

$$R_{xH_{e_n}(x)}(\tau) = E\{x(t)H_{e_n}[x(t-\tau)]\}, \quad n=1,2,\ldots \tag{2-77}$$

had been computed once, orthogonal expansion of $\eta(x)$ makes $R_{xy}(\tau)$ immediately apparent by a simple weighted summation.

It is perhaps germane to clarify the significance of knowing that the MSC is unity. Just as $C_{xy}(f)=1$ for all f ensured that there was some linear filter that mapped x(t) into $y_o(t)=y(t)$ exactly, there also exists a linear filter which maps y(t) into x(t) exactly. That

is, since $|G_{xy}(f)|^2 = |G_{yx}(f)|^2$, $C_{xy}(f) = C_{yx}(f)$ and conclusions drawn with regard to x(t) and y(t) have an analogous relation between y(t) and x(t). Thus, even though one cannot make unqualified statements about the unidentified system, there certainly exists a total detailed knowledge of its output for a given input and therefore, all of its output statistics when the MSC is unity and the input remains unchanged. All this is accomplished through the utilization of a linear (though not necessarily realizable) model.

2B3. Measure of Signal-to-Noise Ratio

The coherence can be used for determining SNR as will be discussed in this section. The results of this section are of interest from two points of view. First, the SNR is a fundamental concern in the basic passive detection problem and parameter estimation problem, and second the results of this section will aid in the interpretation of optimum delay estimation and variance of the estimate of coherence phase. Hence, while these results can be derived independent of the time delay estimation problem, they will form an important role in the understanding of how to estimate time delay or source bearing.

When x(t) is linearly filtered to yield output y(t) and the output is corrupted by uncorrelated additive noise, as depicted in Figure 2-5, then the noise power spectrum is

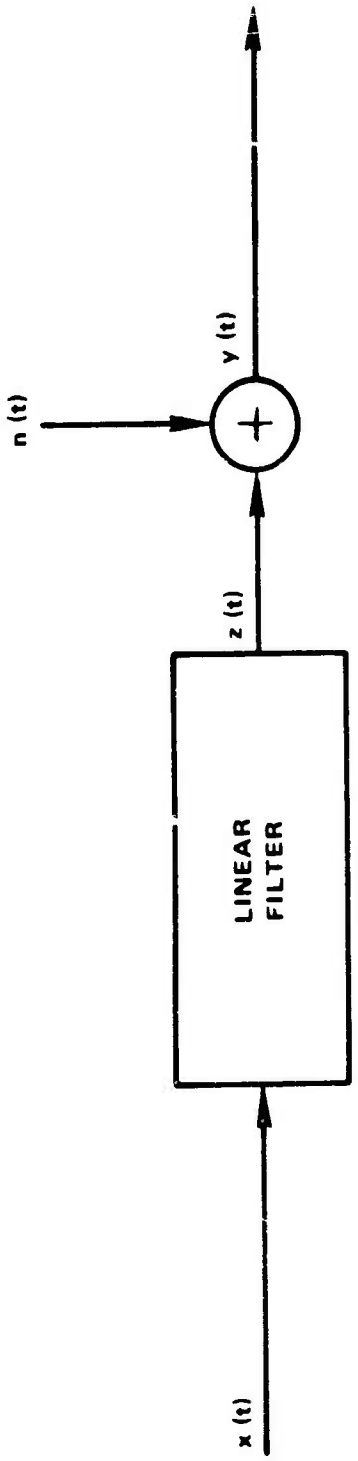

Figure 2-5 Linear Filter Whose Output is Corrupted with Additive Noise

$$G_{nn}(f) = G_{yy}(f)\left[1 - C_{xy}(f)\right] \quad . \tag{2-78}$$

This is an intuitively satisfying result since the MSC is unity if there is no noise, whereas the MSC is zero when the output is all noise. For linear systems, additive noise uncorrelated with the input reduces the MSC according to the ratio of $G_{nn}(f)$ to $G_{yy}(f)$. Measurement of $G_{nn}(f)$ is useful not only in the image processing problem discussed by Cannon (1974) but also in studying the gross effects of digital filtering when viewed as a perfect filter plus additive noise (James (1975) and Weinstein and Oppenheim (1969)). These methods can also be applied to studying special problems such as fast Fourier transform (FFT) noise (Ferrie and Nuttall (1971) and Rabiner and Rader (1972)).

The power spectrum from the output of an arbitrary system can always be viewed in terms of its two components $G_{yy}(f)C_{xy}(f)$ and $G_{yy}(f)\left[1-C_{xy}(f)\right]$ regardless of how $G_{yy}(f)$ is produced (as long as $C_{xy}(f)$ is defined). It is interesting to note that the ratio of these components

$$\frac{G_{y_o y_o}(f)}{G_{ee}(f)} = \frac{G_{zz}(f)}{G_{nn}(f)} = \frac{C_{xy}(f)}{1 - C_{xy}(f)} \tag{2-79}$$

can be considered as either the SNR or the linear to-nonlinear ratio, depending on the application.

For situations like those shown in Figure 2-5, the coherence measures what proportion of an unidentified system output is "linear." Through the use of (2-79), the MSC provides a comparison of the proportion of system

power that is linear with the proportion that is nonlinear in exactly the same way in which the SNR was measured for the output of a linear system corrupted by additive noise. However, in other system configurations, such as that shown in Figure 2-6, where noise and signal have a different interpretation, relation (2-79) will not be useful. Figure 2-6 is of interest to the sonar community since it is analogous to the physical situation in which signal s(t) from an acoustic source is received at two geographically separated sensors. Each observed signal is corrupted by additive stationary noise and is linearly filtered. When $n_1(t)$ and $n_2(t)$ are uncorrelated but have the same power spectra $G_{nn}(f)$, the SNR, $G_{ss}(f)/G_{nn}(f)$ is readily shown to be

$$\frac{G_{ss}(f)}{G_{nn}(f)} = \frac{\sqrt{C_{xy}(f)}}{1-\sqrt{C_{xy}(f)}} \quad , \tag{2-80}$$

which differs from (2-79). (Note from (2-19) that $C_{r_1 r_2}(f)=C_{xy}(f)$.) Ironically it will turn out to be (2-79) and not (2-80) which is critical to our problem. In cases where each transmission path attenuates the source signal differently, the model must be changed to reflect an attenuation in one channel. Unless simplifying assumptions are employed, the net result is that $G_{ss}(f)/G_{nn}(f)$ cannot be determined from $C_{xy}(f)$ unless attenuation in each path is known. (See section 4 of appendix B.)

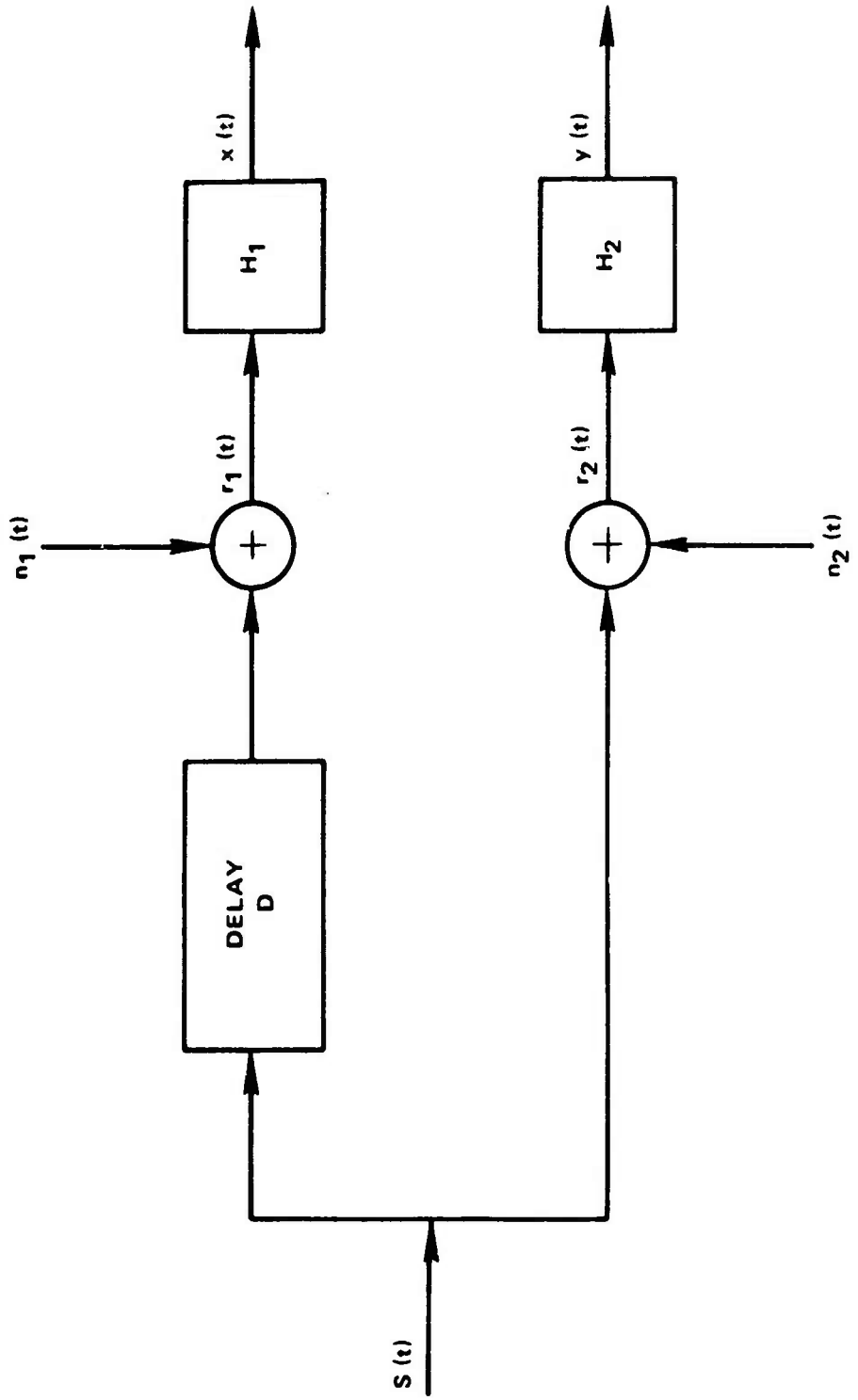

Figure 2-6 Model of Directional Signal Corrupted with Additive Noise and Processed

More generally, the source is transmitted through two ocean medium operators $H_1(f)$ and $H_2(f)$ as shown in Figure 2-7, which can attenuate the signal differently at different frequencies. For illustrative purposes, we assume that the ocean medium operators are linear time invariant filters. Thus $s_1(t)$ and $s_2(t)$ are the outputs of filters $H_1(f)$ and $H_2(f)$, respectively, which have been excited by source $s(t)$. This model of linear filters and noise is mathematically tractable and has been proposed before, as for example, on p. 389 of Whalen (1971). (More sophisticated models are given by Kennedy (1969).) When the noise $n_i(t)$ is uncorrelated with the signal $s_i(t)$, the power spectral density at the output of the i-th sensor is given by

$$G_{x_i x_i}(f) = G_{ss}(f)|H_i(f)|^2 + G_{n_i n_i}(f), \quad i=1,2 \qquad (2\text{-}81a)$$

$$= G_{s_i s_i}(f) + G_{n_i n_i}(f), \quad i=1,2 \ . \qquad (2\text{-}81b)$$

Further, the ratio of the power at the <u>output</u> of the filter to the corruptive noise power depends on the MSC between the <u>source</u> and the <u>sensor</u>. Specifically, from equation (8) of Carter, Knapp and Nuttall (1973a) or (2-79),

$$\frac{G_{s_i s_i}(f)}{G_{n_i n_i}(f)} = \frac{C_{sx_i}(f)}{1 - C_{sx_i}(f)}, \quad i=1,2 \ . \qquad (2\text{-}82)$$

(Note that when $|H_i(f)| \neq 1$, (2-82) does <u>not</u> measure the ratio of source to noise power.) The coherence between

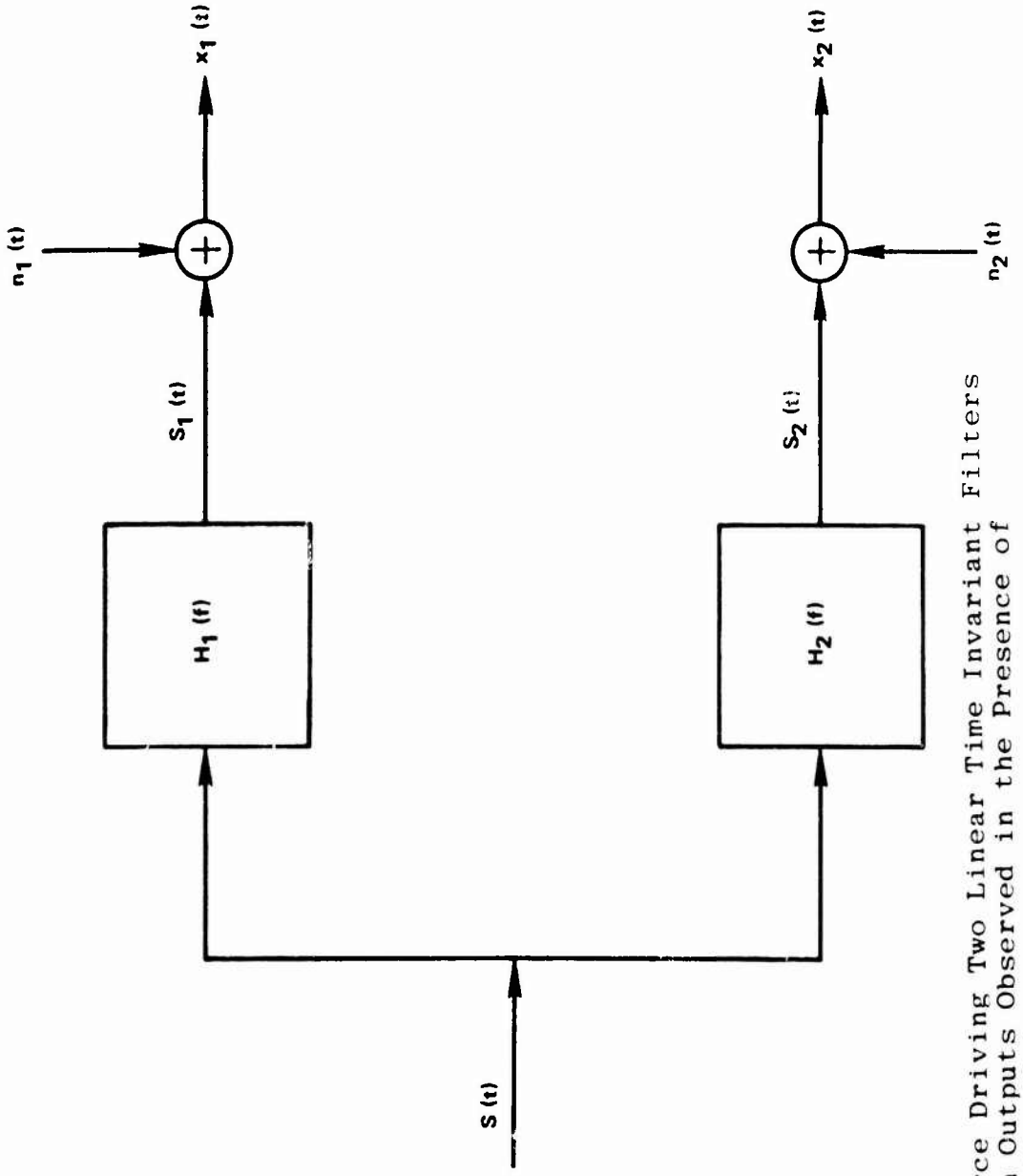

Figure 2-7 Source Driving Two Linear Time Invariant Filters with Outputs Observed in the Presence of Additive Noise

$x_1(t)$ and $x_2(t)$ in Figure 2-7 when and $n_1(t)$ and $n_2(t)$ are uncorrelated is given by

$$\gamma_{x_1x_2}(f) = \frac{G_{ss}(f)H_1(f)H_2^*(f)}{\sqrt{G_{x_1x_1}(f)G_{x_2x_2}(f)}} \quad . \tag{2-83}$$

In order to relate this result to the coherence between the source and each sensor, note that

$$\gamma_{sx_i}(f) = \frac{G_{ss}(f)H_i(f)}{\sqrt{G_{ss}(f)G_{x_ix_i}(f)}} \quad , \quad i=1,2, \tag{2-84}$$

so that

$$\gamma_{x_1x_2}(f) = \gamma_{sx_1}(f)\gamma_{sx_2}^*(f) \quad . \tag{2-85}$$

Taking the magnitude-squared yields

$$C_{x_1x_2}(f) = C_{sx_1}(f)C_{sx_2}(f) \quad . \tag{2-86}$$

Thus, when a source drives two linear time invariant filters whose output is observed in the presence of uncorrelated noise, the MSC between the outputs can be no larger than the MSC between the source and any sensor. In particular, for two sensors the MSC is the product of the two source MSCs, as given in (2-86). However, it is possible to have a source transmitted through some nonlinearity such that the MSC between $s(t)$ and $x_1(t)$ is low and the MSC between $s(t)$ and $x_2(t)$ is low and the MSC between $x_1(t)$ and $x_2(t)$ is high. For example, suppose $s(t)$ is a member function of a stationary random process which is separable in the Nuttall sense. Then the MSC between $x_1(t) = s^2(t)$ and

s(t) is zero; similarly, the MSC between $x_2(t) = s^2(t)$ and s(t) is zero; however, for this example, the MSC between $x_1(t)$ and $x_2(t)$ is unity. Thus, care should be used in interpreting these results since they apply only to the case where the medium can be accurately modeled by linear time invariant filters corrupted by uncorrelated additive noise.

Using (2-86) we can compute a SNR squared quantity, namely,

$$\frac{G_{s_1s_1}(f)}{G_{n_1n_1}(f)} \cdot \frac{G_{s_2s_2}(f)}{G_{n_2n_2}(f)} = \frac{C_{x_1x_2}(f)}{\left[1-C_{sx_1}(f)\right]\left[1-C_{sx_2}(f)\right]} . \quad (2\text{-}87)$$

To be useful (2-87) requires knowledge of the source to sensor MSCs. However, if $C_{sx_1}(f) = C_{sx_2}(f) = \left[C_{x_1x_2}(f)\right]^{\frac{1}{2}}$, then it follows that

$$\left[\frac{G_{s_1s_1}(f)G_{s_2s_2}(f)}{G_{n_1n_1}(f)G_{n_2n_2}(f)}\right]^{\frac{1}{2}} = \frac{\sqrt{C_{x_1x_2}(f)}}{1-\sqrt{C_{x_1x_2}(f)}} . \quad (2\text{-}88)$$

The results on coherence from this chapter will add to the understanding of the role of coherence in ML estimation of time delay as will be seen in the next chapter.

CHAPTER 3

MAXIMUM LIKELIHOOD ESTIMATE OF TIME DELAY

In the first section of this chapter an ML estimator is derived for determining time delay between signals received at two spatially separated sensors in the presence of uncorrelated noise. This ML estimator can be realized as a pair of receiver prefilters followed by a crosscorrelator. The time argument at which the correlator achieves a maximum is the delay estimate. In the second section of this chapter, the variance of the time delay estimate is derived and compared with the Cramér-Rao lower bound, and in the final section, various realizations of the processor are considered.

3A. Derivation

For the purposes of the derivation, a signal emanating from an acoustic source and monitored in the presence of noise at two spatially separated sensors can be mathematically modeled as depicted in Figure 3-1. Mathematically,

$$x_1(t)=s_1(t)+n_1(t) \tag{3-1a}$$

$$x_2(t)=\alpha s_1(t+D)+n_2(t) \ , \tag{3-1b}$$

where $s_1(t)$, $n_1(t)$, and $n_2(t)$ are real, jointly stationary

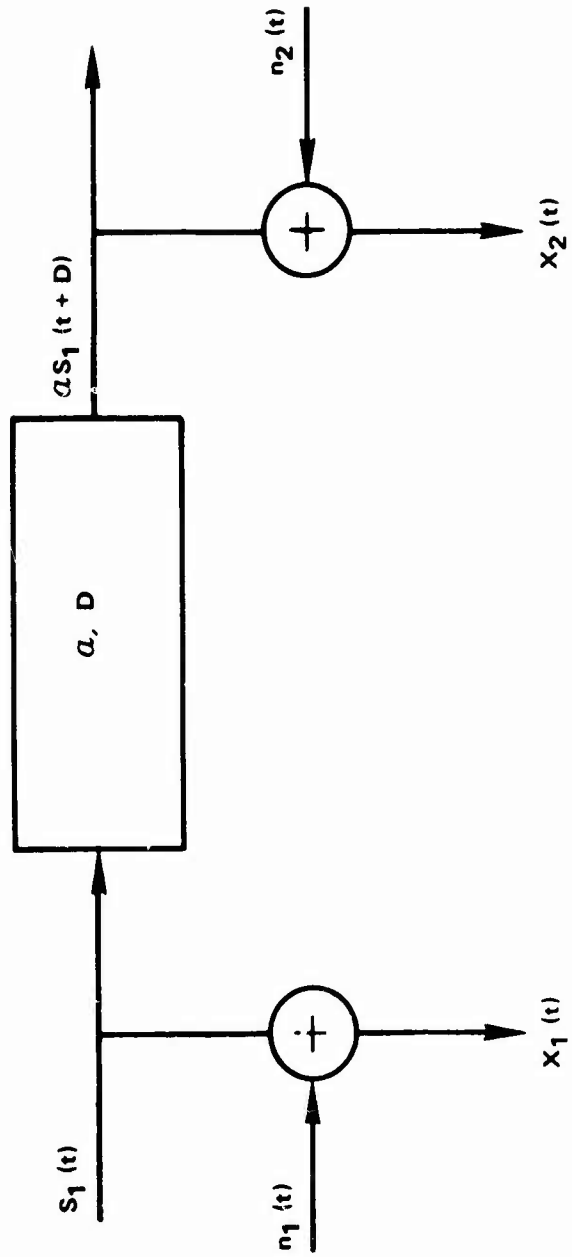

Figure 3-1 Plant with Noise Corrupted Observations of Input and Output

random processes. The delay, D, is the unknown parameter to be estimated. Signal $s_1(t)$ is assumed to be uncorrelated with noise $n_1(t)$ and $n_2(t)$. Later we also assume $n_1(t)$ and $n_2(t)$ are uncorrelated with each other.

More generally, it may be assumed that $s_2(t)$ is linearly related to $s_1(t)$ by the transfer function $H(f)=|\alpha(f)|e^{-j2\pi fD}$. Thus, unlike (3-1) where the Fourier transform of the system output is $\alpha s_1(f)e^{-j2\pi fD}$, the output transform in this case is $|\alpha(f)|s_1(f)e^{-j2\pi fD}$. The linear phase characteristic of such a system is assured when the impulse response is symmetric about $\tau=D$. For realizable systems, this implies that the duration of the impulse response must be finite. Thus, in a sense, we are estimating the midpoint of a symmetric finite impulse response (FIR) filter depicted in Figure 3-2a. Such an impulse response is not necessarily peaked at D (as for example in Figure 3-2b). In the derivation which follows, then, α can (more generally) be interpreted as a frequency dependent attenuation $|\alpha(f)|$.

There are many applications in which it is of interest to estimate the delay D. This chapter derives an ML estimator and evaluates its variance. Chapter 4 compares the estimator with other similar techniques. While the model of the physical phenomena presumes stationarity, the techniques to be developed herein may be employed in slowly varying environments where the characteristics of the signal and noise remain

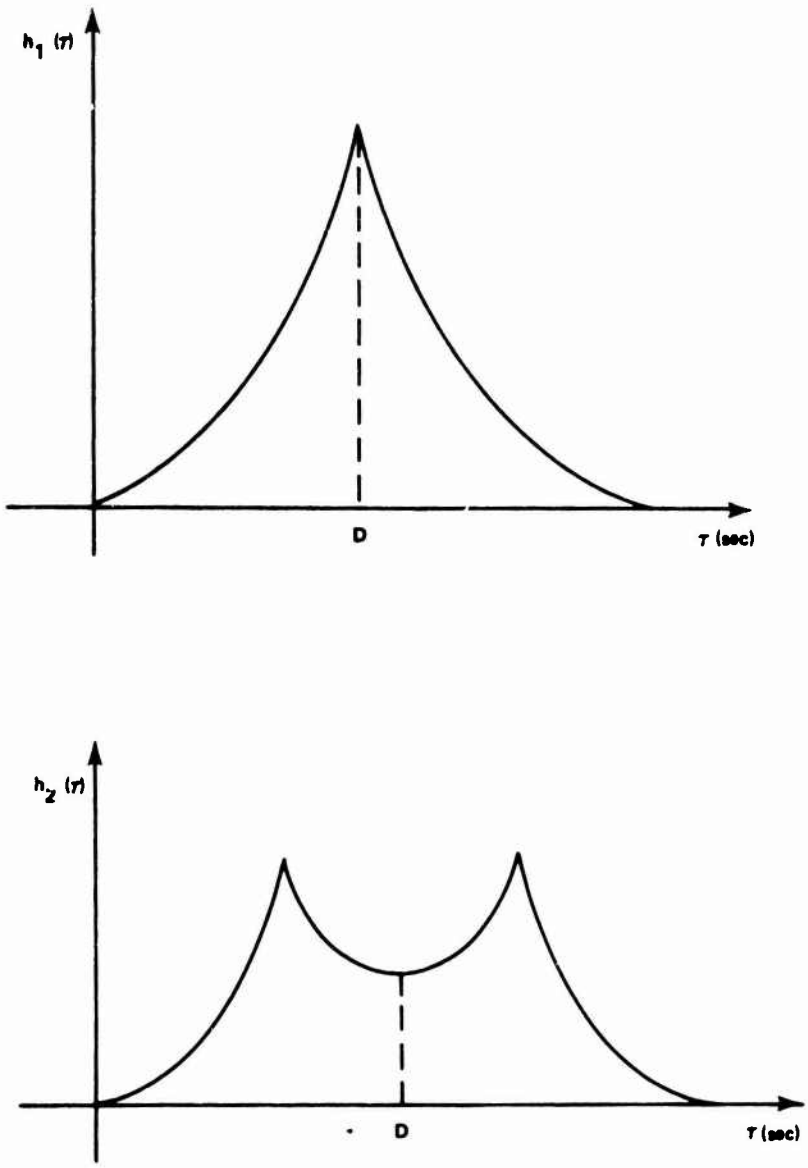

Figure 3-2 Symmetric Impulse Response for Two FIR Linear Phase Filters

stationary only for finite observation time T. Further, the delay D and attenuation α may also change slowly. The estimator is therefore constrained to operate on observations of a finite duration. Having estimated the delay, an estimate of the bearing may be obtained by mapping the delay estimate according to (Nuttall, Carter and Montavon (1974))

$$\hat{\Theta} = \arccos \frac{\xi \hat{D}}{d} , \qquad (3\text{-}2)$$

where ξ is the nominal speed of sound in the non-dispersive medium and d is the sensor separation. (See pp. 93-103 of Urick (1967).) A rigorous derivation for the ML estimator of D using the mathematical model (3-1a) and (3-1b) requires that signal and noise spectra be given (that is, known). (See Hannan and Thomson (1971).) When they are unknown, a heuristic procedure of estimating these spectral characteristics is suggested. The ML estimator of delay can be realized as a pair of receiver prefilters followed by a crosscorrelator. The time argument at which the correlator achieves a maximum is the delay estimate. Qualitatively, the role of the prefilters is to weight the signal passed to the correlator according to the strength of the coherence function. This weighting turns out to be equivalent to that proposed by Hannan and Thomson (1973) and under simplifying assumptions to that proposed by MacDonald and Schultheiss (1969), but apparently differs from the results of Clay, Hinich and Shaman (1973). However, the

development presented here does not presume initially that the estimator is a GCC function. Rather, it is shown that the ML estimate may be realized by prefiltering and crosscorrelating the data $x_1(t)$ and $x_2(t)$. Indeed, other realizations of the ML processor are also possible. (See section 3C of this chapter.) For example, the data can be appropriately filtered, summed, squared and averaged in order to estimate the delay. This latter processor follows directly from the derivation presented here and is discussed fully in 3C.

To make the model (3-1) mathematically tractable, it is necessary to assume that $s_1(t)$, $n_1(t)$ and $n_2(t)$ are Gaussian. Denote the Fourier coefficients of $x_i(t)$ as

$$X_i(k) = \frac{1}{T} \int_o^T x_i(t) e^{-jkt\omega_\Delta} dt, \qquad (3\text{-}3a)$$

where

$$\omega_\Delta = \frac{2\pi}{T} \quad . \qquad (3\text{-}3b)$$

Note that the linear transformation $X_i(k)$ is Gaussian since $x_i(t)$ is Gaussian. In practice, the integral will be replaced by a discrete Fourier transform (DFT) or FFT. When the number of data points in each FFT is large (as will usually be the case) then, by a central limit theorem argument, $X_i(k)$ will tend toward being Gaussian even if the $x_i(t)$ are not Gaussian.[1] This presumption

---

[1]These observations were brought to the authors attention by Dr. G. Mohnkern of the Naval Undersea Center, San Diego, California.

is borne out by Benignus (1969b). Hence, the requirement that $s_1(t)$, $n_1(t)$ and $n_2(t)$ be Gaussian is not a strong requirement.

As the observation time $T \to \infty$,

$$T\, x_i(k) \to \tilde{X}_i(k\omega_\Delta) \quad ,$$

where $\tilde{X}_i$ is the Fourier transform of $x_i(t)$. A more complete discussion on Fourier transforms and their convergence is given in Davenport (1970), Jenkins and Watts (1968), Koopmans (1974), Otnes and Enochson (1972), Bendat and Piersol (1971) and Brillinger (1975). From MacDonald and Schultheiss (1969), it follows for T large compared with $|D|$ plus the correlation time of $R_{s_1 s_1}(\tau)$, that

$$E\left[X_1(k)X_2^*(\ell)\right] \cong \begin{cases} \frac{1}{T}\, G_{x_1 x_2}(k\omega_\Delta), & k=\ell \\ 0, & k\neq\ell \end{cases} \quad . \tag{3-4}$$

Note that $E[X_i(k)] = E[x_i(t)] = 0$, $i=1,2$.

Now let the vector

$$\underline{X}(k) = \left[X_1(k), X_2(k)\right]' \quad , \tag{3-5}$$

where $'$ denotes transpose. Then the covariance of $\underline{X}(k)$ is

$$E\left[\underline{X}(k)\underline{X}^{*'}(k)\right] = E\begin{bmatrix} X_1(k)X_1^*(k) & X_1(k)X_2^*(k) \\ X_2(k)X_1^*(k) & X_2(k)X_2^*(k) \end{bmatrix} \tag{3-6}$$

$$= \frac{1}{T} \begin{bmatrix} G_{x_1x_1}(k\omega_\Delta) & G_{x_1x_2}(k\omega_\Delta) \\ G^*_{x_1x_2}(k\omega_\Delta) & G^*_{x_2x_2}(k\omega_\Delta) \end{bmatrix} \tag{3-7}$$

$$\triangleq \frac{1}{T} \; Q_x(k\omega_\Delta) \quad , \tag{3-8}$$

where $Q_x(\omega)$ is the spectral matrix of $\left[x_1(t), x_2(t)\right]'$.

The vectors $\underline{X}(k)$, $k=-N,-N+1,\ldots,N$ are, as a consequence of (3-4), uncorrelated Gaussian (hence, independent) random variables. More explicitly, the pdf for $\underline{X} \equiv \underline{X}(-N),\underline{X}(-N+1),\ldots,\underline{X}(N)$, given attenuation α and delay D is[1]

$$p(\underline{X}|\alpha,D) = h \cdot \exp - \frac{1}{2} J_1 \quad , \tag{3-9}$$

where

$$J_1 = \sum_{k=-N}^{N} \underline{X}^{*'}(k) Q_x^{-1}(k\omega_\Delta) \underline{X}(k) T \tag{3-10}$$

and h is a function of $|Q_x(k\omega_\Delta)|$ (Van Trees (1968)). Replacing $TX_i(k)$ by $\tilde{X}_i(k\omega_\Delta)$, the Fourier transform of $x_i(t)$, it follows from (3-10) that

$$J_1 = \sum_{k=-N}^{N} \tilde{\underline{X}}^{*'}(k\omega_\Delta) Q_x^{-1}(k\omega_\Delta) \tilde{\underline{X}}(k\omega_\Delta) \frac{1}{T} \quad . \tag{3-11}$$

The ML estimate of D (see, for example, Jenkins and Watts (1968) or Van Trees (1968)) is the value of D which maximizes $p(\underline{X}|\alpha,D)$.

---

[1] More explicitly, since the density function depends on Q_x, one could write $p(\underline{X}|\alpha,Q_x)$. This notation obscures the role of the delay but clarifies the need to know (or estimate) signal and noise spectra. Further, if $\alpha=|\alpha(f)|$ then the pdf is conditioned on knowing $|\alpha(k\omega_\Delta)|$, $k=-N, -N+1,\ldots,N$.

In general, the parameter D affects both h and J_1 in (3-9). However, for uncorrelated noise in (3-1), h is independent of the delay.

For large T, (3-11) becomes

$$J_1 \cong \int_{-\infty}^{\infty} \tilde{\underline{X}}^{*'}(f) Q_x^{-1}(f) \tilde{\underline{X}}(f) df \ . \tag{3-12}$$

From (3-6)-(3-8),

$$Q_x^{-1}(f) = \frac{\begin{bmatrix} G_{x_2x_2}(f) & -G_{x_1x_2}(f) \\ -G^*_{x_1x_2}(f) & G_{x_1x_1}(f) \end{bmatrix}}{G_{x_1x_1}(f)G_{x_2x_2}(f) - |G_{x_1x_2}(f)|^2} \tag{3-13a}$$

$$= \frac{1}{[1-C_{12}(f)]} \cdot \begin{bmatrix} 1/G_{x_1x_1}(f), -G_{x_1x_2}(f) \Big/ \{G_{x_1x_1}(f) \cdot G_{x_2x_2}(f)\} \\ -G^*_{x_1x_2}(f) \Big/ \{G_{x_1x_1}(f) G_{x_2x_2}(f)\}, \ 1/G_{x_2x_2}(f) \end{bmatrix}, \tag{3-13b}$$

where $C_{12}(f) \equiv C_{x_1x_2}(f)$, which will exist provided $C_{12}(f) \neq 1$; that is, $x_1(t)$ and $x_2(t)$ cannot be obtained perfectly from one another by linear filtering (Carter and Knapp (1975)), or equivalently for the model (3-1) that observation noise is present.

When $C_{n_1n_2}(f) = G_{n_1n_2}(f) = 0$

$$G_{x_1x_1}(f) = G_{s_1s_1}(f) + G_{n_1n_1}(f) \ , \tag{3-14a}$$

$$G_{x_2x_2}(f) = \alpha^2 G_{s_1s_1}(f) + G_{n_2n_2}(f) \ , \tag{3-14b}$$

$$G_{x_1x_2}(f)=\alpha G_{s_1s_1}(f)\, e^{-j2\pi fD} \quad , \tag{3-14c}$$

$$C_{12}(f)=\alpha^2 G_{s_1s_1}(f)\Big/ G_{x_1x_1}(f)G_{x_2x_2}(f); \tag{3-14d}$$

and it follows that

$$J_1 = \int_{-\infty}^{\infty} \underline{\tilde{X}}^{*\prime}(f)Q_x^{-1}(f)\underline{\tilde{X}}(f)df=J_2+J_3 \quad , \tag{3-15a}$$

where

$$J_2= \int_{-\infty}^{\infty}\left[\frac{\left|\tilde{X}_1(f)\right|^2}{G_{x_1x_1}(f)}+\frac{\left|\tilde{X}_2(f)\right|^2}{G_{x_2x_2}(f)}\right]\cdot\frac{1}{1-C_{12}(f)}\,df \quad , \tag{3-15b}$$

$$-J_3= \int_{-\infty}^{\infty} A(f)+A^*(f)\,df, \tag{3-15c}$$

$$A(f)=\tilde{X}_1(f)\tilde{X}_2^*(f)\cdot\frac{G_{x_1x_2}^*(f)}{G_{x_1x_1}(f)G_{x_2x_2}(f)[1-C_{12}(f)]} \quad . \tag{3-15d}$$

In order to relate these results to Hannan and Thomson (1973) and others and interpret how to implement the ML estimation technique, note that for $x_1(t)$ and $x_2(t)$ real, $A^*(f)=A(-f)$. Then (3-15c) can be rewritten as

$$-J_3= \int_{-\infty}^{\infty} A(f)df+ \int_{-\infty}^{\infty} A(-f)df=2\int_{-\infty}^{\infty} A(f)df \quad . \tag{3-16}$$

Letting $T\hat{G}_{x_1x_2}(f)\triangleq\tilde{X}_1(f)\tilde{X}_2^*(f)$, (3-16) and (3-15d) can be written as

$$-J_3=2T\int_{-\infty}^{\infty}\hat{G}_{x_1x_2}(f)\frac{1}{\left|G_{x_1x_2}(f)\right|}\cdot\frac{C_{12}(f)}{[1-C_{12}(f)]}e^{j2\pi fD}\,df. \tag{3-17}$$

Notice that the ML estimator for D will minimize $J_1=J_2+J_3$, but the selection of D has no effect on J_2.

Thus, D should maximize $-J_3$. Equivalently, when $\tilde{X}_1(f)\tilde{X}_2^*(f)$ is viewed as T times the estimated cross-power spectrum, $T\hat{G}_{x_1x_2}(f)$, the ML estimator selects as the estimate of delay the value of τ at which

$$R_{y_1y_2}^{(ML)}(\tau)=\int_{-\infty}^{\infty}\hat{G}_{x_1x_2}(f)\frac{1}{|G_{x_1x_2}|}\frac{C_{12}(f)}{[1-C_{12}(f)]}e^{j2\pi f\tau}df, \qquad (3\text{-}18a)$$

where

$$\hat{G}_{x_1x_2}(f)=\frac{\tilde{X}_1(f)\tilde{X}_2^*(f)}{T} \qquad (3\text{-}18b)$$

achieves a peak. That is, the ML estimator selects as the estimate of delay the value of τ at which the GCC

$$\hat{R}_{x_1x_2}^{g}(\tau) = \int_{-\infty}^{\infty}\hat{G}_{x_1x_2}(f)W_g(f)e^{j2\pi f\tau}df \qquad (3\text{-}19)$$

achieves a peak, where $W_g(f)=H_1(f)H_2^*(f)$ is an appropriately selected weighting function (Knapp and Carter (1976)) The ML estimator is equivalent to one proposed by Hannan and Thomson (1973). The ML estimator can be achieved as depicted in Figure 3-3 by shaping $x_1(t)$ with filter $H_1(f)$ and $x_2(t)$ with filter $H_2(f)$ then crosscorrelating the filter outputs and observing what value of delay achieves a maximum. The estimator can also be achieved in other forms. (See section C of this Chapter.) The weighting proposed by Hannan and Thomson (1973) is

$$W_{ML}(f) = \frac{1}{|G_{x_1x_2}(f)|}\cdot\frac{C_{12}(f)}{[1 - C_{12}(f)]}, \qquad (3\text{-}20)$$

where (as required for Q_x^{-1} to exist) $C_{12}(f) \neq 1$. Such

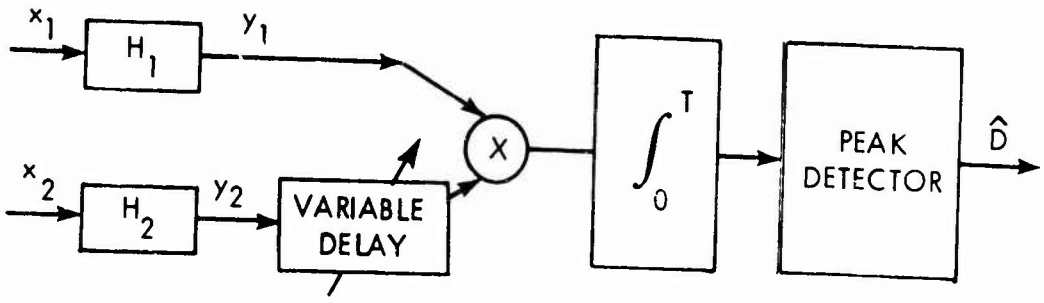

Figure 3-3 Received Waveforms Filtered, Delayed, Multiplied, and Integrated for a Variety of Delays until Peak Output is Obtained

weighting achieves the ML estimator. When $|G_{x_1x_2}(f)|$ and $C_{12}(f)$ are known, this is exactly the proper weighting. An important consideration in estimator design is the available amount of a priori knowledge of the signal and noise statistics. In many problems, this information is negligible. For example, in passive detection, unlike the usual communications problem, the source spectrum is unknown or only known approximately. When the terms in (3-20) are unknown, they can be estimated via techniques of Carter, Knapp and Nuttall (1973a), which are summarized in appendix A and programmed in appendix C. Substituting estimated weighting for true weighting is entirely a heuristic procedure whereby the ML estimator can approximately be achieved in practice. Such techniques have been referred to as approximate ML (AML) techniques by Box and Jenkins (1970) since they are not, truly speaking, ML estimation techniques.

Since the estimation of delay may, in practice, be governed by an AML rather than an ML technique, we should <u>not</u> expect that more complex models will yield to ML techniques without similar heuristic approximation. Rather, the estimation of D with moving sources, for example, will also require AML techniques and may be even more prone to varying interpretations.

3B. Variance of General Time Delay Estimator

The crosscorrelation form of the processor is useful in ascertaining the statistical characteristics of the delay estimate. For each of several different trials a different estimate of delay might be obtained. For example, when the true delay is about 5.0 seconds, six typical trials are sketched in Figure 3-4. One actual example case is given in appendix D. In ascending orders, values of $\hat{D}$ are 4.5, 4.9, 5.0, 5.1, 5.3 and 5.7. For trial number 5, depicted on the Figure 3-4, an estimate 4.9 is obtained. However, there appear to be many ambiguous peaks in trial 5; indeed if the noise had been slightly different, there could have been a different delay estimate, such as: 4.1, 5.7, or 6.5; such an error would increase the variation of the time delay estimate. The derivation of variance of $\hat{D}$, which follows, does not account for errors due to ambiguous peaks. It presumes that the estimated delay is in the neighborhood of the correct delay and not on a secondary peak.

A lower bound on the variance for any delay estimator (which is not necessarily attainable) is given by the Cramér-Rao bound

$$\sigma^2_{\hat{D}} \geq \frac{-1}{E\left\{\frac{\partial^2 \ln p(x|\alpha,\tau)}{\partial \tau^2}\right\}}\Bigg|_{\tau=D} \quad . \tag{3-21}$$

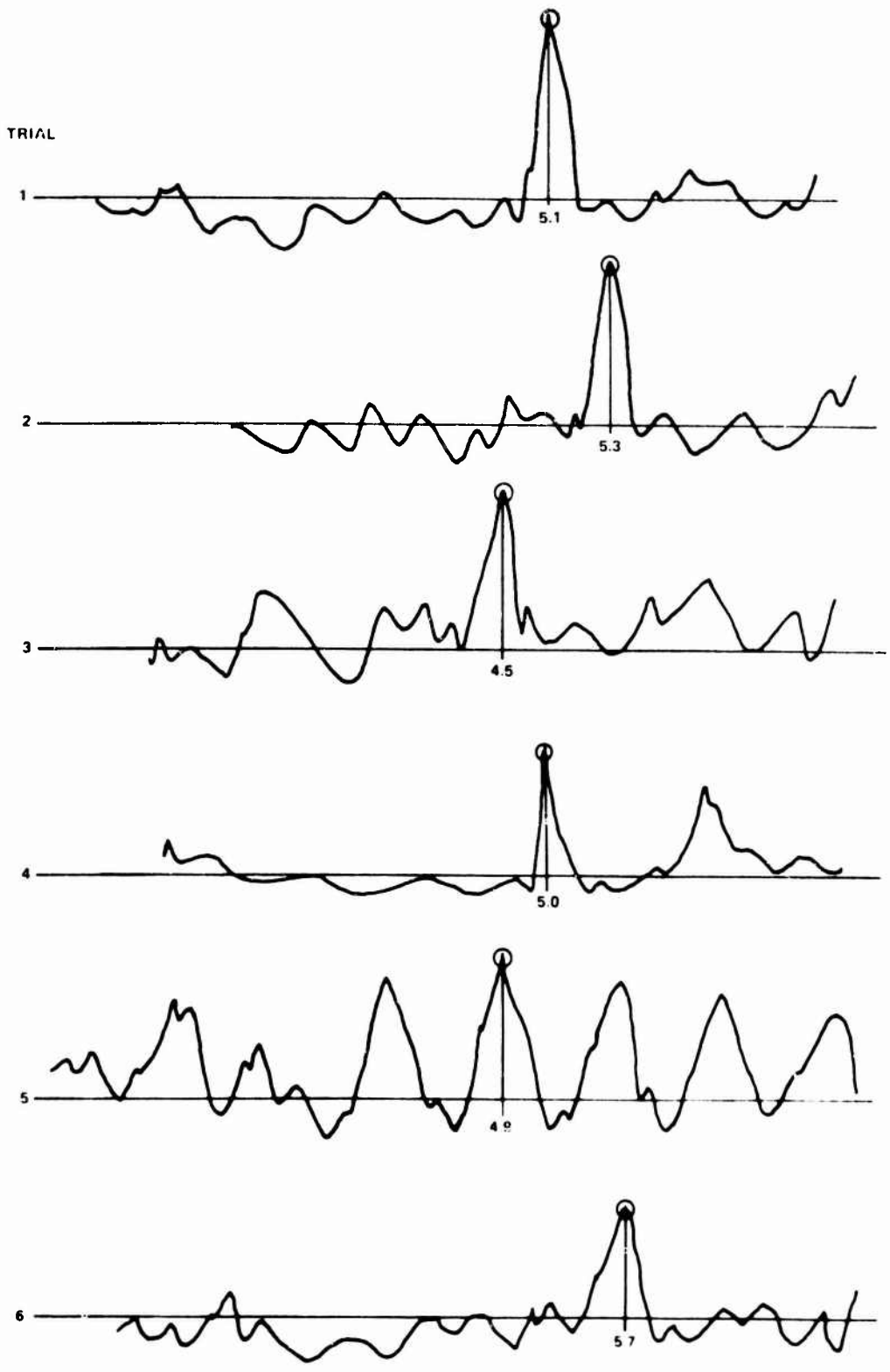

Figure 3-4 Six Hypothetical Correlator Outputs

Cramér-Rao bounds are discussed in Van Trees (1968) and Sage and Melsa (1971). The only part of the log pdf that depends on τ, the hypothesized delay, is J_3 of (3-17). That is,

$$E\left\{\frac{\partial^2}{\partial\tau^2}\ \ln p(\underline{x}|\alpha,\tau)\right\} = \frac{\partial^2}{\partial\tau^2} E(\tfrac{-1}{2}J_3) \ . \qquad (3\text{-}22)$$

If $G_{x_1x_2}(f)=\left|G_{x_1x_2}(f)\right|e^{-j2\pi fD}$, then since $E\left[\hat{G}_{x_1x_2}(f)\right]=G_{x_1x_2}(f)$, it follows that

$$E(\tfrac{-1}{2}J_3)=T\int_{-\infty}^{\infty} e^{j2\pi f(\tau-D)}\ \frac{C_{12}(f)}{[1\ -\ C_{12}(f)]}\ df \ . \qquad (3\text{-}23)$$

Hence, the minimum obtainable variance for delay estimation is (Carter and Knapp (1976a))

$$\text{Minimum Var}(\hat{D})= \left[T\int_{-\infty}^{\infty} (2\pi f)^2 \frac{C_{12}(f)}{[1\ -\ C_{12}(f)]}\ df\right]^{-1} . \qquad (3\text{-}24)$$

For the GCC processor with any weighting $W_g(f)=H_1(f)H_2^*(f)$ we will derive an expression for the local variation of the delay estimator and show that the ML weighting, (3-20), indeed achieves (3-24). The determination of the variance of delay estimates closely parallels a clever method of MacDonald and Schultheiss (1969). Equivalent to the Var $\hat{D}$ =Var $\tau\ \big|_{\tau=D}$ (shown in Figure 3-5) is the left to right variation of the zero crossing of the derivative of the GCC function output

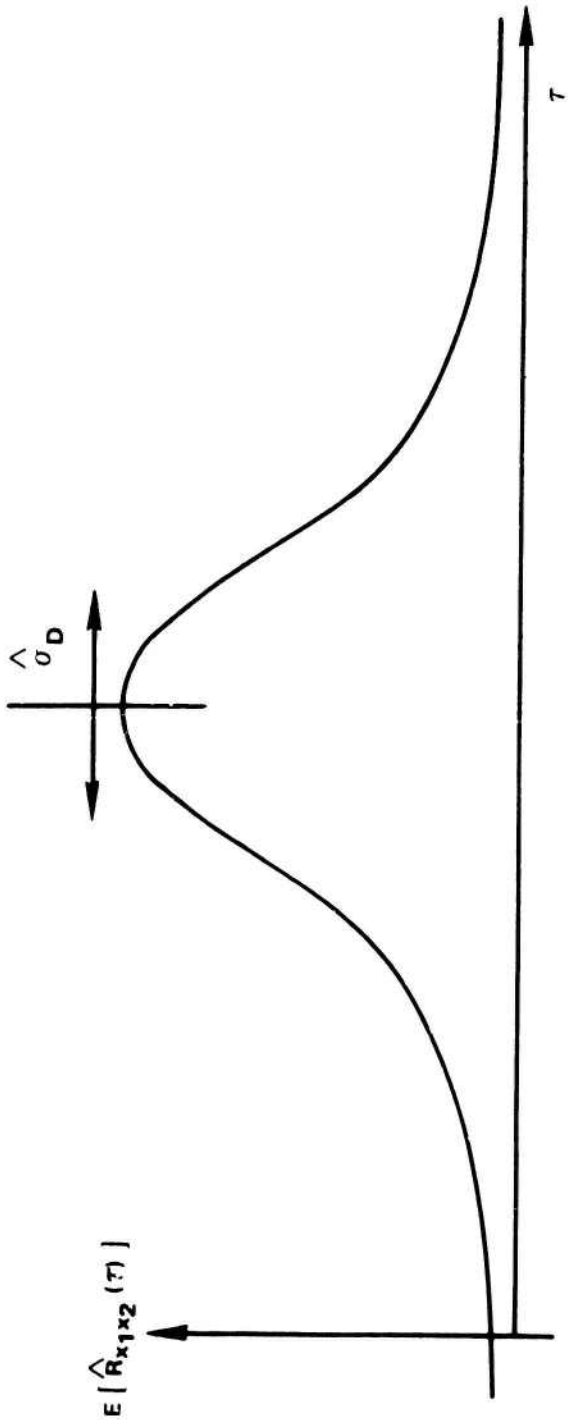

Figure 3-5 Variation of Delay Estimator

with respect to τ (shown in Figure 3-6). Typical mean output of the derivative of the correlator output, z, is plotted in Figure 3-5 together with similar curves σ_z above and below the mean. For σ_z small, so that curves are approximately linear between $D-\sigma_{\hat{D}}$ and $D+\sigma_{\hat{D}}$, the magnitude of the expected value of the slope of the output at the true value of delay is given by

$$\left|\frac{\partial}{\partial\tau}E[z]\right| = \left|\frac{\partial^2}{\partial\tau^2}\, E\ \hat{R}^{g}_{x_1x_2}(\tau)\ \right|_{\tau=D}\Bigg| = \left|\frac{\sigma_z}{\sigma_\tau}\right|_{\tau=D}, \qquad (3\text{-}25)$$

where σ denotes standard deviation. Again using $E\left[\hat{G}_{x_1x_2}(f)\right] = \frac{1}{T}\, E\left[\tilde{X}_1(f)\tilde{X}_2^*(f)\right] = G_{x_1x_2}(f)$, it follows with $G_{x_1x_2}(f) = \left|G_{x_1x_2}(f)\right| e^{-j2\pi D}$ that

$$\left|\frac{\partial^2}{\partial\tau^2}\, E\left[\hat{R}^{g}_{x_1x_2}(\tau)\right]\right|_{\tau=D}\Bigg| = T\int_{-\infty}^{\infty}(2\pi f)^2\left|G_{x_1x_2}(f)\right| W_g(f)\,df. \qquad (3\text{-}26)$$

In order to solve (3-25) for $\sigma_\tau \equiv \sigma_{\hat{D}}$ it is also necessary to solve for σ_z in Figure 3-6. The fundamental problem is to find the variance of the random variable z given by

$$z = \int_0^T y_1(t)y_2(t)\,dt\ . \qquad (3\text{-}27a)$$

(For our particular problem we will later assume that $y_1(t)$ is the output of a filter excited by $x_1(t)$ and $y_2(t)$ is the output of a filter excited by $x_2(t)$.) The variance of z is given by

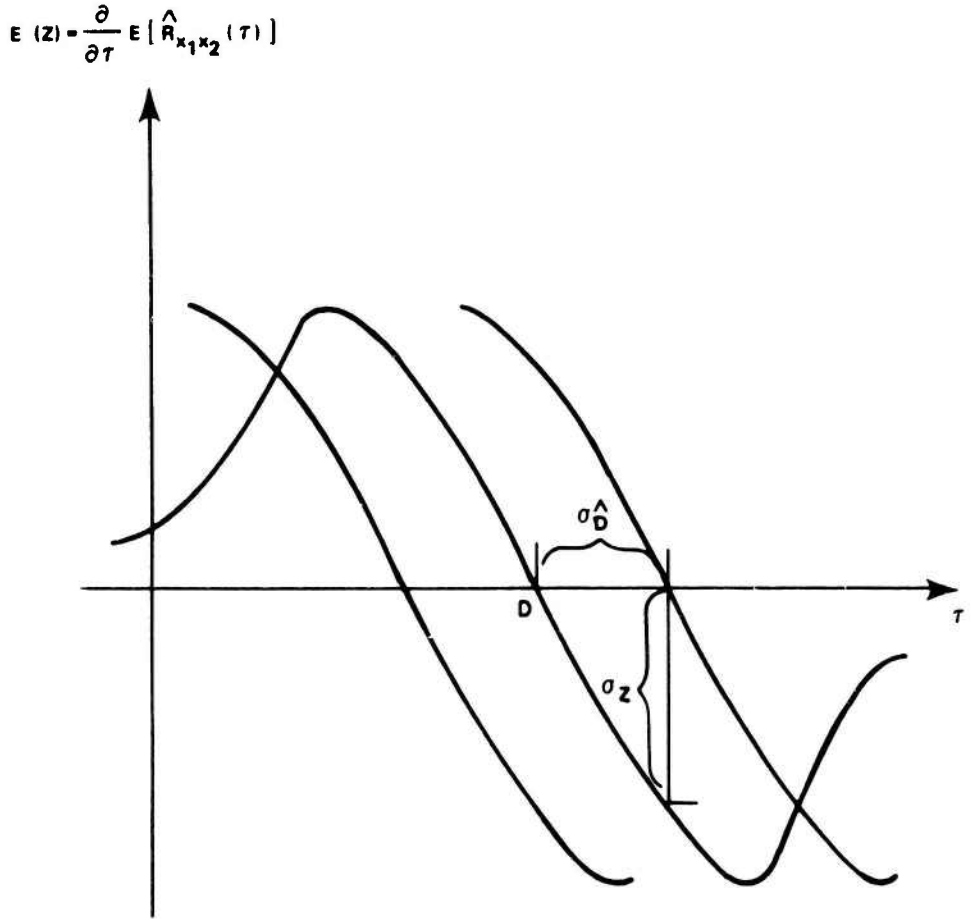

Figure 3-6 Derivative of Typical Output of Generalized Correlator

$$\sigma_z^2 = E[z^2] - E^2[z], \tag{3-27b}$$

where

$$E[z] = E\left[\int_0^T y_1(t)y_2(t)dt\right] \tag{3-27c}$$

$$= \int_0^T E[y_1(t)y_2(t)]\,dt \tag{3-27d}$$

$$= T\,R_{y_1y_2}(0) \tag{3-27e}$$

and

$$E[z^2] = \int_0^T\int_0^T E[y_1(t_1)y_2(t_1)y_1(t_2)y_2(t_2)]\,dt_1dt_2. \tag{3-27f}$$

Evaluation of the fourth moment in (3-27f) can be achieved under Gaussian assumptions. In particular, if $y_1(t)$ and $y_2(t)$ are jointly Gaussian (and stationary), then

$$E[z^2] = \int_0^T\int_0^T\Big[R^2_{y_1y_2}(0)+R^2_{y_1y_1}(t_1-t_2)R_{y_2y_2}(t_1-t_2)$$

$$+ R_{y_1y_2}(t_1-t_2)R_{y_2y_1}(t_1-t_2)\Big]\,dt_1dt_2\,. \tag{3-27g}$$

Letting $\tau=t_1-t_2$ and using (3-27b) and (3-27e), (3-27g) becomes

$$\sigma_z^2 = \int_{-\infty}^{\infty}\int_{-\infty}^{\infty}\Big[R_{y_1y_1}(\tau)R_{y_2y_2}(\tau)+R_{y_1y_2}(\tau)R_{y_2y_1}(\tau)\Big]\cdot$$

$$\Psi(\tau+t_2)\Psi(t_2)d\tau dt_2\,, \tag{3-27h}$$

where

$$\Psi(t) = \begin{cases}1\,, & t\in(0,T)\\ 0\,, & \text{elsewhere}\,.\end{cases}$$

Integrating (3-27h) with respect to t_2 and manipulating yields

$$\sigma_z^2 = T\int_{-T}^{T}\Big[R_{y_1y_1}(\tau)R_{y_2y_2}(\tau)+R_{y_1y_2}(\tau)R_{y_2y_2}(\tau)\Big]\left(1-\frac{\tau}{T}\right)d\tau\,. \tag{3-27i}$$

For large T (3-27i)

$$\sigma_z^2 \cong T\int_{-\infty}^{\infty} [R_{y_1y_1}(\tau)R_{y_2y_2}(\tau)+R_{y_1y_2}(\tau)R_{y_1y_2}(-\tau)]d\tau . \qquad (3\text{-}27j)$$

By Parseval's Theorem

$$\sigma_z^2 \cong T\int_{-\infty}^{\infty} [G_{y_1y_1}(f)G_{y_2y_2}(f)+G^2_{y_1y_2}(f)]df . \qquad (3\text{-}27k)$$

If $y_1(t)$ is the output of a filter $H_1(f)$ cascaded with a differentiator and $y_2(t)$ is the output of a filter $H_2(f)$ cascaded with a variable delay, then

$$G_{y_1y_1}(f) = |H_1(f)|^2 (2\pi f)^2 G_{x_1x_1}(f) \qquad (3\text{-}27l)$$

$$G_{y_2y_2}(f) = |H_2(f)|^2 G_{x_2x_2}(f) \qquad (3\text{-}27m)$$

$$G_{y_1y_2}(f) = H_1(f)H_2^*(f)e^{j2\pi f\tau} G_{x_1x_2}(f) . \qquad (3\text{-}27n)$$

For $\tau=D$ it follows, from (3-27k) - (3-27n), since $W_g(f)=H_1(f)H_2^*(f)$, that

$$\sigma_z^2\Big|_{\tau=D} = T\int_{-\infty}^{\infty} \left|W_g(f)\right|^2 (2\pi f)^2 G_{x_1x_1}(f)G_{x_2x_2}(f)[1-C_{12}(f)]df . \qquad (3\text{-}27o)$$

Combining (3-25) through (3-27o) yields

$$\sigma_{\hat{D}}=\sigma_\tau\Big|_{\tau=D} = \frac{\{\int_{-\infty}^{\infty} \left|W_g(f)\right|^2 (2\pi f)^2 G_{x_1x_1}(f)G_{x_2x_2}(f)[1-C_{12}(f)]\}^{\frac{1}{2}}}{(T)^{\frac{1}{2}}\int_{-\infty}^{\infty} (2\pi f)^2 \left|G_{x_1x_2}(f)\right| W_g(f)\, df} \qquad (3\text{-}28)$$

which is valid for any $W_g(f)$. By substituting the appropriate weighting function into (3-28) the standard deviation of time delay estimates from each processor

can be analytically evaluated.

Parenthetically, we note that the results (3-28) with a particular weighting (3-20) can be related to (20) of MacDonald and Schultheiss (1969) as follows. Define the bearing to an acoustic source, similar to (3-2), as

$$\theta = \arccos\left(\frac{\xi D}{d}\right) , \tag{3-29}$$

where ξ is the (nominal) speed of sound in the nondispersive medium. Consider the case where the estimated D equals the true delay D plus a perturbation η. By a Taylor series expansion it follows that

$$\arccos\left[\frac{\xi}{d}(D+\eta)\right] \cong \arccos\left[\frac{\xi}{d}D\right] + \frac{d}{d\hat{D}} \arccos\left(\frac{\xi\hat{D}}{d}\right)\Bigg|_{\hat{D}=D} (\hat{D}-D) . \tag{3-30}$$

Thus the bearing error

$$e_b \triangleq \arccos\left[\frac{\xi}{d}(D+\eta)\right] - \arccos\left(\frac{\xi}{d}D\right) \tag{3-31a}$$

$$\cong \frac{-\xi}{d\sin\theta}(\hat{D}-D) , \tag{3-31b}$$

and

$$\left[E\left(e_b^2(t)\right)\right]^{\frac{1}{2}} \cong \frac{\xi}{d\sin\theta}\left[\text{Var } \hat{D}\right]^{\frac{1}{2}} . \tag{3-32}$$

The term $d\sin\theta$ can be viewed as the effective array length (sensor separation) physically steered at the source. Assuming equal noise spectra, combining (3-32) with (3-28) and (3-20), and introducing a change of variables yields an expression which agrees with (20) of MacDonald and Schultheiss (1969) when θ is interpreted

as source (not wavefront) angle. Combining (3-28) and (3-32) suggests that in order to reduce to variance of the bearing estimate the observation period and the sensor separation should be made as large as possible. (In practice, there will undoubtedly be limitations on both sensor separation and observation time.) Further, since (3-32) depends on the effective array length physically steered toward the source, this suggests the desirability of sensor mobility to maximize the term $d\sin\theta$.

It has been shown that the variance of the time delay estimate in the neighborhood of the true delay, for general weighting function $W_g(f)$ is given by

$$\underset{\text{Var}}{g}\,\hat{D} = \frac{\int_{-\infty}^{\infty} |W_g(f)|^2 (2\pi f)^2 G_{x_1x_1}(f) G_{x_2x_2}(f) \left[1-C_{12}(f)\right] df}{T\left[\int_{-\infty}^{\infty} (2\pi f)^2 \left|G_{x_1x_2}(f)\right| W_g(f)\, df\right]^2} \quad (3\text{-}33a)$$

which for real processes may also be written

$$\underset{\text{Var}}{g}\,\hat{D} = \frac{\int_{o}^{\infty} |W_g(f)|^2 G_{x_1x_1}(f) G_{x_2x_2}(f) \left[1-C_{12}(f)\right] f^2 df}{8\pi^2 T \left[\int_{o}^{\infty} \left|G_{x_1x_2}(f)\right| W_g(f) f^2 df\right]^2} . \quad (3\text{-}33b)$$

Notice that a scale factor change in $W_g(f)$ does <u>not</u> change the variance of the delay estimator.

The variance of the ML processor is

$$\text{Var}^{ML}\,\hat{D} = \left\{2T \int_{o}^{\infty} (2\pi f)^2 C_{12}(f) / \left[1-C_{12}(f)\right] df\right\}^{-1} , \quad (3\text{-}34)$$

which is the Cramér-Rao lower bound (3-24). It should be reemphasized that (3-33) and (3-34) evaluate the local variation of the time delay estimate and thus do not account for ambiguous peaks which may arise when the averaging time is not large enough for the given signal and noise characteristics. Indeed, when T is not sufficiently large, local variation may be a poor indicator of system performance and the envelope of the ambiguous peaks must be considered[1] (p. 40 of MacDonald and Schultheiss (1969) and p. 41 of Hamon and Hannan (1974)). Further, (3-33) and (3-34) predict system performance when signal and noise spectral characteristics are known. For sufficiently large T, these spectra can be estimated accurately. However, in general, (3-33) and (3-34) must be modified to account for estimation errors; alternatively, system performance can be evaluated by computer simulation. Empirical verification of expressions for variance has not been undertaken by simulation, because to do so without special purpose correlator hardware would be computationally prohibitive. For example, for a given $G_{s_1 s_1}(f)$, $G_{n_1 n_1}(f)$, $G_{n_2 n_2}(f)$, α, and averaging time T, an estimated GCC function can be computed, from which only one number (the delay

---

[1]These observations were brought to the author's attention by C. Stradling and R. Trueblood of the Naval Undersea Center, San Diego, California.

estimate) can be extracted. To empirically evaluate the statistics of the delay estimate (which would be valid only for these particular signal and noise spectra) many such trials would need to be conducted. We have conducted one such trial (with T large) and verified that useful delay estimates can be obtained by inserting estimates $\left|\hat{G}_{x_1x_2}(f)\right|$ and $\hat{C}_{12}(f)$ in place of the true values in (3-20). This might have been expected since the estimated optimum weighting will converge to the true weighting as $T\to\infty$. (The statistics of the MSC estimates are given in appendix B.) In practice, T may be limited by the stationarity properties of the data, and (3-34) may be an overly optimistic prediction of system performance when signal and noise spectra are unknown.

With these qualifications in mind, consider the following example of computing the variance of the ML time delay estimate. Let

$$C_{12}(f) = \begin{cases} C, & f\epsilon(0,B) \\ 0, & \text{otherwise} \end{cases} .$$

Then

$$\text{Var}^{ML}\,\hat{D} = \frac{1}{8\pi^2 T\,\frac{B^3}{3}\left[\frac{C}{1-C}\right]} . \qquad (3\text{-}35)$$

The strong dependence of the estimator variation to the coherence is illustrated in a plot of $\frac{1-C}{C}$ versus C in Figure 3-7. Note since

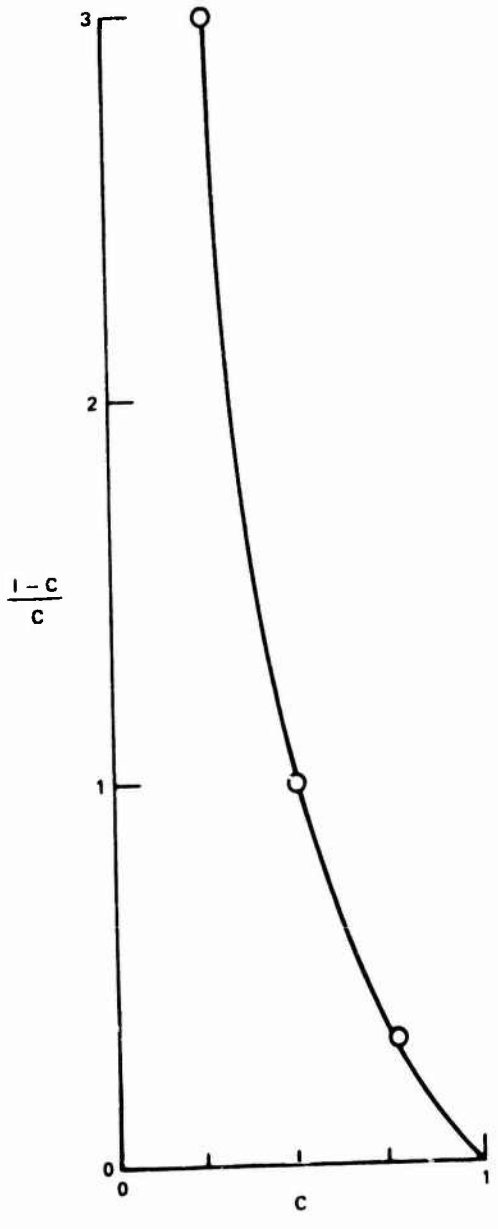

Figure 3-7 Variance of Delay Estimate as a Function of Coherence for Fixed B and T

$$\frac{C}{1-C} = C\,[\,1+C+C^2+\ldots\,]\ , \tag{3-36}$$

that for $C<<1$, (3-36) is

$$\frac{C}{1-C} \cong C\ . \tag{3-37}$$

But for $C=1-\Delta$, where $\Delta<<1$, then

$$\frac{C}{1-C} = \frac{1-\Delta}{\Delta} = \frac{1}{\Delta} - 1 \cong \frac{1}{\Delta}\ . \tag{3-38}$$

An approximate comparison of C=0.01 with C=0.99 shows the variance changed not by a factor of 100 to 1 but 10,000 to 1. The implication is that weakly coherent signals do not contribute much to reducing the variance of the delay estimate. That is not entirely so but is roughly correct. For example, high frequency, low coherent power may be important. A more complete discussion of the variance of several proposed time delay estimators is given in Chapter 4. Prior to Chapter 4, we will discuss other realizations of the ML delay estimator.

3C. Other Realizations of the ML Estimator

This section of Chapter 3 will present four methods for implementing the ML estimator for delay. One (and only) of the methods, the one considered to be most promising, has been programmed. (See appendix C.) The program presumes that signal and noise waveforms are real and that their statistics are unknown; hence the program uses appropriate estimates in lieu of known

values, when forming the weighting function.

The first realization which comes to mind is a bank of allowable delays as depicted in Figure 3-8. Each data waveform $x_1(t)$ and $x_2(t)$ is filtered by $H_1(f)$ and $H_2(f)$, respectively. The output of $H_2(f)$ is delayed for several reasonable values of delay depending on the resolution desired, a priori knowledge and processing cost allowed. Each delayed output is multiplied with the output of $H_1(f)$. After integration for T seconds, the delay that yields the maximum award is the estimate of delay.

The second method is to realize that the bank of delays in Figure 3-8 corresponds to a particular method for computing the GCC function. Indeed we need not be particular about the details of how the GCC function is estimated so long as it is estimated "accurately." The second method uses the overlapped FFT method presented by Carter, Knapp, and Nuttall (1973a) to compute the estimated cross spectrum and MSC. The estimated cross spectrum is appropriately weighted and inverse transformed via an FFT to obtain the estimated GCC function. The delay where the GCC peaks is the estimate of delay. One advantage to methods 1 and 2 is that by computing the crosscorrelation for a large range of delays the presence of more than one delay (acoustic source) can be observed. There are other advantages, too; in the GCC method uncorrelated cross

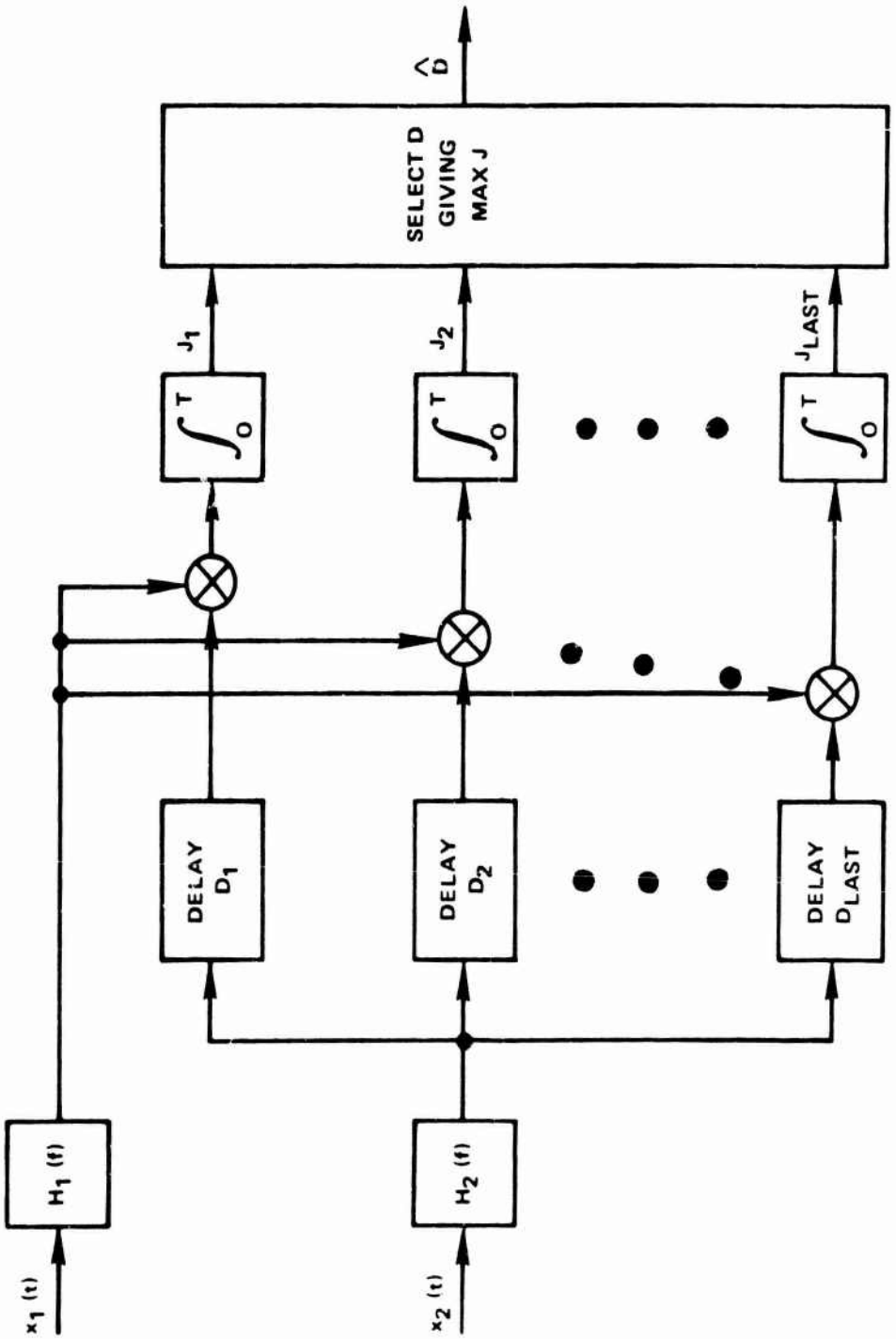

Figure 3-8 Block Diagram of Open Loop ML Time Delay Estimator Realization

terms vanish and there is no unknown residual bias to account for when establishing thresholds (other than the type discussed in appendix B).

If we desire to use a closed loop control scheme to automatically adjust the delay estimate $\hat{D}$, we can instrument the estimator with a derivative in one channel much like our discussion of the variance of the estimator.[1] When we are in the neighborhood of the correct delay, the output in Figure 3-9 should be approximately zero. Any difference from zero (that is, error) is fed back, perhaps smoothed and scaled, and used to adjust the delay estimate in order to drive the system output to zero. For estimating more than one delay (acoustic source) with this realization, more than one variable delay is required. It should be noted as pointed out by Kochenburger (1972) that differentiation is a "noisy" process which should be avoided. However, the filter $H_1(f)$ and the integrator in Figure 3-9 may reduce the adverse effect of this realization.

The final realization to be discussed is the method of Carter and Knapp (1976a). In this method we re-examine our derivation in section 3A. In

---

[1]This idea was brought to the author's attention by J. P. Ianniello of the Naval Underwater Systems Center, New London, Connecticut.

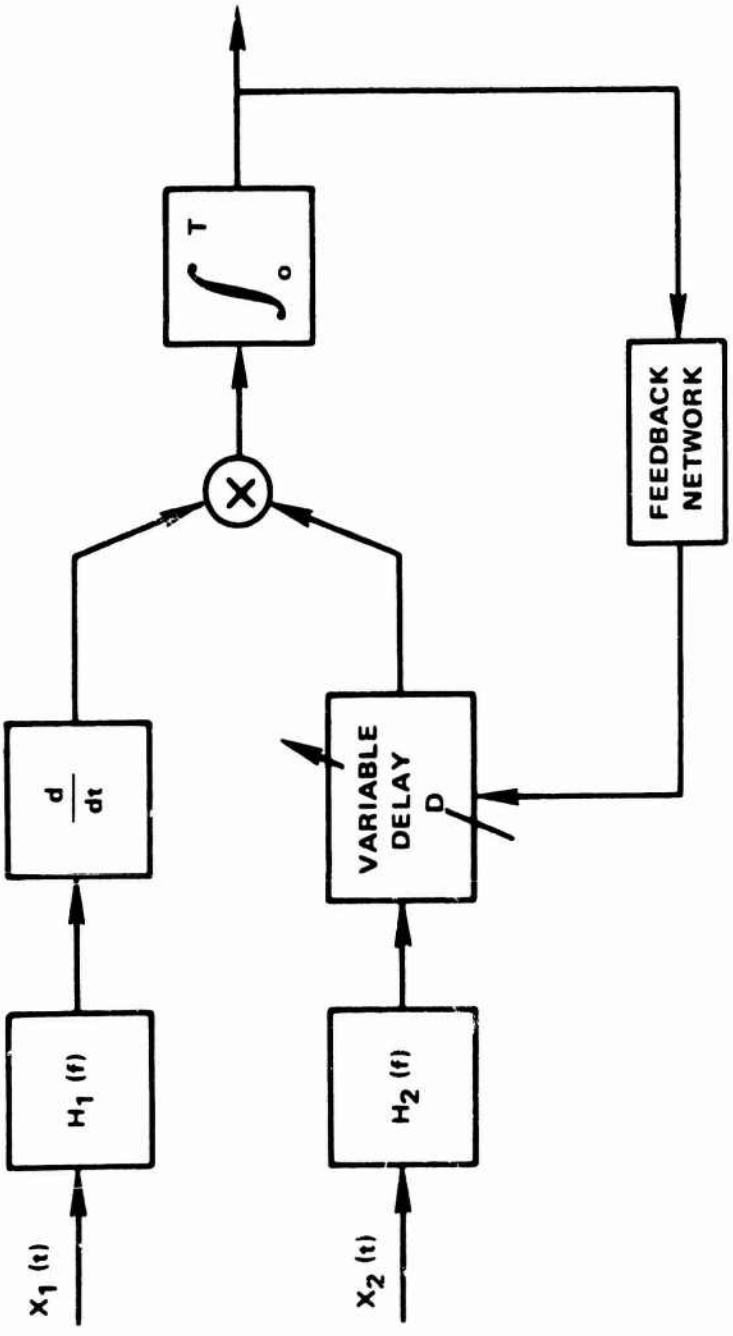

Figure 3-9 Block Diagram of ML Time Delay Estimator with Feedback

particular, the spectral density matrix (3-6), for models like (3-1) which give rise to spectral densities given by (3-14), can be expressed (suppressing the f dependence) as

$$Q_x = Q_n + G_{ss} V^* V' , \tag{3-39}$$

where the steering vector

$$V' = [1, \alpha e^{-j2\pi fD}] \tag{3-40}$$

and, for uncorrelated noises,

$$Q_n = \begin{bmatrix} G_{n_1 n_1} & 0 \\ 0 & G_{n_2 n_2} \end{bmatrix}, \tag{3-41}$$

and (for any given f) G_{ss} is a scalar. The complete award function to be maximized (3-15) requires knowledge of Q_x^{-1}. The inverse of (3-39) is given by Knapp (1966) as

$$Q_x^{-1} = Q_n^{-1} - \frac{G_{ss} Q_n^{-1} V^* V' Q_n^{-1}}{1 + G_{ss} V' Q_n^{-1} V^*} . \tag{3-42}$$

For uncorrelated noises Q_n^{-1} does not depend on D; therefore, the total award is maximized by maximizing

$$J_D = -\frac{1}{2} \int_{-\infty}^{\infty} \tilde{X}^* \tilde{H}^* \tilde{H}' \tilde{X} \, df, \tag{3-43}$$

where the 1x2 vector filter

$$\tilde{H} = [\tilde{H}_1, \tilde{H}_2]' = \frac{Q_n^{-1} V \sqrt{G_{ss}}}{\left[1 + G_{ss} V' Q_n^{-1} V^*\right]^{\frac{1}{2}}} . \tag{3-44}$$

By Parseval's Theorem, (3-43) can be implemented by filtering $x_1(t)$ with filter $\tilde{H}_1(f)$ and filtering $x_2(t)$ with filter $\tilde{H}_2(f)$, then summing, squaring, and averaging.

If we separate from $\tilde{H}_2(f)$ that portion dealing with the hypothesized delay we can realize the delay estimator as shown in Figure 3-10. Moreover, note that

$$Q_n^{-1} V \sqrt{G_{ss}} = \begin{bmatrix} \frac{1}{G_{n_1 n_1}} & 0 \\ 0 & \frac{1}{G_{n_2 n_2}} \end{bmatrix} \begin{bmatrix} 1 \\ \alpha e^{-j2\pi fD} \end{bmatrix} \sqrt{G_{ss}} \qquad (3\text{-}45a)$$

$$= \begin{bmatrix} \frac{\sqrt{G_{ss}}}{G_{n_1 n_1}} \\ \frac{\alpha \sqrt{G_{ss}}\, e^{-j2\pi fD}}{G_{n_2 n_2}} \end{bmatrix}_{2x1} \qquad (3\text{-}45b)$$

Further,

$$1+G_{ss} V' Q_n^{-1} V^* = 1+G_{ss} \left[1, \alpha e^{-j2\pi fD} \right] \begin{bmatrix} \frac{1}{G_{n_1 n_1}} & 0 \\ 0 & \frac{1}{G_{n_2 n_2}} \end{bmatrix} \begin{bmatrix} 1 \\ \alpha e^{j2\pi fD} \end{bmatrix} \qquad (3\text{-}46a)$$

$$= 1+G_{ss} \left[1, \alpha e^{-j2\pi fD} \right] \begin{bmatrix} \frac{1}{G_{n_1 n_1}} \\ \frac{\alpha e^{j2\pi fD}}{G_{n_2 n_2}} \end{bmatrix} \qquad (3\text{-}46b)$$

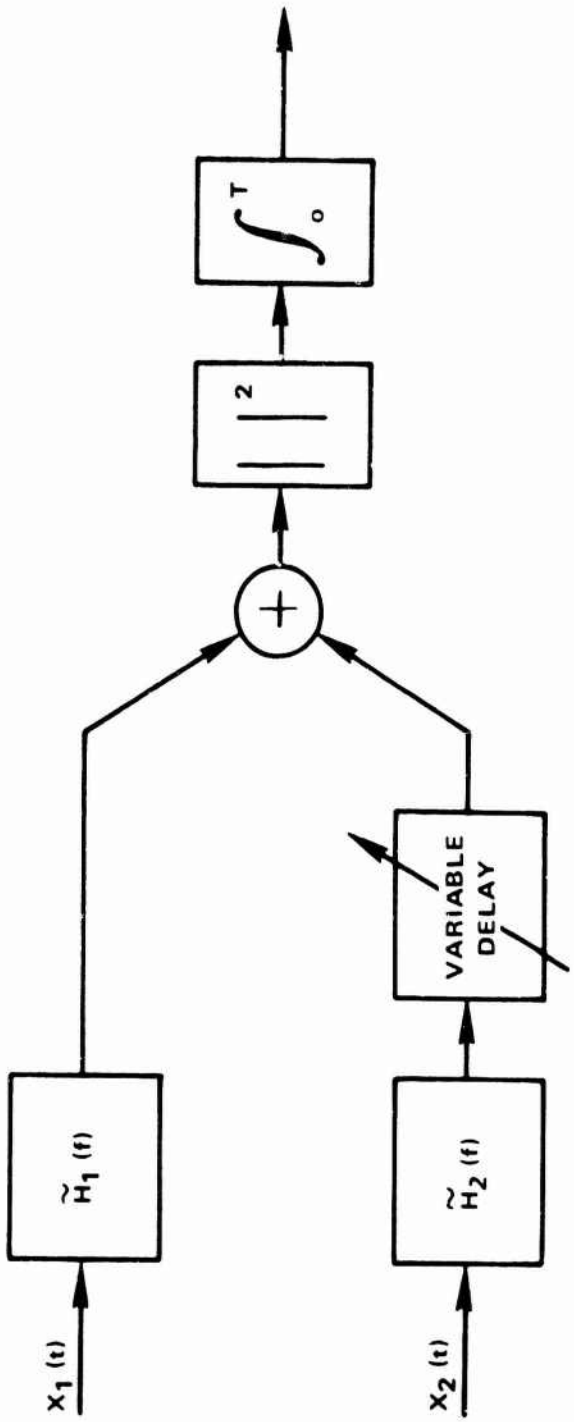

Figure 3-10 Filter and Sum Realization of ML Time Delay Estimator

$$= 1 + \frac{G_{ss}}{G_{n_1 n_1}} + \frac{\alpha^2 G_{ss}}{G_{n_2 n_2}} \quad . \tag{3-46c}$$

Thus, the estimator can be realized as shown in Figure 3-11. For low SNR, that is, when

$$\frac{G_{ss}}{G_{n_1 n_1}(f)} << 1 \text{ and } \frac{\alpha^2 G_{ss}(f)}{G_{n_2 n_2}(f)} << 1 \ ,$$

$$1 + G_{ss} V' Q_n^{-1} V^* \cong 1 \tag{3-47}$$

then the filter following the summation in Figure 3-11 is approximately a unity-gain zero-phase all-pass network. Note in Figure 3-11 that the form of the filters at each sensor depends on the signal and noise spectrum. In particular the estimation of D presented here requires filtering in exactly the fashion as the detection of a signal arrival presented by Knapp (1966). These low SNR filter forms are commonly referred to as Eckart filters after early work done in the detection area by Eckart (1952).

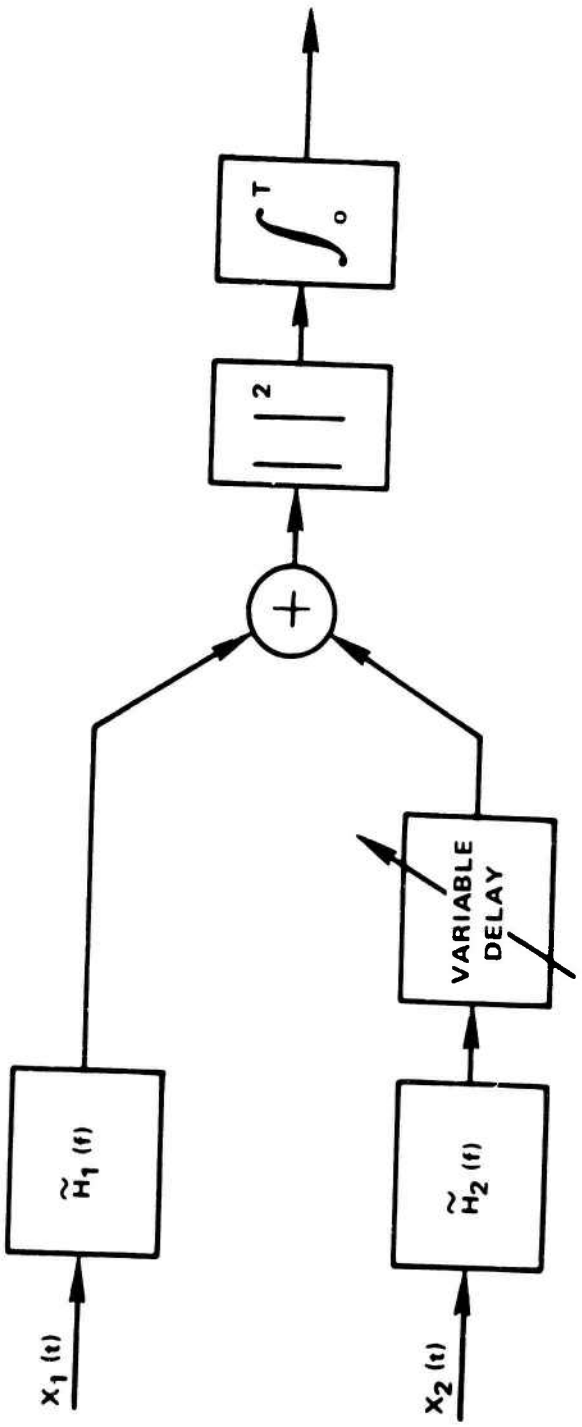

Figure 3-10 Filter and Sum Realization of ML Time Delay Estimator

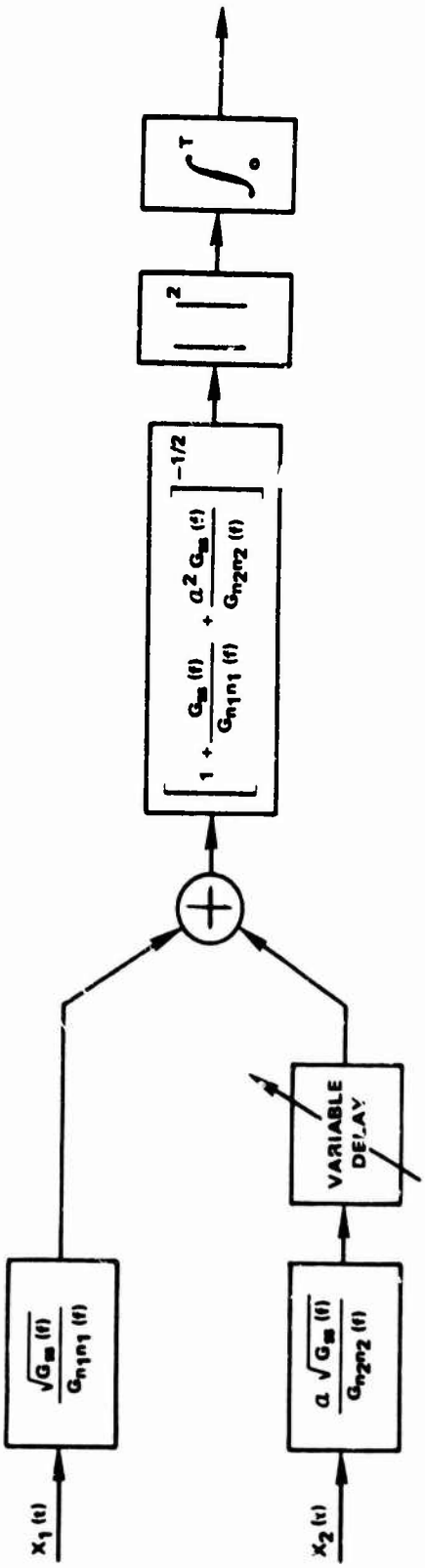

Figure 3-11 Explicit Filter and Sum Realization of ML Time Delay Estimator

CHAPTER 4

COMPARISON OF THE ML ESTIMATOR TO OTHER PROPOSED SUBOPTIMUM PROCESSORS

The objective of Chapter 4 is to compare the ML time delay estimator with several other processors that have been proposed. From Chapter 3, we know that the ML processor will have the minimum local variation. Also, the previously derived expressions for the local variation of any correlation processor can be used to analytically compare other intuitively appealing correlation processors. Additionally, the effect of erroneously identifying the signal spectrum will be investigated, since that will cause the selection of an erroneous weighting function.

The first section of this chapter presents the motivation for the use of crosscorrelation processors. The second section compares several such processors, and the third section considers the interrelationships of these various processors.

4A. Motivation for Crosscorrelation Processors

For the model

$$x_1(t) = s_1(t)+n_1(t) \tag{4-1a}$$

$$x_2(t) = \alpha s_1(t+D)+n_2(t) \tag{4-1b}$$

one common method of estimating the time delay D is to

compute the crosscorrelation function

$$R_{x_1x_2}(\tau)=E[x_1(t)x_2^*(t-\tau)] , \tag{4-2}$$

where E denotes expectation. The argument τ that maximizes (4-2) provides an estimate of delay. For models of the form of (4-1), the crosscorrelation of $x_1(t)$ and $x_2(t)$ is

$$R_{x_1x_2}(\tau)=\alpha R_{s_1s_1}(\tau-D)+R_{n_1n_2}(\tau) . \tag{4-3}$$

The Fourier transform of (4-3) gives the cross-power spectrum

$$G_{x_1x_2}(f)=\alpha G_{s_1s_1}(f)e^{-j2\pi fD}+G_{n_1n_2}(f) . \tag{4-4}$$

If $n_1(t)$ and $n_2(t)$ are uncorrelated ($G_{n_1n_2}(f)=0$), the cross-power spectrum between $x_1(t)$ and $x_2(t)$ is a scaled signal power spectrum times a complex exponential. Since multiplication in one domain corresponds to convolution in the transformed domain (see, for example, Oppenheim and Schafer (1975)), it follows for $G_{n_1n_2}(f)=0$ that

$$R_{x_1x_2}(\tau) =\alpha R_{s_1s_1}(\tau) \circledast \delta(\tau-D) . \tag{4-5}$$

One interpretation of (4-5) is that the delta function has been spread or "smeared" by the Fourier transform of the signal spectrum. If $s_1(t)$ is a white noise source, then its Fourier transform is a delta function and no spreading takes place. An important

property of autocorrelation functions is that $R_{s_1 s_1}(\tau) \leq R_{s_1 s_1}(0)$. Equality will hold for certain τ for periodic functions (see, for example, Davenport (1970), pp. 323-326). However, for most practical applications, equality does not hold for $\tau \neq 0$, and the true crosscorrelation (4-5) will peak at D regardless of whether or not it is spread out. The spreading simply acts to broaden the peak.

In fact, more generally, when $x_1(t)$ and $x_2(t)$ have been filtered by H_1 and H_2, respectively, then the cross-power spectrum between the filter outputs is given on p. 399 Davenport (1970) as

$$G_{y_1 y_2}(f) = H_1(f) H_2^*(f) G_{x_1 x_2}(f) \quad , \tag{4-6}$$

Therefore, the GCC between $x_1(t)$ and $x_2(t)$ is

$$R_{x_1 x_2}^{g}(\tau) = \int_{-\infty}^{\infty} W_g(f) G_{x_1 x_2}(f) e^{j2\pi f} \, df \quad , \tag{4-7a}$$

where

$$W_g(f) = H_1(f) H_2^*(f) \tag{4-7b}$$

denotes the general frequency weighting. The particular weighting selected is denoted by a change in the subscript g.

For all of the proposed weightings which we will investigate, $W(f) = W^*(f)$ and $W(f) = W(-f)$; that is, $W(f)$ is real and even. These properties are also held by the minimum variance ML weighting.

To distinguish which of the proposed general weightings has been applied, we denote

$$G_{y_1y_2}(f)=G^{g}_{x_1x_2}(f) \tag{4-8a}$$

and thus

$$G_{y_1y_2}(f)= W_g(f)[\alpha G_{s_1s_1}(f)e^{-j2\pi fD}+G_{n_1n_2}(f)] \ . \tag{4-8b}$$

When the noises are incoherent, taking the Fourier transform of (4-8b) yields

$$R^{g}_{x_1x_2}(\tau)=R_{ww}(\tau) \circledast \alpha R_{s_1s_1}(\tau) \circledast \delta(\tau-D) \ , \tag{4-9}$$

where $R_{ww}(\tau)$, the inverse Fourier transform of $W_g(f)$, is even. This being the case, the true GCC will also peak at D regardless of the specific weighting. Thus one might be puzzled as to why any weighting is needed. Indeed, the crosscorrelation function alone is a useful technique for estimating time delay.

Two practical reasons why prefiltering is desirable are evident. If the noise is coherent, for example, if

$$G_{n_1n_2}(f)=G_{s_2s_2}(f)e^{-j2\pi fD_2} \ , \tag{4-10}$$

then

$$R^{g}_{x_1x_2}(\tau)=R_{ww}(\tau) \circledast [\alpha R_{s_1s_1}(\tau) \circledast \delta(\tau-D) + R_{s_2s_2}(\tau) \circledast \delta(\tau-D_2)] \ . \tag{4-11}$$

It is clear, from (4-11), that the convolutions by $R_{s_1s_1}(\tau)$ and $R_{s_2s_2}(\tau)$ will produce two peaks which may

be spread into one another. The convolution by $R_{ww}(\tau)$ can aid to undo this smearing. For a single delay broadening of the delay peak may not be a serious problem. However, when the signal has multiple delays, the true crosscorrelation is given by

$$R_{x_1x_2}(\tau)=R_{s_1s_1}(\tau) \circledast \sum_i \alpha_i \delta(\tau-D_i) \ . \qquad (4\text{-}12)$$

In this case also, the convolution with $R_{s_1s_1}(\tau)$ can spread one delta function into another, thereby making it impossible to distinguish peaks or delay times. Under ideal conditions where $\forall f \hat{G}_{x_1x_2}(f) \cong G_{x_1x_2}(f)$, $W_g(f)$ should be chosen to ensure large sharp peaks in $R_{y_1y_2}(\tau)$ rather than a broad one (see Figure 4-1), since this will ensure good time delay resolution.

There is a second important reason why prefiltering is desirable. In practice, only an estimate $\hat{G}_{x_1x_2}(f)$ of $G_{x_1x_2}(f)$ can be obtained from finite observations of $x_1(t)$ and $x_2(t)$. Thus we can never exactly obtain the crosscorrelation from a limited amount of time data. Because of the finite observation time, then, $R_{x_1x_2}(\tau)$ can only be estimated. For example, for real ergodic processes an estimate of the crosscorrelation is given on p. 327 of Papoulis (1965), as:

$$\hat{R}_{x_1x_2}(\tau)= \frac{1}{T-\tau} \int_{\tau}^{T} x_1(t)x_2(t-\tau)dt \ , \qquad (4\text{-}13)$$

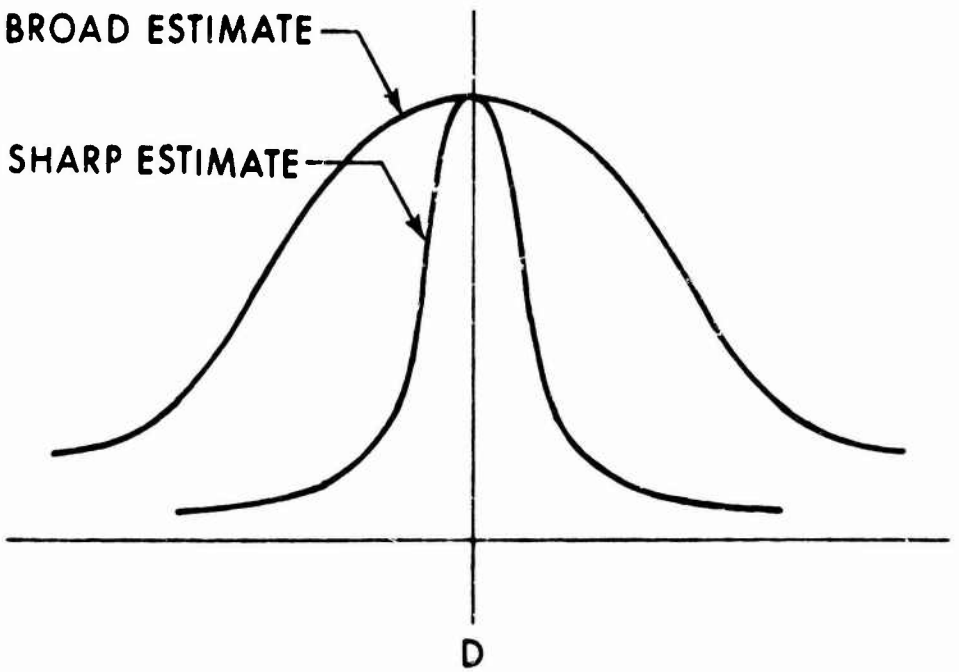

Figure 4-1 Broad and Sharp Estimates of Delay for Infinite Averaging

where T represents the observation interval. For limited duration data records, the accuracy of the delay estimate, $\hat{D}$, can be improved by prefiltering $x_1(t)$ and $x_2(t)$ prior to the integration in (4-13). In practice we can compute (4-13) by weighting the estimated cross spectrum and computing an inverse Fourier transform to obtain an estimated GCC as follows:

$$\hat{R}^{(g)}_{x_1x_2}(\tau)=\int_{-\infty}^{\infty} W_g(f)\hat{G}_{x_1x_2}(f)e^{j2\pi f\tau}df \,. \qquad (4\text{-}14)$$

$W_g(f)$ now serves to improve the estimate of $R_{x_1x_2}(\tau)$ used to estimate time delay.

In practice, depending on the particular form of $W_g(f)$ and the a priori information, it may also be necessary to estimate $W_g(f)$. For example, when the role of the prefilters is to accentuate the signal passed to the correlator at those frequencies at which the SNR is highest, then $W_g(f)$ can be expected to be a function of signal and noise spectra which must either be known a priori or estimated.

Hence, we see that the true crosscorrelation function, for the model (4-1), is sufficient to determine the correct time delay; but for practical (finite data) considerations it is desirable to prefilter $x_1(t)$ and $x_2(t)$ prior to crosscorrelation. Indeed, the problem of selecting $W_g(f)$ to optimize certain performance criteria is not new and has been studied by several investigators. (See, for example, Akaike and Yamanouchi

(1963), Bangs (1971), and Hannan and Thomson (1971).)

Our intuitive discussion of sharply peaked estimators may suggest certain types of weighting. However, sharp peaks are more sensitive to errors introduced by finite observation time, particularly in cases of low SNR. Thus, as with other spectral estimation problems, the choice of $W_g(f)$ is a compromise between good resolution and stability. In the subsequent section we compare several promising weighting functions proposed previously in the literature.

4B. Comparison of Proposed Processors

The preceding discussion provides background for the role that $W_g(f)$ is to play. Now the six versions of the generalized crosscorrelation function listed in Table 4-1 will be examined individually. In the process of comparing the processors in Table 4-1, there will be a tendency to want to look at some simple cases, for example, equal white noises and strong (or weak) white noise signals. In this regard, it can be shown for the case where $G_{n_1n_1}(f)=G_{n_2n_2}(f)=G_{nn}(f)$ is equal to a constant times $G_{s_1s_1}(f)$ (whether or not the signal is white) that five of the processors in Table 4-1 provide for the identical frequency weighting, except for a constant. (The crosscorrelation processor ($W(f)=1, \forall f$) is a delta function smeared out by the Fourier transform of the signal (noise) power spectrum.) In these cases,

Table 4-1. Proposed Processors

Processor Name	Weight $W(f)=H_1(f)H_2^*(f)$
1. Roth Impulse Response	$1/G_{x_1x_1}(f)$
2. Smoothed Coherence Transform (SCOT)	$1/\sqrt{G_{x_1x_1}(f)G_{x_2x_2}(f)}$
3. Phase Transform (PHAT)	$1/\left\|G_{x_1x_2}(f)\right\|$
4. Crosscorrelation	1
5. Eckart	$G_{s_1s_1}(f)/\left[G_{n_1n_1}(f)G_{n_2n_2}(f)\right]$
6. Maximum Likelihood (ML)	$\dfrac{C_{12}(f)}{\left\|G_{x_1x_2}(f)\right\|\left[1-C_{12}(f)\right]}$

the delay estimate from each of these five processors will have the same variance. Hence, a complete comparison can only be made when detailed signal and noise characteristics are provided. Such information is largely dependent on the particular application and a detailed comparison is therefore beyond the intent of this work. For underwater acoustic applications, characteristics of the radiated and self noise of ships, submarines, and torpedoes and the noise background of the sea are given by Urick (1967). For more fundamental signal and noise characteristics, it is useful to provide a brief example of using (3-33) and (3-34). Suppose the example corresponds to (4-1) where $\alpha=1$; $G_{ss}(f)=1$, $\forall f\epsilon(-B,B)$ otherwise $G_{ss}(f)=0$; $G_{n_1n_1}(f)=G_{n_2n_2}(f)=1,\forall f$. It follows from (2-1) and (2-2) that

$$C_{12}(f) = \frac{G_{ss}^2(f)}{[G_{ss}(f)+G_{n_1n_1}(f)][G_{ss}(f)+G_{n_2n_2}(f)]} . \quad (4\text{-}15)$$

Hence,

$$C_{12}(f) = \begin{cases} 0.25 & , \forall f\ (-B,B) \\ 0 & , \text{otherwise} . \end{cases}$$

Other values are given in Table 4-2.

4B1. Roth Processor

The weighting proposed by Roth (1971)

$$W_R(f) = \frac{1}{G_{x_1x_1}(f)} , \quad (4\text{-}16)$$

where the subscript R is to distinguish the choice of

Table 4-2. Comparison Case Data

	$f\varepsilon(0,B)$	$f\varepsilon(+B,H)$
$G_{s_1 s_1}(f)$	1	0
$G_{n_1 n_1}(f)=G_{n_2 n_2}(f)$	1	1
$G_{x_1 x_1}(f)=G_{x_2 x_2}(f)$	2	1
$\left\|G_{x_1 x_2}(f)\right\|$	1	0
$C_{12}(f)$	0.25	0

$W_g(f)$, yields[1]

$$\hat{R}^{(R)}_{x_1x_2}(\tau)=\int_{-\infty}^{\infty} \frac{\hat{G}_{x_1x_2}(f)}{G_{x_1x_1}(f)} e^{j2\pi f\tau} df \ . \qquad (4\text{-}17)$$

Equation (4-17) estimates the impulse response of the optimum linear (Wiener-Hopf) filter,

$$H_m(f)=\frac{G_{x_1x_2}(f)}{G_{x_1x_1}(f)} \ , \qquad (4\text{-}18)$$

which "best" approximates the mapping of $x_2(t)$ to $x_1(t)$ (see, for example, Van Trees (1968), Carter and Knapp (1975) and the discussion of Theorem 2-3). If $n_1(t)\neq 0$, as is generally the case for (4-1), then

$$G_{x_1x_1}(f)=G_{s_1s_1}(f)+G_{n_1n_1}(f) \ , \qquad (4\text{-}19)$$

and ideally

$$R^{(R)}_{x_1x_2}(\tau)=\delta(\tau-D) \Leftrightarrow \int_{-\infty}^{\infty} \frac{\alpha G_{s_1s_1}(f)}{\left[G_{s_1s_1}(f)+G_{n_1n_1}(f)\right]} e^{j2\pi f\tau} df. \qquad (4\text{-}20)$$

Therefore, except when $G_{n_1n_1}(f)$ equals any constant (including zero) times $G_{s_1s_1}(f)$, the delta function will again be spread out. The Roth processor has the desirable effect of suppressing those frequency regions

---

[1]As discussed earlier, W(f) may have to be estimated for this processor and those which follow, because of a lack of a priori information. In this case, (4-16) may require that $G_{x_1x_1}(f)$ be replaced with $\hat{G}_{x_1x_1}(f)$.

where $G_{n_1n_1}(f)$ is large and $\hat{G}_{x_1x_2}(f)$ is therefore more likely to be in error.

From (3-33),

$$\underset{\text{Var}(\hat{D})}{R} = \frac{\int_o^\infty \frac{G_{x_2x_2}}{G_{x_1x_1}}(1-C)f^2df}{8\pi^2T\left[\int_o^\infty \left|G_{x_1x_2}\right|\frac{1}{G_{x_1x_1}}f^2df\right]^2} \quad . \tag{4-21}$$

In the example of Table 4-2 this becomes

$$= \frac{\int_o^B f^2\ \frac{3}{4}\ df+\int_B^H f^2 1df}{8\pi^2\ T\left[\int_o^B f^2\frac{1}{2}df\right]^2} \tag{4-22a}$$

$$= \frac{B^3+\frac{4}{3}H^3-\frac{4}{3}B^3}{\frac{8}{9}\pi^2TB^6} \quad , \tag{4-22b}$$

when B=H (4-22b) agrees with (3-35) as expected; but if H is large in comparison with B, the variance of the Roth processor will be large in comparison to the Cramér-Rao bound (3-24).

4B2. Smoothed Coherence Transform

Errors in $\hat{G}_{x_1x_2}(f)$ may be due to frequency bands where $G_{n_2n_2}(f)$ is large, as well as bands where $G_{n_1n_1}(f)$ is large. One is therefore uncertain whether to form $W_R(f)=1/G_{x_1x_1}(f)$ or $W_R(f)=1/G_{x_2x_2}(f)$; hence,

the smoothed coherence transform (SCOT) proposed by[1] Carter, Nuttall, and Cable (1973) yields

$$W_s(f) = 1/\sqrt{G_{x_1x_1}(f)G_{x_2x_2}(f)} \quad . \tag{4-23}$$

This weighting gives the SCOT

$$\hat{R}^{(s)}_{x_1x_2}(\tau) = \int_{\infty}^{\infty} \hat{\gamma}_{x_1x_2}(f) e^{j2\pi f\tau} df \quad , \tag{4-24}$$

where the coherence estimate[2]

$$\hat{\gamma}_{x_1x_2}(f) \triangleq \frac{\hat{G}_{x_1x_2}(f)}{\sqrt{G_{x_1x_1}(f)G_{x_2x_2}(f)}} \quad . \tag{4-25}$$

For $H_1(f)=1/\sqrt{G_{x_1x_1}(f)}$ and $H_2(f)=1/\sqrt{G_{x_2x_2}(f)}$, the SCOT can be interpreted as prewhitening filters followed by a crosscorrelation. When $G_{x_1x_1}(f)=G_{x_2x_2}(f)$, the SCOT is equivalent to the Roth processor. If $n_1(t)\neq 0$ and $n_2(t)\neq 0$, the SCOT exhibits the same spreading as the Roth processor.

---

[1]The SCOT was originally proposed by G.C.Carter, A.H. Nuttall, and P.G.Cable in 1972 and successfully applied to actual data by G.C.Carter and P.G.Cable in 1972 and Brady (1973) for part of his Ph.D. work.

[2]A more standard coherence estimate is formed when the autospectra must also be estimated, as is usually the case. (See Carter, Knapp and Nuttall (1973a).)

From (3-33)

$$\underset{\text{Var}(\hat{D})}{s} = \frac{\int_o^\infty f^2 [1-C(f)]\,df}{8\pi^2 T\left[\int_o^\infty f^2 \sqrt{C(f)}\,df\right]^2} \quad . \tag{4-26}$$

Note as $C(f)\to 1$, the numerator becomes small and the denominator becomes large. For our example, since $G_{x_1x_1}(f)=G_{x_2x_2}(f)$ the SCOT has the same variance as the Roth processor.

4B3. Phase Transform

To eliminate the spreading evident above, the phase transform (PHAT) uses the weighting[1]

$$W_p(f) = \frac{1}{\left|G_{x_1x_2}(f)\right|} \quad , \tag{4-27}$$

which yields

$$\hat{R}^{(p)}_{x_1x_2}(\tau) = \int_{-\infty}^{\infty} \frac{\hat{G}_{x_1x_2}(f)}{\left|G_{x_1x_2}(f)\right|} e^{j2\pi f\tau}\,df \quad . \tag{4-28}$$

For the model (4-1) with uncorrelated noise (that is, $G_{n_1n_2}(f)=0$),

$$\left|G_{x_1x_2}(f)\right| = \alpha G_{s_1s_1}(f) \quad . \tag{4-29}$$

---

[1]The PHAT was originally suggested by G.C.Carter, A.H. Nuttall and P.G. Cable in 1972.

Ideally, when $\hat{G}_{x_1x_2}(f)=G_{x_1x_2}(f)$,

$$\frac{\hat{G}_{x_1x_2}(f)}{\left|\hat{G}_{x_1x_2}(f)\right|} = e^{j\phi(f)}=e^{j2\pi fD} \tag{4-30}$$

has unit magnitude and

$$R^{(p)}_{x_1x_2}(\tau)=\delta(t-D) \ . \tag{4-31}$$

The PHAT was developed purely as an ad hoc technique. Notice that, for models of the form of (4-1) with uncorrelated noises, the PHAT (4-28), ideally, does not suffer the spreading that other processors do.

From (3-33),

$$\mathrm{Var}(\hat{D}^{(p)}) = \frac{\int_o^\infty f^2 \frac{1}{C}(1-C)\,df}{8\pi^2 T\left[\int_o^\infty f^2 df\right]^2} \ . \tag{4-32}$$

As $C\to 1$, $\frac{(1-C)}{C}\to 0$, so the processor will behave well (that is, low variance). However, as expected, as $C\to 0$ the variance grows without bound. For the example in Table 4-2, assuming the weighting is zero for $f>H$,

$$\mathrm{Var}(\hat{D})^{(p)} = \frac{\int_o^B f^2\cdot 4\cdot\frac{3}{4} + \lim_{C\to 0}\int_B^H f^2\frac{1-C}{C}\,df}{8\pi^2 T\left[\int_o^H f^2 df\right]^2} \ . \tag{4-33}$$

Except when H=B, this processor will suffer a complete breakdown as C tends to zero. When H=B, we obtain the same variance as the Roth and SCOT processors for then

(as indicated earlier) $G_{n_1n_1}(f)=G_{n_2n_2}(f)=G_{s_1s_1}(f)$ and all processors behave equally well. For models of the form of (4-1), the poor behavior of the PHAT suggests that W(f) should not be inversely proportional to signal power. The crosscorrelator is one method of avoiding the application of weight inverse to signal characteristics. Two other processors in Table 4-1 also assign weights or filtering proportionate to SNR: the Eckart filter (Eckart (1952)) and the ML estimator or processor of Hannan and Thomson (1973). We now examine these three processors in depth.

4B4. Crosscorrelation

The variance of the delay estimate from the crosscorrelation processor is

$$\underset{\text{Var}(\hat{D})}{XC} = \frac{\int_o^\infty f^2 G_{x_1x_1} G_{x_2x_2}(1-C)df}{8\pi^2 T\left[\int_o^\infty f^2 \left|G_{x_1x_2}\right| df\right]^2} \quad . \tag{4-34}$$

For the example case in Table 4-2, (4-34) yields

$$\underset{\text{Var}(\hat{D})}{XC} = \frac{\int_o^\infty f^2 \cdot 4 \cdot \frac{3}{4} df + \int_B^H f^2 1 df}{8\pi^2 T\left[\int_o^B f^2 \cdot 1 df\right]^2} \tag{4-35a}$$

$$= \frac{B^3 + \frac{H^3}{3} - \frac{B^3}{3}}{8\pi^2 T \frac{B^6}{9}} \quad . \tag{4-35b}$$

For H=B, (4-35b) agrees with earlier results. The crosscorrelator actually performs better than either the SCOT or the Roth processor for the particular example case in Table 4-2. In general, one can expect to find cases for particular spectra where the cross-correlator performs worse than the SCOT or Roth processors.

4B5. Eckart Filter

The Eckart filter derives its name from work in this area done by Eckart (1952). Derivations in Knapp (1966), and Nuttall and Hyde (1969), are outlined here briefly for completeness. The Eckart filter maximizes the deflection criterion, namely, the ratio of the change in mean correlator output due to signal present to the standard deviation of correlator output due to noise alone. For long averaging time T, the deflection has been shown to be

$$d_f = \frac{L\left[\int_{-\infty}^{\infty} H_1(f)H_2^*(f)G_{s_1s_2}(f)df\right]^2}{\int_{-\infty}^{\infty}\left|H_1(f)\right|^2\left|H_2(f)\right|^2 G_{n_1n_1}(f)G_{n_2n_2}(f)df}, \quad (4\text{-}36)$$

where L is a constant proportional to T, and $G_{s_1s_2}(f)$ is the cross-power spectrum between $s_1(t)$ and $s_2(t)$. For the model (4-1) $G_{s_1s_2}(f)=\alpha G_{s_1s_1}(f)\exp(j2\pi fD)$.

Application of Schwartz's inequality indicates that

$$H_1(f)H_2^*(f)=W_E(f)e^{+j2\pi fD} \quad (4\text{-}37)$$

maximizes d_f where

$$W_E(f) = \frac{\alpha G_{s_1 s_1}(f)}{G_{n_1 n_1}(f) G_{n_2 n_2}(f)} \quad . \tag{4-38}$$

Notice that the weighting (4-38), referred to as the Eckart filter, possesses some of the qualities of the SCOT. In particular, it acts to suppress frequency bands of high noise, as does the SCOT. Also note that the Eckart filter unlike the PHAT attaches zero weight to bands where $G_{s_1 s_1}(f)=0$. In practice, the Eckart filter requires knowledge or estimation of the signal and noise spectra. For (4-1), when $\alpha=1$ this can be accomplished by letting

$$W_E(f)=\left|\hat{G}_{x_1 x_2}(f)\right| \Big/ \left\{\left[\hat{G}_{x_1 x_1}(f)-\left|\hat{G}_{x_1 x_2}(f)\right|\right]\cdot\left[\hat{G}_{x_2 x_2}(f)-\left|\hat{G}_{x_1 x_2}(f)\right|\right]\right\}. \tag{4-39}$$

The variance of the time delay estimate using Eckart filtering is

$$\underset{\mathrm{Var}(\hat{D})}{E} = \frac{\int_o^\infty f^2 \dfrac{G_{ss}^2}{G_{n_1 n_1}^2 G_{n_2 n_2}^2} G_{x_1 x_1} G_{x_2 x_2} (1-C)\,df}{8\pi^2 T\left[\int_o^\infty f^2 \left|G_{x_1 x_2}\right| \dfrac{G_{ss}}{G_{n_1 n_1} G_{n_2 n_2}}\right] df}^2 \quad . \tag{4-40}$$

For the example case in Table 4-2,

$$\underset{\mathrm{Var}(\hat{D})}{E} = \frac{\int_o^B f^2 4\frac{3}{4}\,df}{8\pi^2 T\left[\int_o^B f^2 df\right]^2} \tag{4-41a}$$

$$= \frac{1}{\frac{8}{9}\pi^2 TB^3}; \qquad (4\text{-}41b)$$

that is, for this example the Eckart filter achieves the Cramér-Rao lower bound (3-24). In general this will not always occur. In the next section we see that (4-41b) is the variance achieved by the ML processor. This might be expected since both the Eckart and ML processors pass nothing in the signal frequency band (B,H) and both have constant weighting over the band (0,B). Actually, the ML estimator is closely related to the Eckart filter, as will be seen in section 4C of this chapter.

4B6. Maximum Likelihood Processor

As shown in Chapter 3 the ML processor always has minimum variance. For the Table 4-2 example, the correct weighting from (3-20) is W(f)=1/3 for $f\varepsilon(-B,B)$ and zero otherwise. Now from (3-34)

$$\mathrm{Var}^{ML}(\hat{D}) = \left[\frac{8}{9}\, T\pi^2 B^3\right]^{-1} . \qquad (4\text{-}42)$$

Thus, the minimum variance depends on a time bandwidth product, TB multiplied by the bandwidth squared, B^2. Suppose an error had been made identifying the frequency band of the signal. Then if we presumed that the weighting was W(f)=1/3 for, say, $f\varepsilon(-aB,aB)$, in lieu of $f\ (-B,B)$, we would obtain from (3-33)

when $a \geq 1$

$$\mathrm{Var}(\hat{D}) = \frac{(2+a^3)}{3}\left[\frac{8}{9}\, T\pi^2 B^3\right]^{-1} , \qquad (4\text{-}43)$$

which reduces to (4-42) when a=1. For example, in this case, a 10 percent error (that is, a=1.1) leads to more than an 11 percent increase in variance. If $a \leq 1$ then (3-33) becomes

$$\mathrm{Var}(\hat{D}) = \frac{1}{a^3}\left[\frac{8}{9}\, T\pi^2 B^3\right]^{-1} , \qquad (4\text{-}44)$$

which agrees with (4-42) when a=1. Thus a 10 percent error (a=0.9) leads to an increase in variances of 37 percent. Thus our example suggests it may be more desirable to let in extra noise than to omit signal power. Finally, if our error led to processing the band $f\varepsilon(aB,B)$ and $f\varepsilon(-B,-aB)$, we would obtain

$$\mathrm{Var}(\hat{D}) = \frac{1}{1-a^3}\left[\frac{8}{9}\, T\pi^2 B^3\right]^{-1} , \qquad (4\text{-}45)$$

which agrees with (4-42) when a=0.

The ratio of variances (4-45) to (4-42) for $a \ll 1$ is

$$\frac{1}{1-a^3} \cong 1+a^3 . \qquad (4\text{-}46)$$

If we again err by 10 percent (i.e., a=0.1), then (4-46) yields 1.001 or little change in the variance. (This error is at lower frequencies in the signal band and as (3-33) suggests, proper weighting is most critical at higher frequencies.) Thus, for this example,

depending on how we make a 10 percent error in frequency band selection, we can have anywhere from 0.1 percent to a 37.0 percent increase in variance of the time delay estimate.

4C. Interpretation of Relationship Between Correlation Processors

For the case where $\alpha=1$

$$W_{ML}(f)=\frac{1}{G_{s_1s_1}(f)}\left\{\frac{G^2_{s_1s_1}(f)}{\left[G_{s_1s_1}(f)+G_{n_1n_1}(f)\right]}\right. \left.\frac{1}{\left[G_{s_1s_1}(f)+G_{n_2n_2}(f)\right]-G^2_{s_1s_1}(f)}\right\} \tag{4-47a}$$

$$= \frac{\dfrac{G_{s_1s_1}(f)}{G_{n_1n_1}(f)G_{n_2n_2}(f)}}{1+\dfrac{G_{s_1s_1}(f)}{G_{n_2n_2}(f)}+\dfrac{G_{s_1s_1}(f)}{G_{n_1n_1}(f)}} , \tag{4-47b}$$

which agrees with equation (28) of MacDonald and Schultheiss (1969) if in (4-47b) $G_{n_1n_1}(f)=G_{n_2n_2}(f)$.[1] For low SNR,

$$\frac{G_{s_1s_1}(f)}{G_{n_1n_1}(f)} \ll 1 \text{ and } \frac{G_{s_1s_1}(f)}{G_{n_2n_2}(f)} \ll 1 ,$$

it follows that

$$W_{ML}(f) \approx \frac{G_{s_1s_1}(f)}{G_{n_1n_1}(f)G_{n_2n_2}(f)} = W_E(f) ; \tag{4-48}$$

---

[1] Notice that agreement requires $\alpha=1$.

that is, for $\alpha=1$ and low SNR, the ML processor is identical to the Eckart filter. Similarly, for low SNR,

$$W_s(f) \cong 1/\sqrt{G_{n_1n_1}(f)G_{n_2n_2}(f)} \quad . \tag{4-49}$$

Therefore, if $\alpha=1$,

$$W_{ML}(f) \cong \frac{G_{s_1s_1}(f)}{\sqrt{G_{n_1n_1}(f)G_{n_2n_2}(f)}} \; W_s(f) \quad . \tag{4-50a}$$

Furthermore, for $G_{n_1n_1}(f)=G_{n_2n_2}(f)=G_{nn}(f)$,

$$W_{ML}(f) \cong \frac{G_{s_1s_1}(f)}{G_{nn}(f)} \; W_s(f) = \left[\frac{G_{s_1s_1}(f)}{G_{nn}(f)}\right]^2 W_p(f). \tag{4-50b}$$

Thus, under low SNR approximations with $\alpha=1$, both the Eckart and ML prefilters can be interpreted either as SCOT prewhitening filters with additional SNR weighting or PHAT prewhitening filters with additional SNR squared weighting.

We can rewrite (4-47) as

$$W_{ML}(f)=\frac{\dfrac{1}{\sqrt{G_{n_1n_1}G_{n_2n_2}}}}{\sqrt{\dfrac{G_{n_1n_1}G_{n_2n_2}}{G_{s_1s_1}}}+\sqrt{\dfrac{G_{n_1n_1}G_{n_2n_2}}{G_{n_1n_1}}}+\sqrt{\dfrac{G_{n_1n_1}G_{n_2n_2}}{G_{n_2n_2}}}} \tag{4-51}$$

for uniformly high SNR,

$$\sqrt{\frac{\lim}{\frac{G_{n_1n_1}G_{n_2n_2}}{G_{s_1s_1}}\to 0}} W_{ML}(f) = \frac{1}{G_{n_2n_2}+G_{n_1n_1}} ; \qquad (4\text{-}52)$$

that is, giving the weighting characteristics similar to the SCOT at low SNR. Note that, like the ML processor, the PHAT computes a type of transformation on

$$\left|\frac{\hat{G}_{x_1x_2}(f)}{G_{x_1x_2}(f)}\right| \cong \exp\ j\hat{\phi}(f) \quad . \qquad (4\text{-}53)$$

However, the ML processor, like the SCOT, weights the phase according to the strength of the coherence. From p. 379 of Jenkins and Watts (1968), comparing (B-22) with equation (9.2.19) and (9.2.20) of Jenkins and Watts (1968) the variance of the phase estimates is given by

$$\text{Var}\ \hat{\phi}(f) \cong \frac{(1-C)}{C}\cdot\frac{1}{(2N)} \ , \qquad (4\text{-}54)$$

where N is the number of independent FFTs used to estimate phase. Notice as C→1, Var $\hat{\phi}$ →0. Thus,

$$R^{(ML)}_{x_1x_2}(\tau) = \frac{1}{N}\int_{-\infty}^{\infty} e^{j\hat{\phi}(f)}\cdot\frac{1}{\text{Var}\ \hat{\phi}(f)} e^{j2\pi f\tau} df \ . \qquad (4\text{-}55)$$

Comparison of (4-55) with (4-53) reveals that the ML estimator is the PHAT inversely weighted according to the variability of the phase estimates.

The ML processor has been compared with five other candidate processors to demonstrate the interrelation of all six estimation techniques. The derivation of the ML delay estimator (in Chapter 3),

together with its relation to various ad hoc techniques of intuitive appeal (in this chapter), suggests the practical significance of ML processing for estimation of time delay and, thence, bearing. The remainder of this thesis deals with extensions of the ML processor to more complex models and a discussion of the results and suggestions for future work.

CHAPTER 5

MORE COMPLEX MODELS

Chapter 3 answered, for a simple model, the fundamental question of this thesis: What is the "best" method of estimating time delay" Chapter 4 compared this method with several other candidate processors. Chapter 5 considers three conceptually straightforward extensions of the problem considered in Chapter 3: (1) multiple source models, (2) moving source models, and (3) multiple sensor models. The "solution" to these problems is more difficult than the problem of estimating a single time delay for a stationary source. For example, in the multiple source and multiple sensor models, there is more than one delay to be estimated. Indeed, if we treated multiple sources and multiple sensors together, we would need to estimate a parameter vector for each source, corresponding to the (relative) delays between that source and each sensor; thus, a (nonsquare) matrix of delays (comprised of a parameter vector for each source) would need to be estimated. Finally, it is necessary, in effect, to estimate the motion of each source so as to be able to Doppler correct the received signals prior to crosscorrelation. Failure to apply some sort

of Doppler correction will cause the received signals to be essentially uncorrelated even if a common (but frequency shifted) signal is present.

Both notationally and analytically, the methods applied to estimate the unknown parameters become more complex than the methods in Chapter 3. Yet even in Chapter 3 where a "solution" for the ML estimate of time delay was possible, we noted that, in practice, it would be necessary to resort to an AML estimation technique; for more complex models there is no reason to expect that the solution will become simpler; indeed, in this chapter (especially with regard to moving sources), we appeal more to approximate and ad hoc techniques based on the ideas of Chapter 3 than to rigorous methodologies. The reasons for this approach are apparent in section B and have to do with the nonstationarities introduced by the source motion.

5A. Multiple Source Models

The simplest multiple source model is a two source case where receiving sensors are physically steered at one source and the second source acts as an interference. Such a model is depicted in Figure 5-1 (Carter and Knapp (1975)). Mathematically,

$$x_1(t) = s_1(t)+s_2(t)+n_1(t) \tag{5-1a}$$

and

$$x_2(t) = s_1(t)+s_2(t-D)+n_2(t) \ . \tag{5-1b}$$

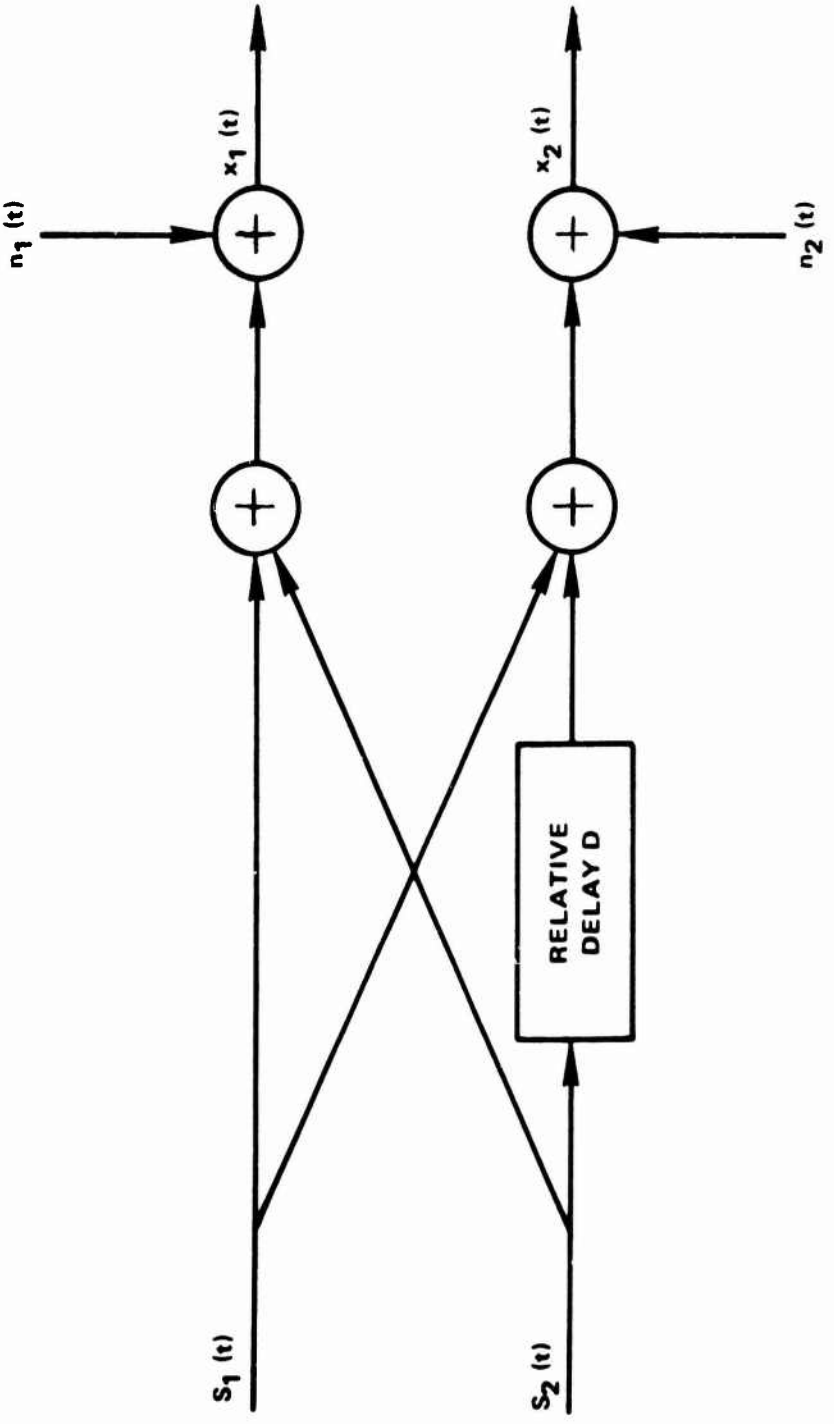

Figure 5-1 Two Directional Source Signals Received with Noise

(The effect of an interfering source on detection is considered by Schultheiss (1968).) The problem is to estimate the parameter D. In effect $s_1(t)$ accounts for correlated noise insofar as estimation of D is concerned.

When $s_1(t)$ and $s_2(t)$ are stationary uncorrelated signals with power spectra $G_{s_1s_1}(f)$ and $G_{s_2s_2}(f)$ and when $n_1(t)$ and $n_2(t)$ are stationary uncorrelated noises with the same power spectrum $G_{nn}(f)$, it has been shown by Carter and Knapp (1975) that

$$\gamma_{x_1x_2}(f)=\left[1+\frac{G_{s_2s_2}(f)}{G_{s_1s_1}(f)}e^{-j2\pi fD}\right]\frac{G_{s_1s_1}(f)}{G_{s_1s_1}(f)+G_{s_2s_2}(f)+G_{nn}(f)}. \tag{5-2}$$

In the special case when $G_{nn}(f)=0$ and $G_{s_1s_1}(f)=G_{s_2s_2}(f)$

$$\gamma_{x_1x_2}(f)=\frac{1}{2}(1+e^{-j2\pi fD})=e^{-j\pi fD}\cos\pi fD \tag{5-3}$$

and

$$C_{x_1x_2}(f)=\cos^2\pi fD=\frac{1}{2}(1+\cos 2\pi fD). \tag{5-4}$$

Because of the sinusoidal oscillation between 0 and 1 of $C_{x_1x_2}(f)$, the Fourier transform of (5-3) will exhibit a peak at the value of time delay. This suggests the usefulness of computing the Fourier transform of the coherence or SCOT (Carter, Nuttall and Cable (1973)).

A more general, multiple source, two sensor model is

$$x_1(t)=\sum_i s_i(t)+n_1(t) \tag{5-5a}$$

$$x_2(t)=\sum_i \alpha_i s_i(t+D_i)+n_2(t)\ . \tag{5-5b}$$

The limit on the sum depends on the number of sources. Since each source will be presumed to be independent of the others, the sources will be mutually uncorrelated. For the general two source case depicted as a multi-input, multi-output system in Figure 5-2, it follows that

$$x_1(t) = s_1(t)+s_2(t)+n_1(t) \tag{5-6a}$$

$$x_2(t) = \alpha_1 s_1(t+D_1)+\alpha_2 s_2(t+D_2)+n_2(t) \tag{5-6b}$$

and therefore

$$G_{x_1x_1}(f) = G_{s_1s_1}(f)+G_{s_2s_2}(f)+G_{n_1n_1}(f) \tag{5-7a}$$

$$G_{x_2x_2}(f) = \alpha_1^2 G_{s_1s_1}(f)+\alpha_2^2 G_{s_2s_2}(f)+G_{n_2n_2}(f) \tag{5-7b}$$

and

$$G_{x_1x_2}(f) = \alpha_1 G_{s_1s_1}(f)e^{-j2\pi fD_1} + \alpha_2 G_{s_2s_2}(f)e^{-j2\pi fD_2} + G_{n_1n_2}(f) \quad . \tag{5-7c}$$

However, we can accommodate coherent noise through the inclusion of additional sources so that without loss of generality $G_{n_1n_2}(f)=0$ for all frequencies. From the two-source model with incoherent noise, we generalize that

$$G_{x_1x_1}(f) = G_{n_1n_1}(f)+\Sigma_i G_{s_is_i}(f) \tag{5-8a}$$

$$G_{x_2x_2}(f) = G_{n_2n_2}(f)+\Sigma_i \alpha_i^2 G_{s_is_i}(f) \tag{5-8b}$$

and

$$G_{x_1x_2}(f) = \Sigma_i \alpha_i G_{s_is_j}(f)e^{-j2\pi fD_i} \quad . \tag{5-8c}$$

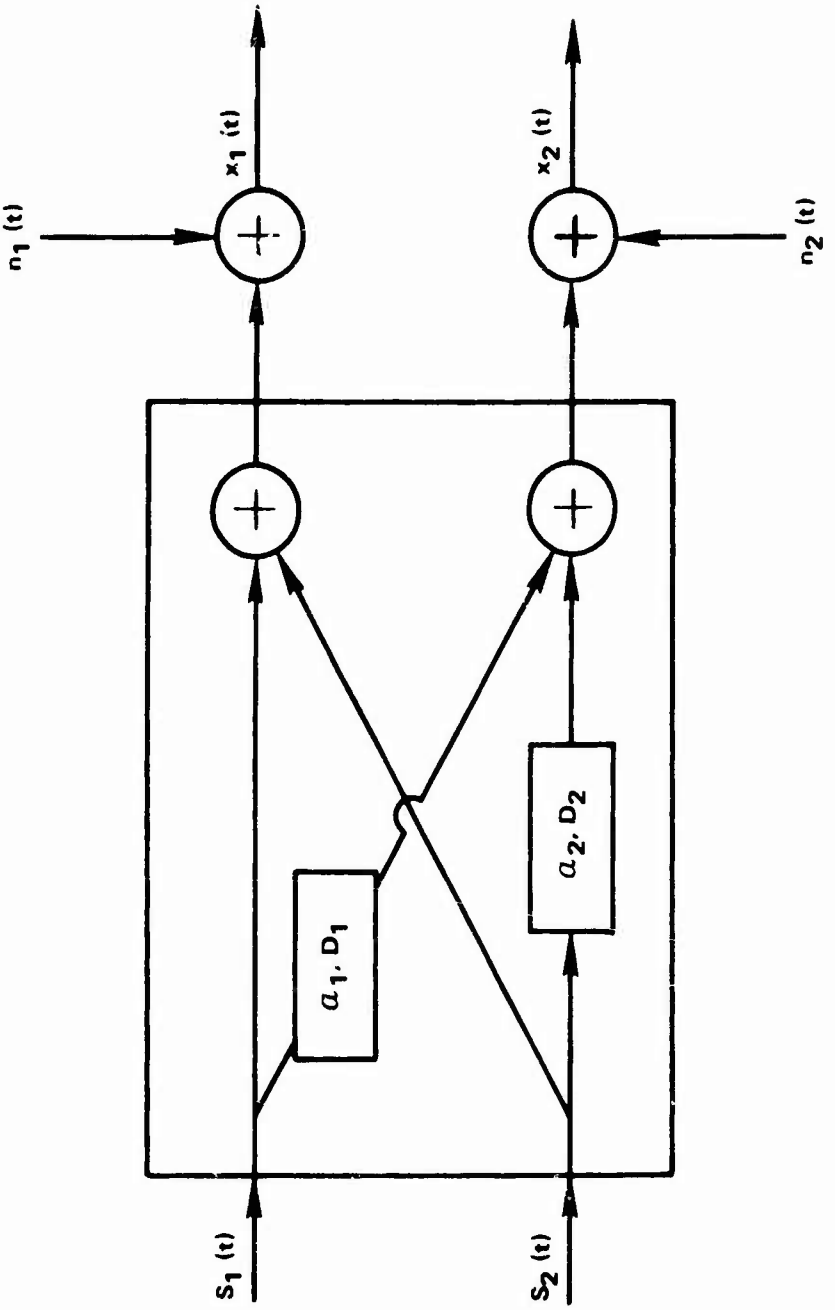

Figure 5-2 General Two Source, Two Sensor Model

In the ML estimation procedure earlier the determinant of Q_x could be ignored since it did not depend on D. Now, however, for the two-source model, we see (suppressing f) that

$$|Q| = \begin{vmatrix} G_{s_1s_1}+G_{s_2s_2}+G_{n_1n_1}, & \alpha_1 G_{s_1s_1} e^{-j2\pi fD_1}+\alpha_2 G_{s_2s_2} e^{-j2\pi fD_2} \\ \alpha_1 G_{s_1s_1} e^{+j2\pi fD_1}+\alpha_2 G_{s_2s_2} e^{+j2\pi fD_2}, & G_{x_2x_2} \end{vmatrix} \quad (5\text{-}9a)$$

does depend on (D_1D_2). For example, even when $G_{n_1n_1}=G_{n_2n_2}=G_{nn}$, $\alpha_1=\alpha_2=1$ and $G_{s_1s_1}=G_{s_2s_2}=G_{ss}$,

$$|Q| = (2G_{ss}+G_{nn})^2 - G_{ss}^2 (e^{-j2\pi fD_1}+e^{-j2\pi fD_2})(e^{+j2\pi fD_1}+e^{+j2\pi fD_2}) \quad (5\text{-}9b)$$

$$|Q| = 4G_{ss}^2+2G_{ss}G_{nn}+G_{nn}^2-G_{ss}^2\left[2+e^{-j2\pi f(D_2-D_1)}+e^{+j2\pi f(D_2-D_1)}\right]. \quad (5\text{-}9c)$$

In general, $|Q|$ depends on the parameter vector (D_1D_2). Thus, we must be concerned by the $|Q|$ as well as the exponent in (3-9), for the multiple source model. Specifically, we want to maximize the sum of both (3-17) and the $\log_c|Q|$ term. The latter is given by

$$h = \sum_{k=-N}^{N} \log_e |Q|^{-\frac{1}{2}}, \quad (5\text{-}10)$$

but

$$|Q| = \begin{vmatrix} G_{x_1x_1} & G_{x_1x_2} \\ G^*_{x_1x_2} & G_{x_2x_2} \end{vmatrix} = G_{x_1x_1} G_{x_2x_2} [1-C_{x_1x_2}] . \quad (5\text{-}11)$$

Thus,

$$\log_e |Q|^{-\frac{1}{2}} = -\frac{1}{2}[\log_e G_{x_1x_1} G_{x_2x_2} + \log_e (1-C_{x_1x_2})]. \qquad (5\text{-}12)$$

But $\log_e G_{x_1x_2} G_{x_2x_2}$ does not depend on $(D_1, D_2, \ldots)$ so that the critical parameters in the $|Q|$ term are approximately given by

$$-\frac{1}{2}T \int_{-\infty}^{\infty} \log_e [1-C_{x_1x_2}(f)]\,df. \qquad (5\text{-}13)$$

In practice, x_1 and x_2 will have finite bandwidth; therefore the limits of the integral (5-13) will also be finite. It is noteworthy that the second term is related to the definition by Shannon (1949) for the amount of information about $x_2(t)$ contained in $x_1(t)$. More specifically, Gelfand and Yaglom (1959) and Nettheim (1966) have shown that the amount of information about x contained in y (or vice versa) is given by[1]

$$I_{xy} = -\frac{1}{2} \int \log_e [1-C_{xy}(f)]\,df, \qquad (5\text{-}14)$$

where the limits of integration are over the nonzero range of the integrand. Hence, for $C_{xy}(f)=0$, there is no information (in the linear sense)[2] contained in one

---

[1] These results can be combined with (2-79) for models like Figure 2-5 to show that I_{xy} is the integral of the logarithm of 1 plus received signal to noise ratio.

[2] See Carter and Knapp (1975) or Chapter 2 for a discussion of nonlinear relations which can yield $C_{xy}(f)=0$ and yet y(t) can be entirely due to x(t). as for example, when $y(t)=x^2(t)$.

time series with regard to the other. Alternatively, if $C_{xy}(f)=1$, for some particular f_p, then there is an infinite amount of information about x(t) knowing y(t) at the particular frequency f_p. More generally, for nonzero $C_{xy}(f)<1$, the amount of information depends on the bandwidth (limits of integration in (5-14)) and the MSC in that band.

Thus, following (3-15) and (5-10) through (5-14), we see that it is desired to maximize

$$J=T\left[I_{x_1x_2}+2\int_{-\infty}^{\infty}\frac{\hat{G}_{x_1x_2}G_{x_1x_2}^{*}}{G_{x_1x_1}G_{x_2x_2}(1-C_{x_1x_2})}df\right] . \qquad (5\text{-}15)$$

For the two source model,

$$J=T\left[I_{x_1x_2}+2\int_{-\infty}^{\infty}\frac{\hat{G}_{x_1x_2}\alpha_1 G_{s_1s_1}e^{+j2\pi fD_1}}{|Q|}df + 2\int_{-\infty}^{\infty}\frac{\hat{G}_{x_1x_2}\alpha_2 G_{s_2s_2}e^{+j2\pi fD_2}}{|Q|}df\right] , \qquad (5\text{-}16)$$

or for two-sensor, multiple source model we maximize

$$J=T\left[I_{x_1x_2}+2\int_{-\infty}^{\infty}\frac{\hat{G}_{x_1x_2}(f)\Sigma\alpha_i G_{s_is_i}(f)e^{+j2\pi fD_i}}{|Q(f)|}df\right] . \qquad (5\text{-}17)$$

Thus, the important regions of the estimated cross spectrum for determining D_i are those frequency bands where $G_{s_is_i}(f)$ is large. However, even when the signal spectrum is strong, if the intersource interference is such that the intersensor coherence $C_{x_1x_2}(f)$ is low, the

weight attached to the estimated cross spectrum is degraded, as shown above.

While we can estimate auto spectra and coherence between sensors, more sophisticated methods must be applied in order to estimate the source signal spectrum. The mathematics shows how to process for known signal spectrum. In the communications problem, signal spectrum will generally be known, although α, which more generally could be a function of frequency, will probably not be known. In other problems, methods involving classification and data bank retrieval need to be studied. In the absence of a priori knowledge, we might assume that every frequency band where the coherence was high was a different source. Tracking (that is, estimating bearing continuously) for each frequency band then becomes a classification problem where the number of sources is ascertained by noting the number of clustered sources. The fewer the sources for a given total source power the easier tracking will be. However, repeated clustering analysis will be desirable to ascertain whether two or more sources are being classified as one.

In "real world" problems, there may well be more than one source; hence, the application of Chapter 3 results must include the concepts of multiple sources. There are other concerns, too, in the practical application of our Chapter 3 results. The next generalization which we will discuss is the moving source

problem.

5B. Moving Source Models

The model we shall consider is a simplified one characterized by the observed waveforms (Carter and Knapp (1976b))

$$x_1(t)=s(t)+n_1(t) \tag{5-18a}$$

$$y_2(t)=\alpha s(\beta t+D)+n_2(t)\ , \tag{5-18b}$$

where $s(t)$, $n_1(t)$ and $n_2(t)$ are zero mean jointly stationary Gaussian random processes which are mutually uncorrelated. The problem addressed here is ML estimation of the time compression and delay parameters β and D, respectively; the problem is related to the Doppler shift work by Van Trees (1971). The characteristics of the signal and noise are such that $x_1(t)$ is a member function of a zero mean stationary Gaussian random process. Further, despite the attenuation, delay and time compression, $y_2(t)$ is also stationary and Gaussian. That is, both autocorrelation functions given by

$$R_{x_1x_1}(\tau) = R_{n_1n_1}(\tau)+R_{ss}(\tau) \tag{5-19a}$$

and

$$R_{y_2y_2}(t_1,t_2)=R_{n_2n_2}(t_2-t_1)+\alpha R_{ss}(\beta(t_2-t_1)) \tag{5-19b}$$

depend only on the time difference t_2-t_1.

However, the crosscorrelation for model (5-18) depends on β as follows:

$$R_{x_1y_2}(t_1,t_2)=\alpha E[s(t_1)s(\beta t_2+D)]=\alpha R_{ss}(t_1-\beta t_2-D) \qquad (5\text{-}19c)$$

$$R_{y_2x_1}(t_1,t_2)=\alpha E[s(\beta t_1+D)s(t_2)]=\alpha R_{ss}(\beta t_1+D-t_2) \ . \qquad (5\text{-}19d)$$

As required,

$$R_{x_1y_2}(t_1,t_2) = R_{y_2x_1}(t_2,t_1) \ . \qquad (5\text{-}20)$$

Notice the crosscorrelation depends on β as well at t_1 and t_2, and not simply the difference between t_1 and t_2. Hence the processes $x_1(t)$ and $y_2(t)$ are <u>not</u> jointly second order stationary, but depend on the absolute time origin. Thus, the introduction of time compression β in our model thereby complicates the theory through the imposition of a second order nonstationarity. [For a variety of practical reasons, we desire to operate on $y_2(t)$ in order to ensure complete stationarity.]

An ad hoc technique for estimating D is to operate on $y_2(t)$ to remove (or adjust) the time scale change β. The result, referred to as $x_2(t)$, may then be used with $x_1(t)$ in the usual ML estimator of Chapter 3. This indeed turns out to be the ML estimator for this problem (as is subsequently shown). A major problem, of course, is that β as well as delay D must be estimated to undo the time scaling introduced by motion of the source. Suppose β_a, for example, is one estimate (or hypothesis) of β (like τ was a hypothesized delay in Chapter 3) and let

$$x_2(t) \triangleq y_2(t/\beta_a) \qquad (5\text{-}21a)$$

$$= \alpha s(\beta t/\beta_a + D) + n_2(t/\beta_a) \quad . \tag{5-21b}$$

Now the crosscorrelation of $x_1(t)$ with $x_2(t)$ is given by

$$R_{x_1x_2}(t_1,t_2) = E[x_1(t_1)x_2(t_2)] \tag{5-22a}$$

$$= \alpha R_{ss}(t_1 - \frac{\beta}{\beta_a}t_2 - D) . \tag{5-22b}$$

Thus, for $\beta_a=\beta$, we see that $x_1(t)$ and $x_2(t)$ are second order jointly stationary, for then $R_{x_1x_2}(t_1,t_2)$ depends only on the time difference $\tau=t_1-t_2$. For $\beta_a=\beta$, it is possible to compute a single Fourier transformation on τ to achieve

$$G_{x_1x_2}(f) = \int_{-\infty}^{\infty} R_{x_1x_2}(\tau)e^{-j2\pi f\tau}d\tau \tag{5-23a}$$

$$= \alpha G_{ss}(f)e^{-j2\pi fD} \quad . \tag{5-23b}$$

Similar results can be obtained using the concept of locally stationary random processes (Silverman (1957)). However, in general, when $\beta \neq \beta_a$, a two-dimensional Fourier transformation must be performed. For convenience let $\tilde{\beta}=\beta/\beta_a$ (where we ultimately hope to make $\tilde{\beta}\cong 1$ by proper choice of β_a)[1]; then it follows that

$$E\left[X_1(k)X_2^*(l)\right] = \frac{\alpha}{T^2}\int_0^T dt_1 \int_0^T dt_2 R_{ss}(t_1 - \tilde{\beta}t_2 - D) \quad . \tag{5-24a}$$

$$e^{-j\omega_o(kt_1 - lt_2)}$$

---

[1] In the following it may be assumed that $\beta_a=1$ and $\tilde{\beta}=\beta$; that is, that $y_2(t)$ has not been preprocessed. Results can then be applied with $\beta\cong 1$ (rather than $\tilde{\beta}\cong 1$); for many problems $\beta\cong 1$.

However,

$$R_{ss}(t_1-\tilde{\beta}t_2-D) = \frac{\alpha}{2\pi}\int_{-\infty}^{\infty} G_{ss}(\omega)e^{j\omega(t_1-\tilde{\beta}t_2-D)}d\omega \qquad (5\text{-}24b)$$

so that

$$E\left[X_1(k)X_2^*(l)\right] = \frac{1}{2\pi}\int_{-\infty}^{\infty} G_{ss}(\omega)e^{-j\omega D}d\omega \cdot \frac{1}{T}\int_0^T e^{j(\omega-k\omega_\Delta)t_1}dt_1 \; \frac{1}{T}\int_0^T e^{-j(\tilde{\beta}\omega-l\omega_\Delta)t_2}\,dt_2 \qquad (5\text{-}24c)$$

$$= \frac{1}{2\pi}\int_{-\infty}^{\infty} G_{ss}(\omega)e^{-j\omega D}\left[\frac{e^{j(\omega-k\omega_\Delta)T}-1}{j(\omega-k\omega_\Delta)T}\right]\left[\frac{1-e^{-j(\tilde{\beta}\omega-l\omega_\Delta)T}}{j(\tilde{\beta}\omega-l\omega_\Delta)T}\right]d\omega \qquad (5\text{-}24d)$$

$$= \frac{1}{2\pi}\int_{-\infty}^{\infty} G_{ss}(\omega)e^{-j\omega D}e^{j(\omega-k\omega_\Delta)T/2}e^{-j(\tilde{\beta}\omega-l\omega_\Delta)T/2}\left[\frac{\sin(\omega-k\omega_\Delta)T/2}{(\omega-k\omega_\Delta)T/2}\cdot\frac{\sin\tilde{\beta}T/2(\omega-\frac{l\omega_\Delta}{\tilde{\beta}})}{\tilde{\beta}T/2(\omega-\frac{l\omega_\Delta}{\tilde{\beta}})}\right]d\omega \qquad (5\text{-}24e)$$

$$= \frac{1}{2\pi}\int_{-\infty}^{\infty} G_{ss}(\omega)e^{-j\omega D}e^{j\omega T/2(1-\tilde{\beta})}e^{j(1-k)T}\,\frac{\sin(\omega-k\omega_\Delta)T/2}{(\omega-k\omega_\Delta)T/2}\cdot\frac{\sin\tilde{\beta}T/2(\omega-l\omega_\Delta/\tilde{\beta})}{\tilde{\beta}T/2(\omega-l\omega_\Delta/\tilde{\beta})}\;d\omega\,. \qquad (5\text{-}24f)$$

Equation (5-24) offers a more rigorous interpretation of (5-23). For large T and $\tilde{\beta}$ near unity, it follows from (5-24f) (since the discrepancy between the sinc functions is minor) that

$$G_{x_1x_2}(f) = T\,E[X_1(k)X_2^*(l)] \tag{5-25a}$$

$$= \begin{cases} \alpha G_{ss}(k\omega_\Delta)e^{-jk\omega_\Delta D}, & l=k\tilde{\beta} \\ 0, & l\neq k\tilde{\beta}\ . \end{cases} \tag{5-25b}$$

Also,

$$T\,E[X_1(k)X_1^*(l)] = \begin{cases} G_{n_1n_1}(k\omega_\Delta)+G_{ss}(k\omega_\Delta), & l=k \\ 0, & l\neq k \end{cases} \tag{5-25c}$$

and

$$T\,E[X_2(k)X_2^*(l)] = \begin{cases} \beta_a G_{n_2n_2}(\beta_a k\omega_\Delta)+\frac{\alpha}{\tilde{\beta}}G_{ss}(\frac{k\omega_\Delta}{\tilde{\beta}}), & l=k \\ 0, & l\neq k \end{cases}. \tag{5-25d}$$

Note in (5-25d) $G_{n_2n_2}$ is evaluated at $\beta_a k\omega_\Delta$ not $k\omega_\Delta$. Similarly, it can be shown for $\tilde{\beta}\cong 1$ and large T, that

$$E[X_2(k)X_1^*(l)] = \begin{cases} \alpha G_{ss}(k\omega_\Delta)e^{jk\omega_\Delta D} & l=k/\tilde{\beta} \\ 0 & l\neq k/\tilde{\beta}\ . \end{cases} \tag{5-26}$$

We now proceed as in Chapter 3, Section A. In particular, we desire to maximize a total award function J_A, as depicted in Figure 5-3, through the adjustment of hypothesized compression β_a and hypothesized delay τ; when J_A is maximized, the ML estimates $\hat{\beta}$ and $\hat{D}$ depicted in Figure 5-3 are achieved.

It is important to the discussion that follows to note that if β_a is incorrectly selected such that $\tilde{\beta}$ is

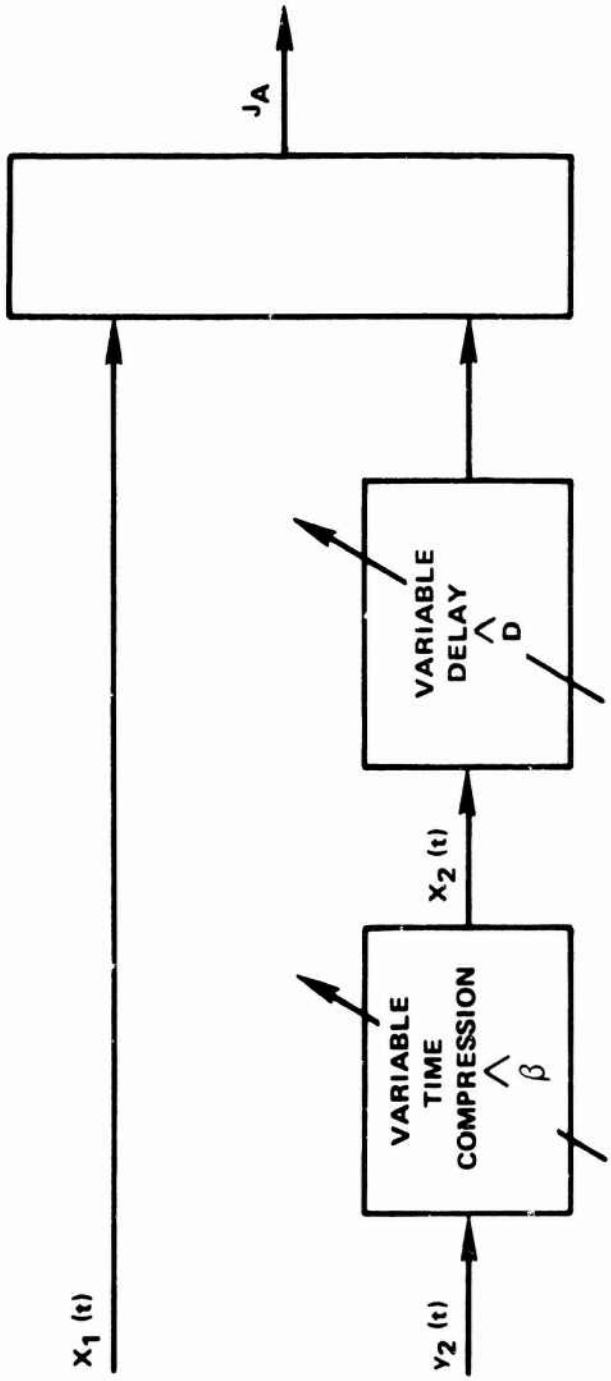

Figure 5-3 Processing to Estimate β and D

much different from unity, the processes $x_1(t)$ and $x_2(t)$ are second order jointly nonstationary and the estimators are not ML estimators. However, once we have begun to estimate delay and compression correctly, the processor is an ML estimator; that is, in the sequential estimation problem where several observation intervals are available, then ML or at least AML estimation is possible in the last intervals. Before proceeding, we also note that if $\tilde{\beta}\neq 1$ any crosscorrelation (coherence) terms in the award J_A will be zero. More specifically, if β is much different from unity, then time delay cannot be estimated without some type of Doppler or time compression preprocessing. The importance of this statement is that Chapter 3 cannot be applied to estimate bearing to moving sources which are nearfield (relative to the sensor separation) unless time compression preprocessing is done. Denote the Fourier coefficients of $x_1(t)$ and $x_2(t)$ as in Chapter 3. The 2N+1 vectors $\underline{X}(k)\cong[X_1(k),X_2(\tilde{\beta}k)]'$, k= -N, -N+1,...,N for $\tilde{\beta}\cong 1$, are uncorrelated Gaussian (hence, independent) random variables. More explicitly, because of the independence, the pdf for

$$\underline{X}\equiv\{X_1(-N),X_2(-N\tilde{\beta})\}',\{X_1(-N+1),X_2[(-N+1)\tilde{\beta}]\}',\ldots\{X_1(N),X_2(N\tilde{\beta})\}'$$

given the true values of attenuation α, delay D and time compression β (actually we also are given β_a; hence are "given" $\tilde{\beta}=\beta/\beta_a$) is the product of the individual densities.

Specifically when $\beta_a=1$ and $\beta\cong 1$ the pdf of $\underline{X}$ is

$$p(\underline{X}|\alpha,\beta,D) = \prod_{k=-N}^{N} [h_k \exp(-\tfrac{1}{2}J_k)] \tag{5-27a}$$

where

$$J_k = T[x_1^*(k)x_2^*(k)]Q_x^{-1}(k\omega_\Delta)\begin{bmatrix} x_1(k) \\ x_2(k) \end{bmatrix}, \tag{5-27b}$$

and

$$h_k = [(2\pi)|Q_x(k\omega_\Delta)|^{\frac{1}{2}}]^{-1}, \tag{5-27c}$$

and $Q_x(f)$ is the power spectral density matrix between the random processes $x_1(t)$ and $x_2(t)$.

For ML estimation, it is desired to simultaneously choose as $\hat{D}$ and $\hat{\beta}$ those values which maximize the pdf evaluated for hypothesized compression β_a and hypothesized delay τ. Equivalently, $\hat{\beta}$ and $\hat{D}$ are selected to maximize any monotonically increasing transformation of the pdf. Hence, $\hat{\beta}$ and $\hat{D}$ are selected to maximize the log pdf, namely,

$$J_A = \ln p(\underline{X}|\alpha,\beta,D) \sum_{k=-N}^{N} \ln h_k - \frac{1}{2} \sum_{k=-N}^{N} J_k \quad . \tag{5-28}$$

While the derivation provides sufficient information on estimating the parameters β and D, it is valuable to interpret (5-28) in order to understand both its meaning and its implementation. The award to be maximized (5-28) can be written (assuming large T) as three terms substituting (5-14) and (3-15)

$$J_A = I_{x_1x_2} - \int_{-\infty}^{\infty} \frac{1}{2}\left[\frac{\hat{G}_{x_1x_1}}{G_{x_1x_1}} + \frac{\hat{G}_{x_2x_2}}{G_{x_2x_2}}\right]\left[\frac{1}{1-C_{12}}\right] df + \int_{-\infty}^{\infty} \frac{\hat{G}_{x_1x_2}}{|G_{x_1x_2}|}\frac{C_{12}}{[1-C_{12}]} e^{+j2\pi f\tau} df \cdot \quad (5\text{-}29)$$

Unlike Chapter 3, C_{12} depends on β. Equation (5-29) is difficult to interpret; it is comprised of three terms. For ML estimation (versus AML estimation), only the last two terms of (5-29) depend on the data. However, the parameters β and D appear in all three terms of (5-29); hence, all three terms must be considered. The first term of (5-29) is small with respect to the second term (because, from (5-14), the information has a logarithm in it); also, the first term of (5-29) is small with respect to the third term. Hence, we might expect that the first term can be ignored. However, under some common degenerate cases (specifically, τ=D and T very large) the sum of the second and third terms does <u>not</u> depend on the parameters β and D. For example, for τ=D and very large T, $\hat{G}_{x_ix_i} = G_{x_ix_i}$, i=1,2 and $\hat{G}_{x_1x_2} = |G_{x_1x_2}|e^{-j2\pi fD}$ and the sum of the last two terms of (5-29) becomes $-\int_{-\infty}^{\infty} \frac{1-C}{1-C} df$, which is a constant. This situation is perplexing since the remaining term in (5-29) (namely, the information (5-14)) does <u>not</u> depend on the data, but only on the (assumed known) statistics of the data. It is interesting that when this is the case and when we apply AML techniques (that is, we use estimated data statistics for assumed known statistics), the data do

appear in the expression for the information.

Finally, we notice if as a suboptimum technique, we were to take the first or last term in (5-29) and simply maximize it, that to do so would require adjusting the parameter estimates so as to attempt to increase the coherence across the entire frequency band; the second term of (5-29) does just the opposite. Notice when the time compression is estimated incorrectly, $C_{12}=0$ and only the information I_{12} (or $\hat{I}_{12}$) is needed to estimate compression. Having estimated compression correctly, only the last term of (5-29) is needed to estimate delay. This suggests a suboptimum ad hoc technique for estimating β and D, namely, maximize the information to estimate β then use that $\hat{\beta}$ to estimate D with the award function of Chapter 3. In practice, this suboptimum technique should compare favorably with maximizing (5-29), since there are a number of assumptions and approximations leading to the award function (5-29); most notably, (5-29) presumes $\tilde{\beta}\cong 1$ so that joint second order stationarity holds. When this is not the case, maximizing (5-29) becomes simply an advisable but ad hoc estimation procedure.

There are some degenerate cases of the model (5-18) that are easier to work with analytically (namely, D known and equal to zero, $n_2(t)=0$ and $\alpha=1$). Such models have rather predictable results (namely, the cross-correlation terms are important except as $G_{n_1 n_1}(f)\to\infty$,

that is, as one of the observation channels becomes noise dominated; in the later case, the hypothesized time compression attempts to align the estimated auto spectrum with the (known) signal spectrum). Thus, the degenerate cases do not add insight into the fundamental issue of stationarity. We are thus led to state that maximizing (5-29) (or first (5-14) and then the last term of (5-29)) by choice of $\hat{\beta}$ and $\hat{D}$ (respectively) is merely an intuitively appealing ad hoc technique.

5C. Multiple Sensor Models

The problem we address here is estimation of a parameter vector $\underline{D}$ from a set of sensors with received voltages

$$x_i(t) = \alpha_i s(t+D_i)+n_i(t) \quad i=1,2\ldots \quad . \tag{5-30}$$

Although the notation for D_i is the same as Section A, this model should <u>not</u> be confused with a multiple source model, since this model is only one source but many sensors. To extend the problem to many moving sources received at many sensors requires that

$$x_i(t) = \left\{\sum_k \alpha_{i,k} s\left[\beta_{i,k} t+D_{i,k}\right]\right\}+n_i(t) \quad . \tag{5-31}$$

In the model (5-30), we assume (without loss of generality) that $\alpha_1=1$ and $D_1=0$; thus

$$x_1(t) = s(t)+n_1(t) \tag{5-32}$$

$$\begin{aligned} x_2(t) &= \alpha_2 s(t+D_2)+n_2(t) \\ &\vdots \qquad\qquad \vdots \\ x_M(t) &= \alpha_M s(t+D_M)+n_M(t) \end{aligned}$$

and we desire to estimate the M-1 dimension relative delay vector $(D_2-D_1,\ D_3-D_1,\ldots,D_M-D_1)$.

The general solution to this problem is simply an extension of the alternate realization in Chapter 3, Section 3C. In particular, the steering vector is now

$$V' = [1,\ \alpha_2 e^{-j2\pi fD_2},\ldots,\alpha_M e^{-j2\pi fD_M}] \quad . \tag{5-33}$$

For uncorrelated noises

$$Q_n = \text{diag}[G_{n_i n_i}] \quad . \tag{5-34}$$

The 1xM vector filter is given by

$$\tilde{H} = [\tilde{H}_1,\tilde{H}_2,\ldots,\tilde{H}_M] = \frac{Q_n^{-1}V\sqrt{G_{ss}}}{[1+G_{ss}V'Q_n^{-1}V^*]^{\frac{1}{2}}} \quad . \tag{5-35}$$

Hence, the generalization is realized by extending Figure 3-10 to M prefilters with one at each sensor location as shown in Figure 5-4. A more explicit realization is given in Figure 5-5, which is the extension of Figure 3-11.

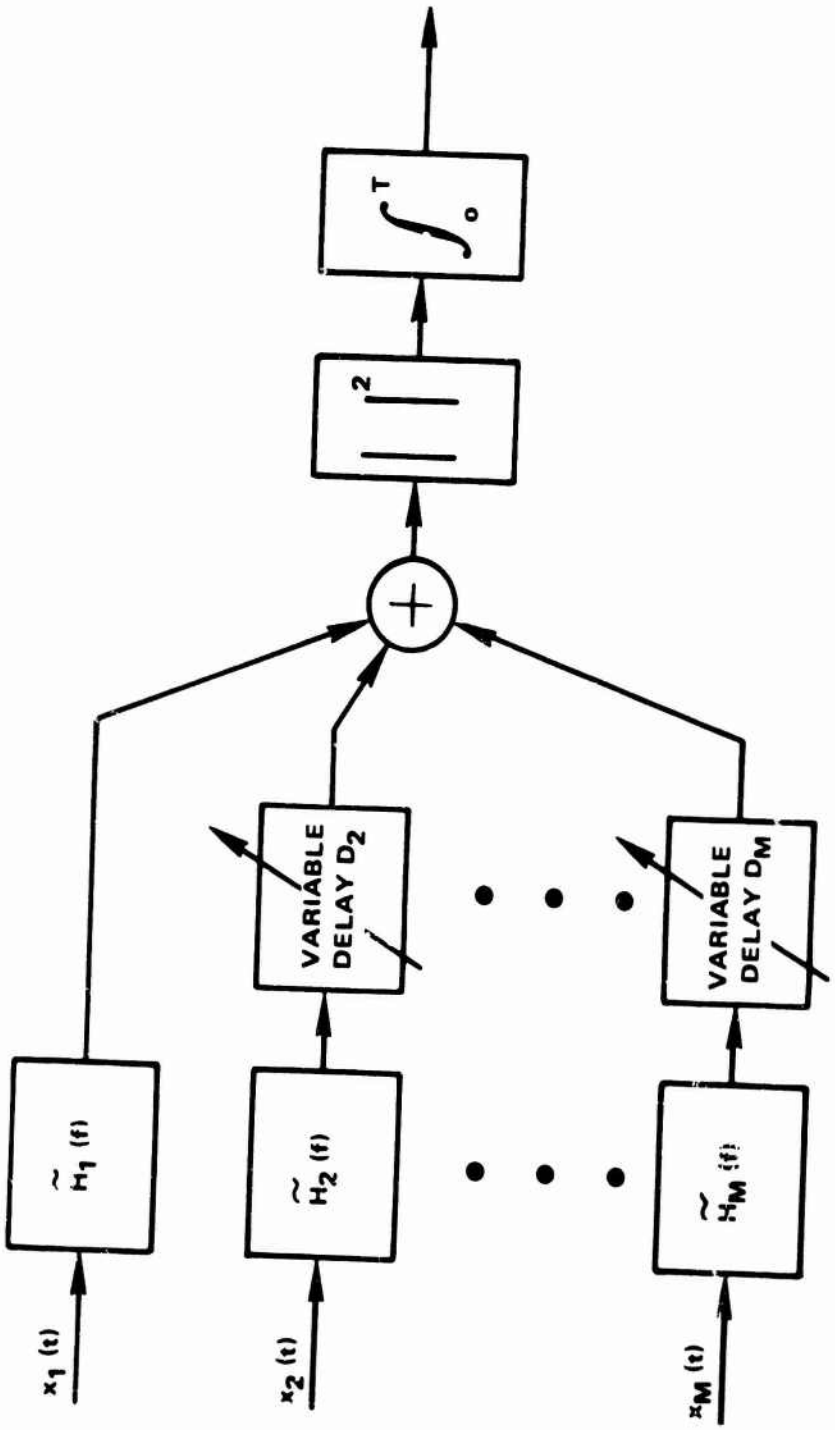

Figure 5-4 Multiple Sensor Estimation of Delay Vector

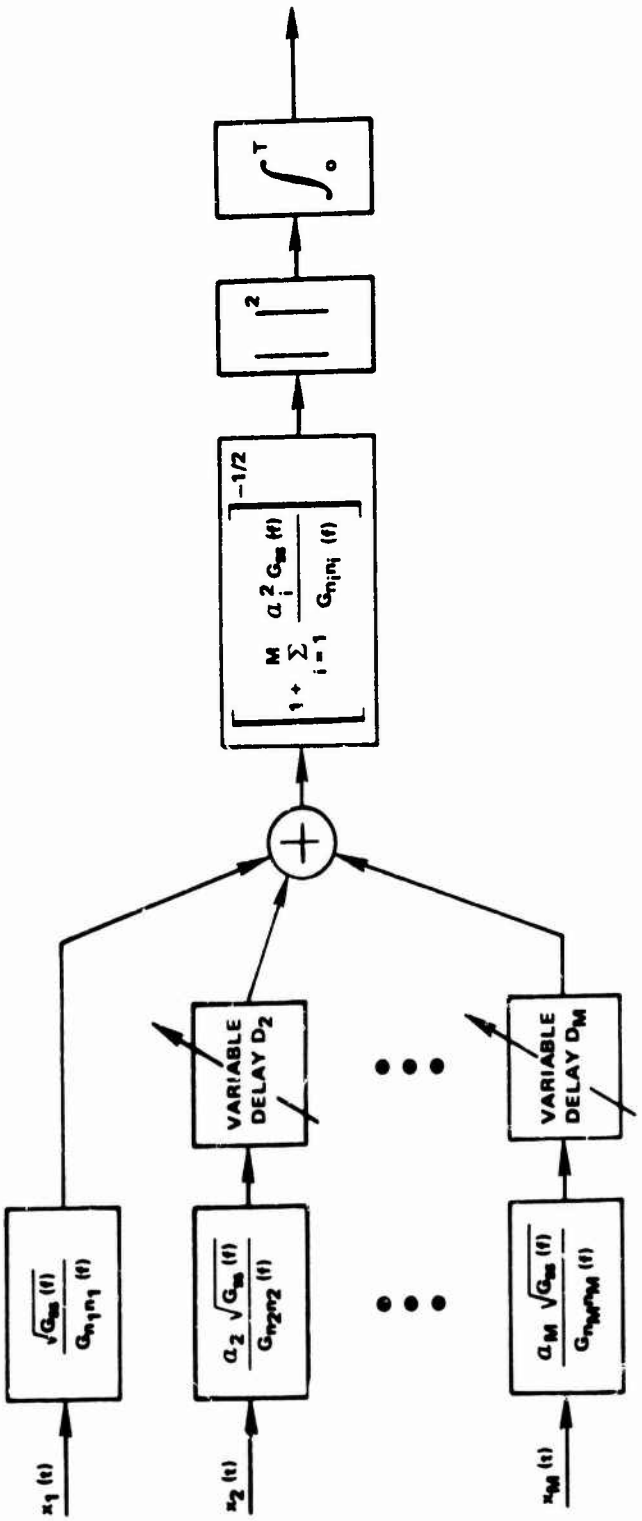

Figure 5-5 Explicit Multiple Sensor Processor for Estimating Delay Vector

CHAPTER 6

DISCUSSION

6A. Applications and Summary

The purpose of this section is to briefly summarize and discuss the applications of this work. Most of the applications are intimately tied to the theoretical results already presented which are summarized in the subsequent paragraphs. The primary purpose of this section is to highlight applications of the theory with a minimum of reliance on mathematical notation. There are three main applications for the theory of time delay estimation discussed in the following three subsections. First, it is a useful vehicle for parameter identification. Second, we can use it to obtain bearing estimates. Finally, under certain conditions we can estimate source position. These applications rely on the theory developed in the preceding text, which is summarized in the following two paragraphs.

This dissertation has investigated methodologies for passive estimation of the bearing to a slowly moving acoustically radiating source. As demonstrated, the mathematics for the solution to this problem is analogous to estimating the time delay between two time series. Because the estimation of time delay is

closely related to the coherence between two time series an extensive investigation of coherence has been presented. New results on using coherence to provide information about linear and nonlinear systems have been presented and proved.

The ML estimate of time delay (under jointly stationary Gaussian assumptions) has been derived. The explicit dependence of the time delay estimate on coherence is evident in the estimator realization in which the two time series are prefiltered (to accentuate frequency bands according to the strength of the coherence) and subsequently crosscorrelated. The hypothesized delay at which the GCC function peaks is the time delay estimate. From the GCC realization the variance of the time delay estimate has been obtained. By use of a different interpretation of the ML estimator derivation, other realizations have been obtained. The GCC realization with ML weighting is compared to several other proposed weightings. The estimation formulation has been extended to three important generalizations: multiple sources, moving source and multiple sensors. Nonstationarities introduced as a result of source motion are studied. These results can now be applied to three problem areas of interest.

6A1. Parameter Identification

In the system identification problem we are given a system with unknown description. We design a probe

to excite the system and ensure that the probe is sufficiently rich in frequency content ($G_{xx}(f)>0$, $f\varepsilon(-B,B)$). Then we simultaneously observe (perhaps record) the probe (input) and response (output) of the system. The objective of these observations is to characterize the system. In Chapter 2 it has been shown that there exists a linear filter which will characterize the system if the MSC is unity at all frequencies. (Appendix C provides a computer program for estimating MSC between two waveforms (input and output).) When the MSC is not unity, the characterization is considerably more complex. We have looked at certain no memory nonlinearities and shown how they can be characterized by orthogonal polynomial expansions.

The main thrust of the dissertation, however, has been to estimate one parameter (delay) when the system is linear, but the observations are corrupted by noise. Proper estimation of just this one parameter requires knowledge of the magnitude transfer function α (or more generally $|\alpha(f)|$), and finally knowledge of the noise spectral densities. When this a priori knowledge is not available, we have proposed estimating the unknown quantities and substituting them in place of the known quantities. There is no rigorous derivation to support this procedure other than to note that as the observation time becomes large the estimated quantities converge to the true ones. Thus, the

methodologies applied to the time delay estimations can be expected to be even more complex if, for example, the filter output were $x_2(t)=\alpha_1 S(t+D_1)+\alpha_2 S(t+D_2)+n_2(t)$. More generally, if $x_2(t)$ was the output of an FIR digital filter of unknown order then the problem of estimating the order, the delays and the attenuations (see Hannan and Thomson (1971), Hannan and Robinson (1973) and Carter and Knapp (1976a)) is a more general problem than the one addressed here. However, to solve the bearing estimation problem motivating this research, the added generality is not required. Thus, the problem considered here is only a subset of the parameter identification problem. Further, note that the solution to the time delay estimation problem does not involve the Fourier transform of the optimum Wiener-Hopf filter (Roth processor), which maps $x_1(t)$ closest to $x_2(t)$; that is, the technique does not look at the peaks or midpoint of the impulse response of the filter that in the MMSE sense filters $x_1(t)$ to obtain an optimum $x_2^o(t)$. With these comments in mind, we have generalized our model to an important class of nonstationarities in order to estimate bearing.

6A2. Bearing Estimation

The bearing estimate follows directly from the delay estimate according to the simple arccos transformation (3-2). The range does not need to be too great relative to the sensor separation in order for the

angle that the hyperbola asymptote makes with the baseline to accurately represent the source bearing. For stationary sources or closely spaced sensors, the relative Doppler (or more generally, the time compression) can be ignored. However, to apply these techniques to widely separated sensors and moving sources, it is necessary to process the data in order to perform Doppler correction (that is, a time scale correction or time scale expansion). To ignore this processing would result in an apparent uncorrelated behavior between the two received waveforms. One contribution of this work has been to specify an ML estimate of time compression. However, because of the nonstationarity of the processes involved, the results tend to be more heuristic and more difficult to interpret (and implement) than those for the time delay estimation problem. In fact, the implementation is hindered by practical computational issues of achieving the time compression. Nevertheless, in the future as computational methods allow for broadband time compression, the methods hypothesized here could actually be tested in practical environments. This should not be interpreted to mean that time compression cannot currently be accomplished. Exact time compression can be achieved, as for example, with variable speed tape recorders or with exact DFT's. Approximate time compression can also be achieved through complex inter-

polation of FFT points or nearest FFT bin approaches. In practice, all of these techniques are expensive to implement; hence, any production application of the theory will benefit from advances in methodologies and mechanizations for achieving time compression. Having techniques for estimating the bearing to moving acoustic sources, we can extend the applications of our theory to estimating range.

6A3. Passive Ranging

In the two sensor models, we are able to estimate delay from which we can estimate bearing. In the multiple sensor situation more information is available. Indeed, with three sensors we can also estimate source location. For example, in Figure 6-1 three equispaced collinear sensors are depicted. As indicated in section 5C, the estimate of θ_1, θ_2 requires simultaneously processing data from all three sensors (one suboptimum processor would be to estimate each bearing from generalized crosscorrelations between only two sensors). When the sensor-pair midpoints are separated by distance d (meters), the range (meters) to the source is given by

$$R = \frac{d\sin\theta_2}{\sin(\theta_1-\theta_2)} \quad . \tag{6-1}$$

An estimated range is obtained by inserting estimated

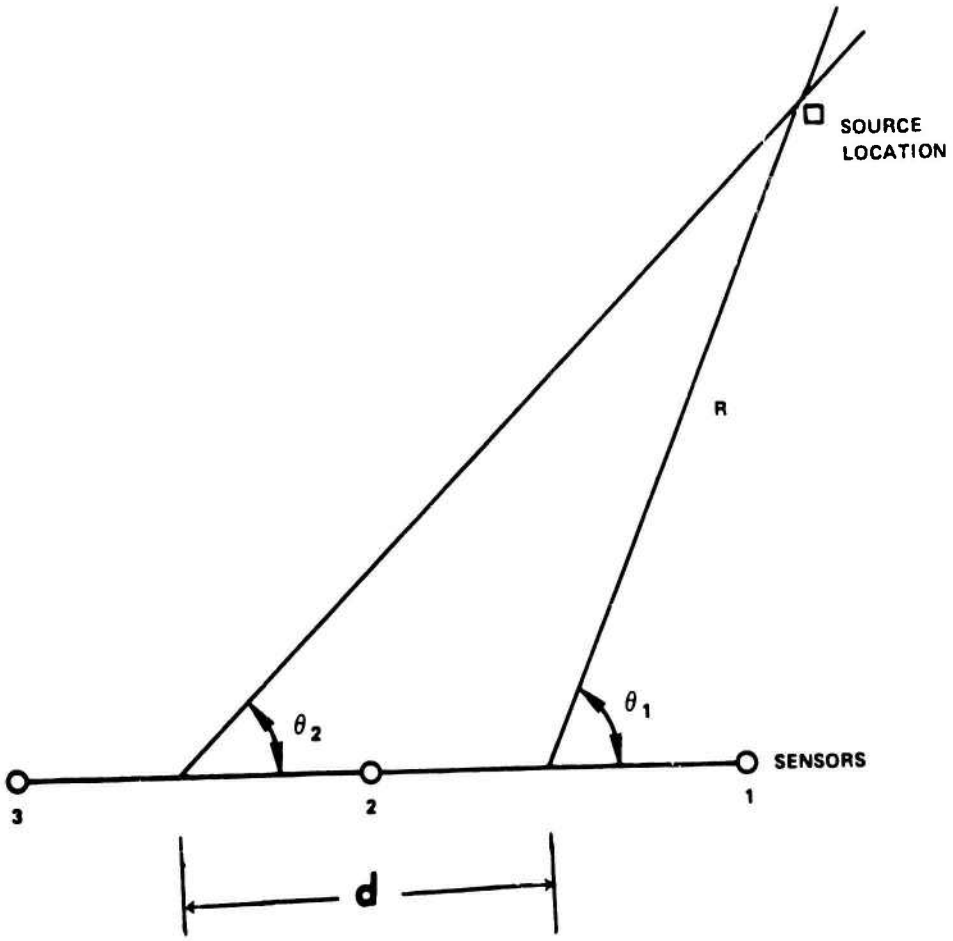

Figure 6-1 Three Collinear Sensors, Single Source Passive Ranging Geometry

bearings in (6-1).[1] The asymptotes depicted in Figure 6-1 are upper bounds (biased estimates of hyperbolic LOP's); hence, the actual source location will be slightly "below" the intersection depicted. For R>>d, the bias will not be a practical concern.

For more complicated sensor geometries (see Figure 6-2), the bearings Θ_1 and Θ_2 are used to obtain effective bearings Θ_1^e and Θ_2^e. When the sensor geometry is known, the effective bearings are easily obtained by the addition of a correction term to the observed bearing. Similarly, the effective separation d_e is simply the shortest distance between the midpoints of the sensor pairs (1,2) and (2,3). The range estimate is then obtained by substituting effective measurements into (6-1). When four or more sensors are used to estimate three or more LOP's, source position may be ambiguously specified, as shown by points A, B, C in Figure 6-3. In such a case, it is reasonable to presume that the source is the least squares distance from existing LOP's; although it is possible for two or three sources to be present.

---

[1]The estimated position (range and bearing, in polar coordinates) obtained by substituting ML estimates of the bearings into (6-1) is <u>not</u> necessarily the ML estimate of position.

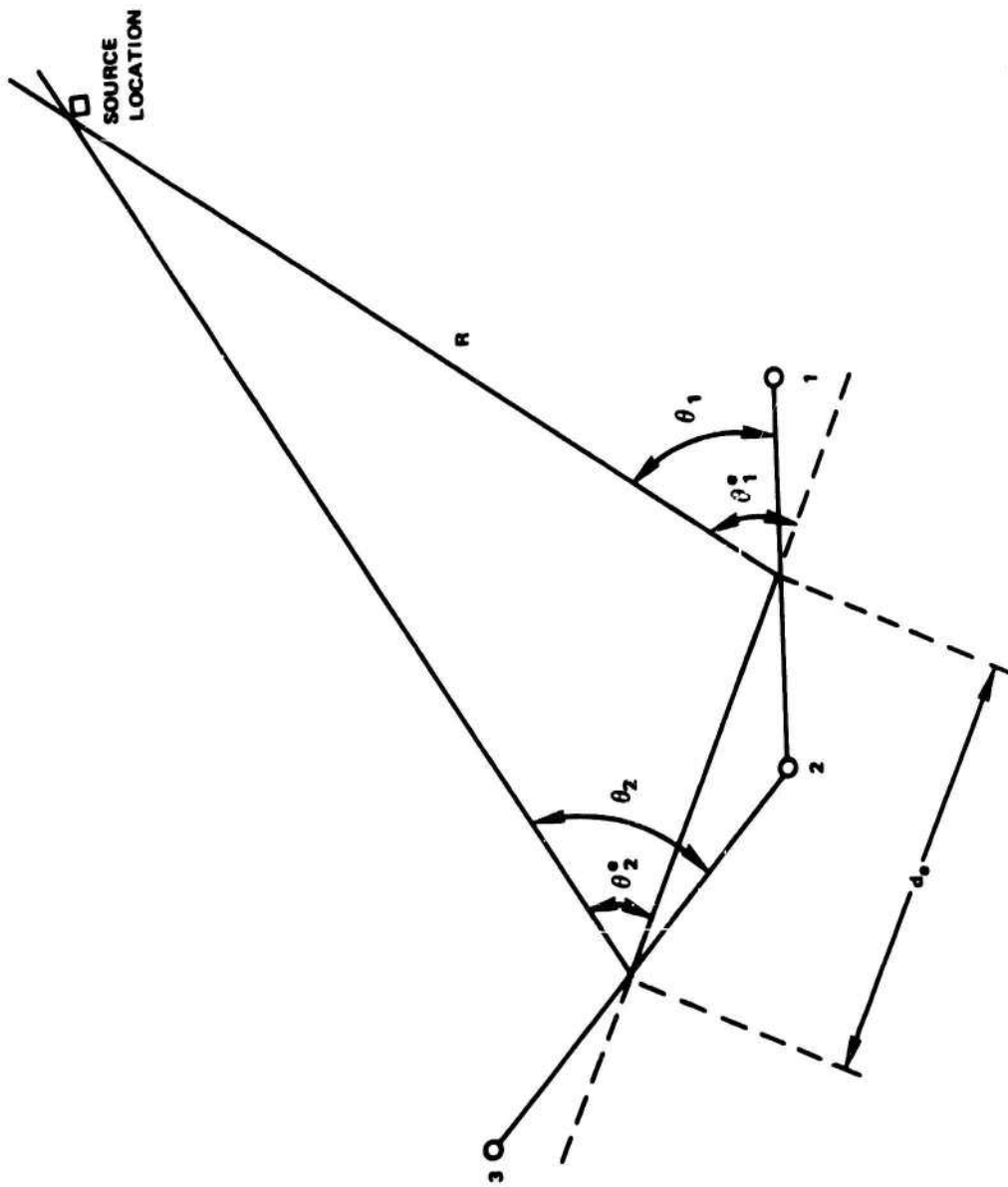

Figure 6-2 Three Noncollinear Sensors, Single Source Passive Ranging Geometry

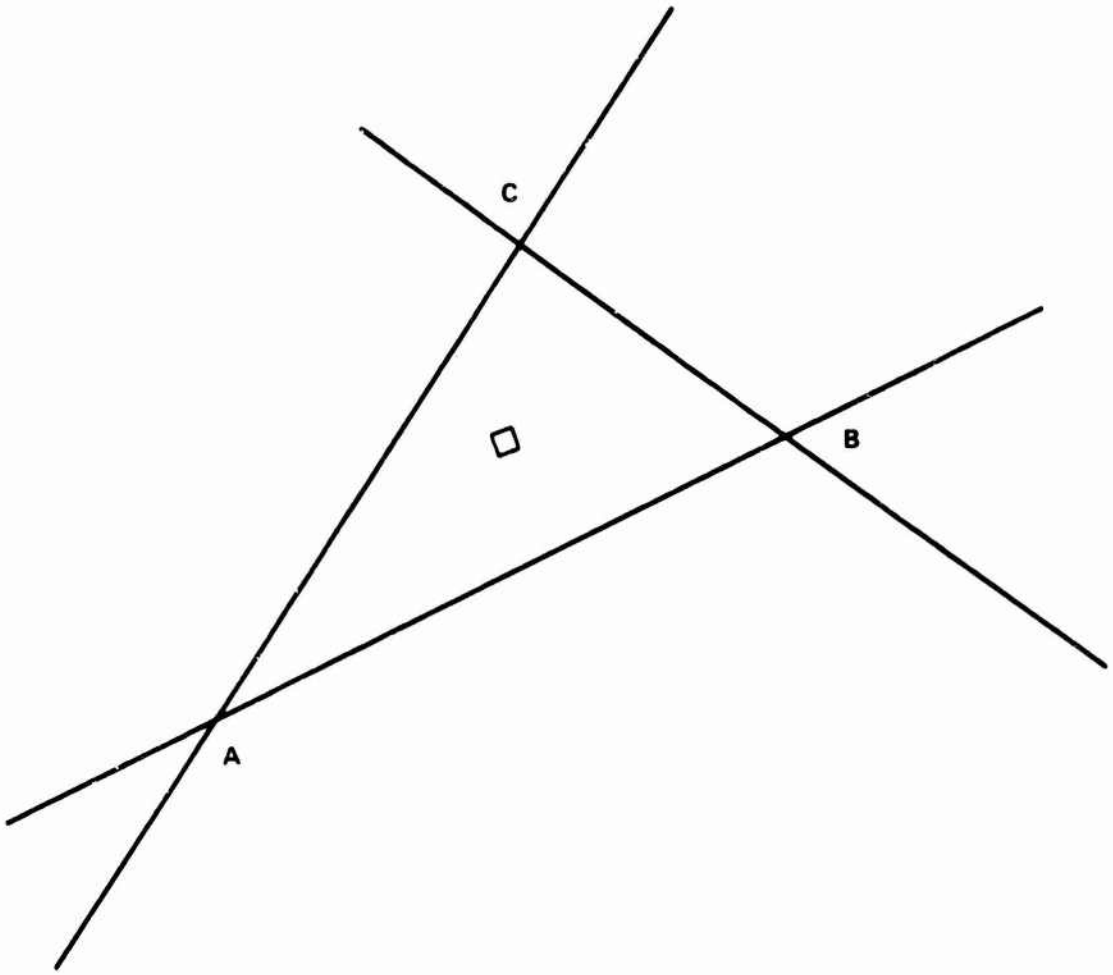

Figure 6-3 Three Estimated LOPs to One Source

6B. Suggestions for Future Work

This section suggests four areas for future work. In a sense, it provides an insight into what we still do not know about the problem at hand. Or stated differently, having solved the problem we set out to solve, we now understand how to pose new problems which we have uncovered. First, in the parameter identification area there appear to be several fruitful research questions: How to identify parameters for (1) general (or particular) nonlinear systems, (2) multi-input, multi-output linear systems, (3) general linear systems, and finally (4) "real world" socio-economic systems. The complexity of estimating time delay suggests that the solution to these problems will be more complex.

The second area is verification of the theory by simulation. We have already conducted one costly computer experiment (Appendix D) which substantiates our belief that insertion of estimated spectra for true spectra enhances the estimation of time delay. However, without running many such experiments, we have no statistical argument to substantiate the theory. Because the cost of running this analysis is prohibitive on a large scale, digital computer, special purpose FFT hardware should be used to empirically validate the theory. The cost of such a system will be significant.

The third area of investigation is an extension of the theory to sequential estimation. In practice, our observation interval will not be just T seconds; rather there will be several consecutive periods of T seconds. Knowing that the source is constrained in its rate of speed, we should be able to rule out certain ambiguous estimates of delay (bearing). More generally, we could model the ship's track and use Kalman filter techniques to extrapolate best projected position (bearing) based on the filter outputs.

Finally, the theory presumes a great deal about (1) ocean acting as a linear time invariant filter over the observation period T, (2) the characteristics of the noise, and (3) the source motion. Thus, the true engineering test is to make controlled measurements with actual acoustic sources in the ocean in order to test the hypothesis. Based on what we currently know, there is every reason to believe such an endeavor will be successful.

APPENDIX A

TECHNIQUES FOR SPECTRAL ESTIMATION

The basic objective of this appendix is to briefly describe two (similar) techniques used to estimate the elements of the power spectral density matrix. The estimates obtained are then used to form an AML estimate of time delay. The two techniques are the overlapped FFT technique (discussed by Carter, Knapp, and Nuttall (1973a)) and the Chirp-Z transform (CZT) technique (discussed by Carter and Knapp (1975)). The methods discussed are sometimes referred to as direct methods (as opposed to indirect correlation methods) and have been discussed in part by Knapp (1966), Welch (1967), Bingham, Godfrey and Tukey (1967), Benignus (1969a), Nuttall (1971), Williams (1971), and Rabiner and Rader (1972).

Both methods begin with two (one from each process) digital waveforms (or with analog waveforms that have been lowpass filtered and digitized). Briefly, there are four steps in the estimation procedure: First, each time series is segmented into N segments, each having P-data points. Second, each segment is multiplied by a smooth weighting function. Third, the Z transform of the weighted P-point sequence is evaluated on the unit

circle in the Z-plane. Finally, the Fourier coefficients thus obtained are used to estimate the elements of the power spectral density matrix by averaging "raw" power spectral estimates over all the N segments. The two methods of spectral estimation differ in how the Z transform is evaluated. One method uses the FFT; the other uses the Partitioned and Modified CZT (PAM-CZT).

More explicitly, two random processes that are jointly stationary over N data segments are processed as follows (Carter and Knapp (1975)):

1. Each of the two time series is segmented into N segments of P points. The segments may either be disjoint or overlapped. Then one segment of P data points with the same time origin is selected from each of two time records. Even if each of the N data segments is large (for example, greater than 4096), P should be selected to ensure that the sampling frequency divided by P will afford adequate spectral resolution.

2. Each of the two P point segments is multiplied by a smooth weighting function. Here smooth means that the ℓ-th order derivative is continuous over the full interval of data points, for ℓ=0, 1, 2, ... up to some reasonable limit. The smoother the weighting function, the more rapidly the side lobes of its Fourier transform, or window function, will decay. The more impulse-like the window, the less leakage there will be of extraneous power, which corrupts spectral measurements.

Hence, good weighting functions result in better spectral estimates. The price paid for impulse-like window functions with rapidly decaying side lobes is a wider main lobe, that is, poorer frequency resolution when P is held fixed. If better resolution is desired, more data points per segment will be required. This in turn requires both that the data be available and that they can be efficiently processed. Moreover, from a stability point of view, increasing P decreases the available number of independent data segments when the data duration is finite.

The specific selection of a weighting function involves a number of tradeoffs. A commonly used weighting (or windowing) function is the cosine (Hanning) function defined at the p-th instant in the interval (0,P) as

$$\frac{1}{2}\left(1 - \cos\frac{2\pi p}{P}\right);$$

such a function starts out at zero for p=0 smoothly rises to unity by p=P/2 and smoothly decays to zero at p=P.

The application of a cosine-weighting function, which is necessary to reduce errors due to side lobe leakage, has the disadvantage of apparently wasting the available data. This apparent wastage can be overcome through overlapped processing. In particular, Nuttall (1971) has shown that the same stability (as measured by the number of equivalent degrees of freedom) can be obtained from a fixed amount of data via overlapped

processing as with Blackman and Tukey (1958) correlation processing for both auto and cross spectral density estimation. (Results on cross spectra processing followed in a supplemental report.)

Quite naturally, there is an increase in computational cost associated with overlapped processing. Specifically, the number of FFTs to be performed (a measure of the computational cost) increases with the percent overlap specified. For example, the number of FFTs required for 50-percent overlap is approximately twice the number for 0-percent overlap. Increasing the overlap from 50-percent to 62.5 percent requires 32-percent more FFTs. For Hanning weighting, the improvement to be derived from using 62.5-percent overlap, as opposed to 50-percent overlap, will not usually warrant the increased computational costs (Carter, Knapp, and Nuttall (1973a)).

Note that if there is no overlap, each segment would be virtually independent of the previous one (except for correlated edge effects). Independent data segments facilitate certain analytic computations. Hence, all theoretical results here are concerned with the case of independent segments; that is, no overlap. This is true even though overlapped processing is recommended for actual data processing. The amount of overlap desirable can be predicted by picturing the apparent wastage for a specific weighting.

3. The transform of the weighted P-point sequence is evaluated on the unit circle in the z plane. The two sided Z-transform of an infinite sequence is defined by Gold and Rader (1969) and Oppenheim and Schafer (1975) as

$$X_n(z) = \sum_{p=-\infty}^{\infty} x_n(p) z^{-p}, \quad n=1,2,\ldots,N \ , \qquad \text{(A-1)}$$

where z equals any complex variable.

Similarly, $Y_n(z)$ is defined as the Z-transform of $y_n(p)$. When $x_n(p)$, $y_n(p)$ are finite in duration, the infinite series (A-1) becomes finite. Evaluation of the Z-transform at P equally spaced points around the circle yields the DFT:

$$X_n(k) = \sum_{p=0}^{P-1} x_n(p) e^{-j2\pi pk/P} \ . \qquad \text{(A-2)}$$

Similarly, $Y_n(k)$ is the DFT of the n-th weighted data segment $y_n(p)$, $p=0,1,\ldots,P-1$. The DFT can rapidly be evaluated by two methods: the Cooley-Tukey (1965) or the PAM-CZT (see, for example, Rabiner, Schafer, and Rader (1969), Schilling (1972), Ferrie, Nawrocki, and Carter (1973), and Carter and Knapp (1975)). The FFT is a fast algorithm for evaluating the DFT. If the DFT, (A-2), is evaluated for P frequencies ($k=0,1,\ldots,P-1$) it requires P^2 (complex) multiplications and additions (MADs). The FFT uses an ingenious computation method to evaluate (A-2) in just $P\log_2 P$ MADs. Thus, for P=4096, the number of MADs is reduced by a factor of more than 340. Thus,

computations requiring more than 5 hours can be done in less than 1 minute using FFTs in lieu of DFTs. Specific details of the FFT are beyond the scope of this dissertation.

The DFT, (A-2), is a special case of the CZT, which was introduced by Rabiner, Schafer, and Rader (1969) and amplified, including software implementation, by Schilling (1972)[1] and hardware development by Alsup, Means, and Whitehouse (1973), and Buss, Collins, Bailey and Reeves (1973). Given sufficient data, it is a fast and efficient technique for computing the Z-transform of a sequence on any Z-plane spiral. The modified CZT (MCZT) evaluates equispaced frequency points on the unit circle in the Z-plane. With proper spacing and starting points, it is equivalent to the DFT. Computationally, the MCZT requires three FFTs each of size greater than N (for example, 2N) to compute the DFT, (A-2). However, the tradeoffs are really more complex than this. (For example, if many MCZTs are to be performed one of the three required FFTs does not need to be repeated after its first computation since it is a transformed cosine data table.) The major advantage of the MCZT occurs when the number of data points P (in each of the N data segments) is large.

---

[1]This work was brought to the author's attention by Dr. N. Ahmed, Kansas State University, Manhattan, Kansas.

In such cases, the original P point data segment can be again segmented into R partitions each disjoint with size P/R data points. The R partitions are processed with R MCZTs; the outputs are summed together with appropriate phasing to achieve a PAM-CZT that is equivalent to the DFT, (A-2),. The mathematical details of this technique are covered in length by Ferrie, Nawrocki, and Carter (1975); their inclusion here does not appreciably add to the discussion but does considerably complicate the notation due to conflicts with assigned symbols. For most broad band cases of interest (and certainly the example case in Appendix D), the FFT will be preferable to the PAM-CZT. A complete discussion of the tradeoffs is given by Carter and Knapp (1975).

Having computed the DFT, (A-2), either by an FFT or PAM-CZT, we are ready to proceed with the fourth step in the spectral estimation algorithm.

4. The spectral estimates are

$$\hat{G}_{xx}(k) = c_g \sum_{n=1}^{N} |X_n(k)|^2, \qquad \text{(A-3a)}$$

$$\hat{G}_{yy}(k) = c_g \sum_{n=1}^{N} |Y_n(k)|^2, \qquad \text{(A-3b)}$$

$$\hat{G}_{xy}(k) = c_g \sum_{n=1}^{N} X_n(k) Y_n^*(k), \qquad \text{(A-3c)}$$

where the constant

$$c_g = \frac{1}{N \cdot f_s \cdot P} \quad , \tag{A-3d}$$

and $f_s \equiv$ sampling frequency. (The estimated cross spectrum (A-3c) is complex.) The estimate of MSC

$$\hat{C}_{xy}(k) = \frac{|\hat{G}_{xy}(k)|^2}{\hat{G}_{xx}(k)\hat{G}_{yy}(k)} \quad . \tag{A-4}$$

The AML estimation of time delay requires substituting the estimates $\hat{C}_{xy}$ in place of the true (but unknown) value of MSC. Therefore, we are concerned about the statistical variability of the MSC. Further, the statistical characteristics of $\hat{C}$ are of interest in their own right, since $\hat{C}$ is useful not only in time estimation (Chapter 3) but also for other applications (Chapter 2). Appendix B discusses the statistics of the MSC estimate.

APPENDIX B

STATISTICS OF THE MSC ESTIMATE

The MSC estimate, from (A-3) through (A-4), is

$$\hat{C}_{xy}(k) = \frac{\left| \sum_{n=1}^{N} X_n(k) Y_n^*(k) \right|^2}{\sum_{n=1}^{N} \left| X_n(k) \right|^2 \sum_{n=1}^{N} \left| Y_n(k) \right|^2} , \qquad \text{(B-1)}$$

where N is the number of data segments employed and $X_n(k)$, $Y_n(k)$ are the DFTs of the n-th weighted data segments of x(t), y(t), respectively. Under certain assumptions the statistical characteristics of $\hat{C}$ can be evaluated. This appendix is divided into four sections. The first section gives the pdf, cumulative distribution function (cdf), and m-th moment of $\hat{C}$, given C and N. The second section gives the bias of the estimate $\hat{C}$ including a discussion of when the analytic results fail and simulations to support the theory. The third section gives the variance of $\hat{C}$. The fourth section gives a computer program for evaluating receiver operating characteristics (ROC) of a linearly thresholded coherence estimation processor. The results in all four sections are based on the derivation by Goodman (1957) of an analytical expression for the pdf of the MC estimate and the subsequent extensions to

MSC by Carter, Knapp, and Nuttall (1973a). These results are based on two zero-mean stochastic processes that were jointly stationary, Gaussian, and had been segmented into N independent segments.[1] Each segment was assumed large enough to ensure adequate spectral resolution. Further, each segment was assumed perfectly weighted (windowed), in the sense that the Fourier coefficient at some k-th frequency was to have "leaked" no power from other bins. The statistics do not hold at the zero-th or folding frequencies (Hannan (1970)). Extensions to Goodman's work are given by Alexander and Vok (1963), Amos and Koopmans (1963), Enochson and Goodman (1965), Nettheim (1966), Wahba (1966), Tick (1967), Carter and Nuttall (1972), Carter, Knapp and Nuttall (1973b), Halvorsen and Bendat (1975), and Nuttall and Carter (1976a).

B1. Probability Density, Cumulative Distribution and m-th Moment of $\hat{C}$

The first-order pdf, cdf and m-th moment of the estimate of MSC, given the true value of MSC and the number, N, of independent segments processed, are presented in this section in closed form.

---

[1] Despite the fact that it is only mathematically tractable to obtain analytic expressions when the segments are independent, we would in practice use some overlapped processing to regain the apparent data wastage incurred by the necessity of data weighting. Carter, Knapp, and Nuttall (1973a) report the results of an empirical study that demonstrates how bias and variance decrease as a function of increased data segment overlap. Fifty percent overlap is recommended with cosine weighting.

The conditional pdf for $\hat{C}$, between two processes, given C and N, is (Carter, Knapp, and Nuttall (1973a))

$$p(\hat{C}|N,C) = (N-1)(1-C)^N(1-\hat{C})^{N-2}\ (1-C\hat{C})^{1-2N}\ {}_2F_1(1-N,1-N;1;C\hat{C}). \tag{B-2}$$

The ${}_2F_1$ is a hypergeometric function with two numerator terms and one denominator term. (It is a special case of (B-7) and is discussed more fully in Section B4.) For present, we note equation (B-2) is desirable because ${}_2F_1(1-N,1-N;1;C\hat{C})$ can be expressed as an (N-1)st order polynomial (Abramowitz and Stegun (1964), Equation (15.5.1)).

A special case of the density function occurs when C=0. In that event,

$$p(\hat{C}|N,C=0) = (N-1)(1-\hat{C})^{N-2}\ . \tag{B-3}$$

Using a result of Fisher (1950), Carter, Knapp, and Nuttall (1973a) have determined (in closed form) the cumulative distribution of the estimate of MSC, namely,

$$P(\hat{C}|N,C)=\hat{C}\left(\frac{1-C}{1-C\hat{C}}\right)^N \sum_{k=0}^{N-2}\left(\frac{1-\hat{C}}{1-C\hat{C}}\right)^k \cdot\ {}_2F_1\left(-k,1-N;1;C\hat{C}\right). \tag{B-4}$$

A digital computer program to evaluate equation (B-4) is given in Section B4. In the special case when C=0, the cdf can be simplified to give

$$P(\hat{C}|N,C=0) = 1-(1-\hat{C})^{N-1}\ . \tag{B-5}$$

Equation (B-5), when differentiated, yields the pdf equation (B-2).

The m-th moment of the MSC estimate can be found by application of Equation 7.512(12) by Gradshteyn (1965) to

a different form of (B-1) to yield (Carter, Knapp, and Nuttall (1973a))

$$E[(\hat{C}^m|N,C)] = (1-C)^N \frac{\Gamma(N)\,\Gamma(m+1)}{\Gamma(N+m)}$$

$$\cdot\ {}_3F_2(m+1,\ N,\ N;\ m+N,\ 1;C) \quad . \qquad \text{(B-6)}$$

These results can be confirmed using Carter (1972a) and Anderson (1958).

The ${}_3F_2$ hypergeometric functions (with three numerator terms and two denominator terms) are given by

$${}_3F_2(a,b,c;\ d,e;\ z) = \sum_{k=0}^{\infty} \frac{(a)_k(b)_k(c)_k}{(d)_k(e)_k} \frac{z^k}{k!} \quad , \qquad \text{(B-7a)}$$

where the $(a)_k$ notation is Pochhammer's symbol (Abramowitz and Stegun (1964)) defined by

$$(a)_k \triangleq \frac{\Gamma(a+k)}{\Gamma(a)} \quad , \qquad \text{(B-7b)}$$

where $\Gamma(\ )$ is the Gamma function. Similarly, the F two-one function has two numerator and one denominator terms.

B2. Bias of $\hat{C}$

This section deals with the bias of the MSC estimate. Exact and approximate expressions are presented. In addition, computer evaluation of the exact expressions is presented to lend meaning to these results, and two computer simulations are presented. The first simulation demonstrates the need to have adequate spectral resolution. The second simulation verifies the theoretical results for bias (and also variance, which is discussed in the next section, B3).

Consider now the first moment of the estimate of MSC which can be written as

$$E[\hat{C}|N,C] = \frac{(1-C)^N}{N} \; {}_3F_2(2,N,N;N+1,1;C) \quad , \tag{B-8}$$

which can be manipulated into the form (Carter (1972a))

$$E(\hat{C}|N,C) = \frac{1}{N} + \frac{N-1}{N+1} C \; {}_2F_1(1,1;N+2;C) \quad . \tag{B-9}$$

The bias or expected estimation error is defined as

$$\text{Bias} = B(\hat{C}|N,C) = E(\hat{C}|N,C) - C \quad . \tag{B-10}$$

An exact expression for the bias is

$$B(\hat{C}|N,C) = \frac{1}{N} + \frac{N-1}{N+1} C \; {}_2F_1(1,1;N+2;C) - C \quad . \tag{B-11}$$

The maximum bias is 1/N (regardless of N and C). The bias is plotted in Figure B-1. It should be noted that

$$\lim_{N\to\infty} (\text{Bias}) = 0 \quad ; \tag{B-12}$$

therefore, the estimator may be referred to as asymptotically unbiased. By expanding ${}_2F_1$ in (B-11) in a power series in C and retaining terms to order N^{-2}, the following approximation is obtained (Nuttall and Carter (1976b)):

$$B_1(C,N) = \frac{1}{N}(1 - C)^2\left(1 + \frac{2C}{N}\right) \quad . \tag{B-13}$$

Plots of N B(C,N) and N B_1(C,N) are presented in Figure B-2 for N=4 (they cross near C=0.4). Approximation (B-13) is seen to be excellent over the entire range of C. Furthermore, the discrepancy between the approximation (B-13) and the true bias (B-11) is even less for larger

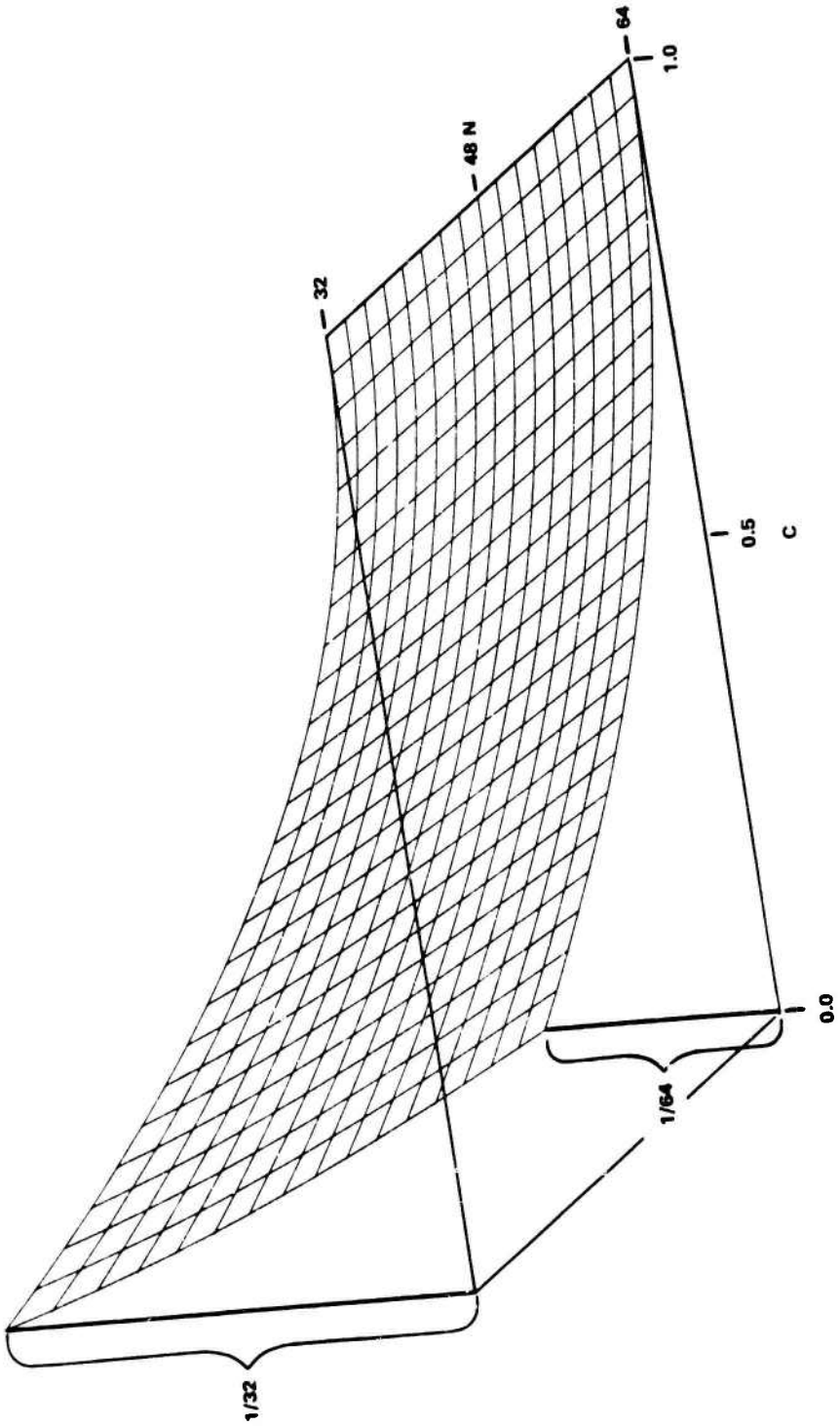

Figure B-1 Bias of $\hat{C}$ versus C and N

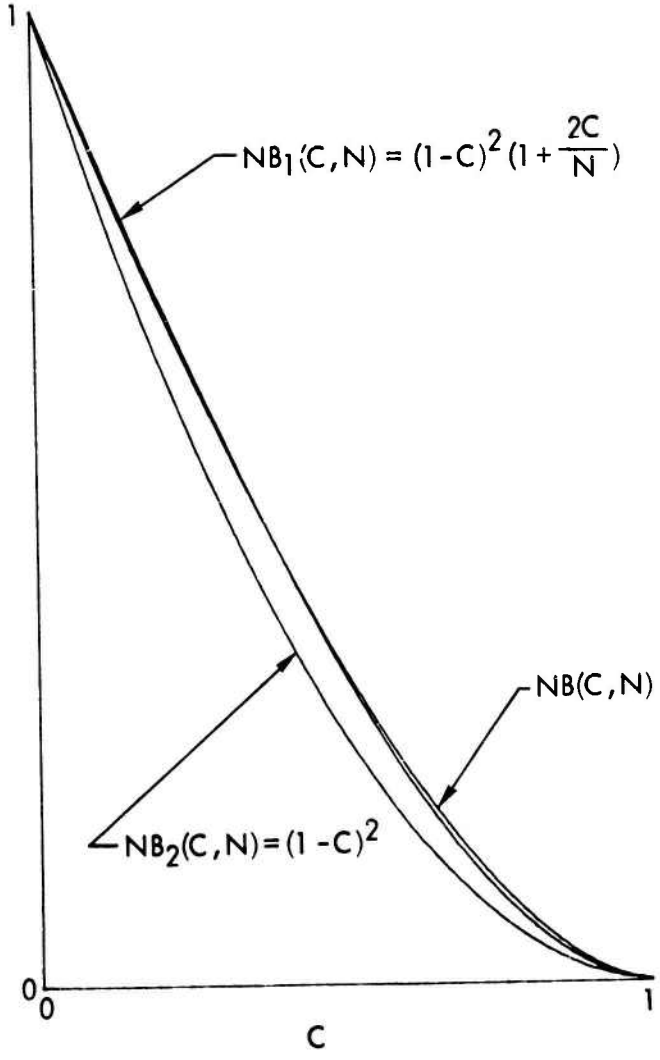

Figure B-2 Bias of $\hat{C}$ and Approximations for N=4

values of N.

For large N, (B-13) is further reduced to the approximation given by Carter, Knapp, and Nuttall (1973a):

$$B_2(C,N) = \frac{1}{N}(1-C)^2; \text{ good for large } N \ . \qquad (B\text{-}14)$$

Therefore, as N leads to infinity, N B(C,N) tends to $(1-C)^2$, which is also plotted in Figure B-2; furthermore, the approach is monotonic.

In Benignus (1969a), (2), an approximate expression for the bias, based upon a simulation approach, is presented as

$$B_3(C,N) = \frac{1}{N}(1-C) \ . \qquad (B\text{-}15)$$

Whereas the results in Haubrich (1965) and (B-14) dictate a quadratic behavior for bias, the approximation by (B-15) indicates a linear behavior. Since (B-11) through (B-14) is based upon theory and (B-15) is based upon simulation, it was decided to verify (or invalidate) (B-11) through (B-14) by a simulation approach. Two computer simulations were conducted.

In order to verify the theory, the simulation must preserve those assumptions present in the derivation of the theoretical expression (B-11) for bias. Specifically, as pointed out by Carter and Knapp (1975), (B-11) holds under the following assumptions:

1. jointly Gaussian stationary processes
2. N independent (non overlapped) data segments

3. smooth weighting function to reduce side lobe leakage

4. adequate frequency resolution

When any of the specified assumptions are violated, analytic results derived for bias (and variance) of the estimator can be grossly misleading. (The Gaussian part of the first assumption is weak; see the discussion after (3-3).) As an empirical verification of this statement, consider the study reported by Carter and Knapp (1975), where $C_{xy}(f) = 1, \forall f$. Specifically, consider a simple linear second-order digital filter of the form

$$Y_n = 1.97300Y_{n-1} - 0.98202Y_{n-2} + 0.00872X_n . \quad \text{(B-16)}$$

The system behavior was studied by probing the filter with a white pseudorandom noise source. The sampling rate was set equal to 2048 Hz; hence, the Nyquist rate of π radians is depicted as 1024 Hz in the figures that follow.

The filter phase characteristics were estimated, Figure B-3, with P=1024, cosine weighting, and 64 independent segments. Despite the fact that the MSC between input and output should equal unity (hence, the bias of the estimator would normally be zero), the estimate of MSC is grossly biased when a rectangular weighting function is used. Specific MSC estimates are depicted in Figure B-4 for the rectangular weighting case. The bias attributable to improper windowing, while

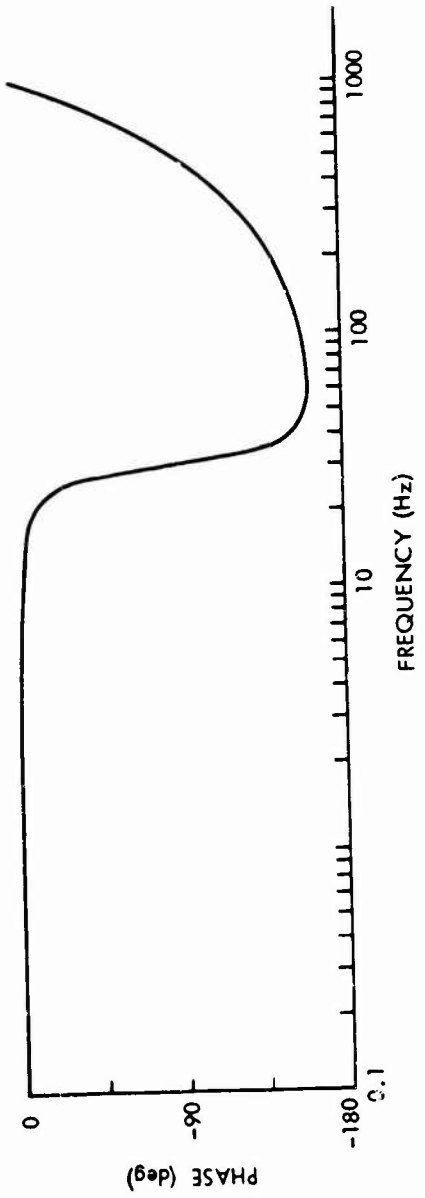

Figure B-3 Phase Characteristics of Second Order Linear Filter

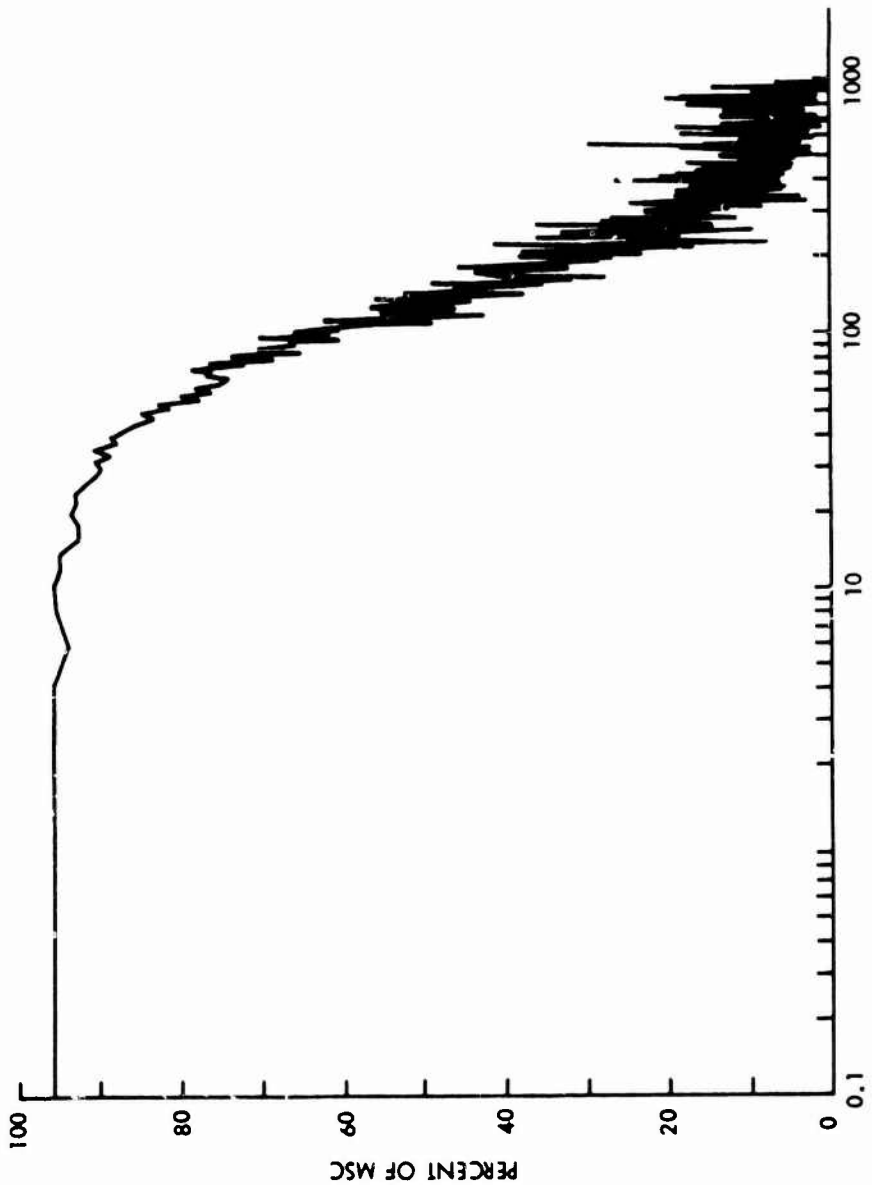

Figure B-4 Biased Estimates of C (True Value of C is Unity) Due to Rectangular Weighting Function

severe, can be substantially eliminated through selection of a leakage-suppressing window. When a cosine or Hanning window is utilized and the data are reprocessed, estimates depicted in Figure B-5 are obtained. Notice now that the bias, though greatly improved, still exists in the vicinity of 30 Hz. Referring to Figure B-3, notice that 30 Hz is the center of a frequency band in which the first derivative of the phase is large. The dependence of the bias of the MSC estimate on this characteristic of phase is predicted in Jenkins and Watts (1968), Hannan (1970), and Koopmans (1974).

Once sufficient resolution has been achieved, this bias no longer exists. To determine whether the bias in Figure B-5 could be reduced by more averaging, as analytically predicted by the approximation in Jenkins and Watts (1968), additional independent data segments were processed in the simulation (that is, N was made larger without changing P). In this case of insufficient resolution, the maximum bias error was observed to be independent of the number of segments averaged; that is, the estimator is biased as $N \to \infty$ when the number of data points per segment is small.

When large amounts of data are used, as in the case of a computer simulation, better resolution can be obtained without loss of averaging (variance reduction) capability. However, when the data are of limited

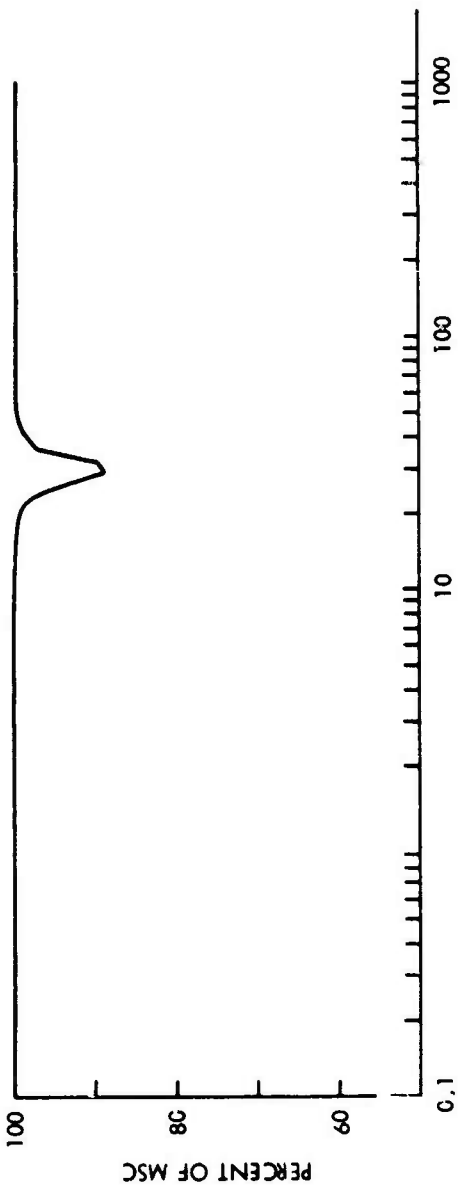

Figure B-5 Example of Biased Estimates of C Due to Inadequate Frequency Resolution

duration then--dependent on the length of actual data cuts and the stationarity of events over that duration--another method can be employed to improve MSC estimation in the face of rapidly changing phase angles. These methods are referred to as alignment, or translation methods, and are used to remove the time delay or group delay of a filter. Translation (that is, prefiltering by a single time delay) of one time series with respect to another permits the rate of change of the phase in a particular frequency band to be controlled and reduced to yield better MSC estimates in that frequency band. The implication is that MSC estimates are valid in frequency bands where the phase has little or no slope. Various methods for estimating the time delays are discussed in Chapter 4.

Translation was applied to align the time series for the example presented here. After alignment, unbiased estimates were obtained in a 20 Hz band about 30 Hz; however, as expected, outside that band, biases were severe, making interpretation meaningless. In general, translation must be applied for "all" time delays and the results combined into one result (graph); hence, when sufficient data are available, the author's preference is for finer frequency resolution rather than for the piecemeal approach which may be dictated for reasons of limited data or limited stationarity. In the latter case (of P sufficiently large), $\hat{C}$ will not depend on D.

The example used here exhibited biases of one tenth (see Figure B-5); furthermore the trend was clearly indicative of the fact that any bias (less than one) could be expected with insufficient frequency resolution even when as many as 64 independent data segments have been processed (Carter (1972b)). The practical implication of this limitation is that it is highly desirable that the actual number of data points per segment, P, be large. For a finite duration data set, this will mean increased instability in the estimator (that is, smaller N and hence larger variance). It should be noted that one cannot simply increase P by adding zeros or by increasing the sampling rate of the original data, for then no additional information content is added. Quite the contrary, the minimum data sampling rate should be selected, for this ensures the maximum amount of actual time per data segment for a given value of P. Good resolution, that is, large P, apparently requires computation of a large size FFT. An alternative computation that reduces the required FFT size is the PAM-CZT (Appendix A).

The results of the first simulation show two critical things: first, when estimating MSC (or any spectral quantities) it is important to use both smooth weighting functions and adequate frequency resolution. Second, simulation experiments to validate expressions for bias of $\hat{C}$ can give misleading results due to the sensitivity

of the four fundamental assumptions upon which the theory rests. Another difficulty in experimentally estimating bias is that when the assumptions do hold, the bias is a small quantity to measure. For example, for C=0.3, N=32, we find B(C,N)=0.0156. However, the standard deviation of $\hat{C}$ is approximately 0.3. (See Section 3 of Appendix B.) Thus a large number of independent trials, in each of which C is computed, must be used in order to obtain a sample mean that has statistical significance. We use 10,000 different independent trials at each value of C=0 (.1).9; the results of Benignus (1969a) employed less than 1,000 trials.

Lastly, the smallness of the bias dictates that the desired value of C be accurately realized in the simulation. As an example of the danger of not doing so, consider the following: suppose we believe we have generated processes with a desired coherence of 0.300, and subsequently observe a sample mean of 0.315; in such a situation, the estimated bias is 0.015. But if the generated coherence is not precisely under the experimenter's control and is off by only 1 percent (giving rise to a true coherence in this example of 0.303), then the bias should have been reported as 0.315-0.303=0.012. Thus, a 1 percent error in true coherence gives rise to a 25 percent error in estimated bias in this example. We generate our correlated

processes according to

$$x(t) = a(t) , \tag{B-17a}$$

$$y(t) = b(t) + g\,a(t), \tag{B-17b}$$

where a(t) and b(t) are uncorrelated complex Gaussian processes, and

$$g = \sqrt{\frac{C}{1-C}} \quad . \tag{B-18}$$

The statistical characteristics of $\hat{C}$ in (B-1) are derived on the fact that X(k) and Y(k) are Gaussian. This will be the case if x(t) and y(t) are Gaussian; however, the essence of the theory does <u>not</u> require X(k) and Y(k) to be DFT outputs but merely complex Gaussian random variables. Thus, we can simply avoid the issues of weighting and frequency resolution by simulating the DFT outputs directly; this technique reduces the cost of the experiment (and indeed will verify the theory). The essential features of the simulation are given in Figure B-6.

The results of the simulation for N=4 are superposed in Figure B-7 on the exact bias curve.

In particular, the sample mean of 10,000 independent trials at each value of C=0(.1..9 is plotted, along with a vertical bar between the $\pm\sigma$ points of the random variable. In seven out of the ten cases of selected MSC, the $\pm\sigma$ points bracket the theoretical curve, and the remaining three out of ten are included within the $\pm 2\sigma$ points. The possibility of (B-15) falling within

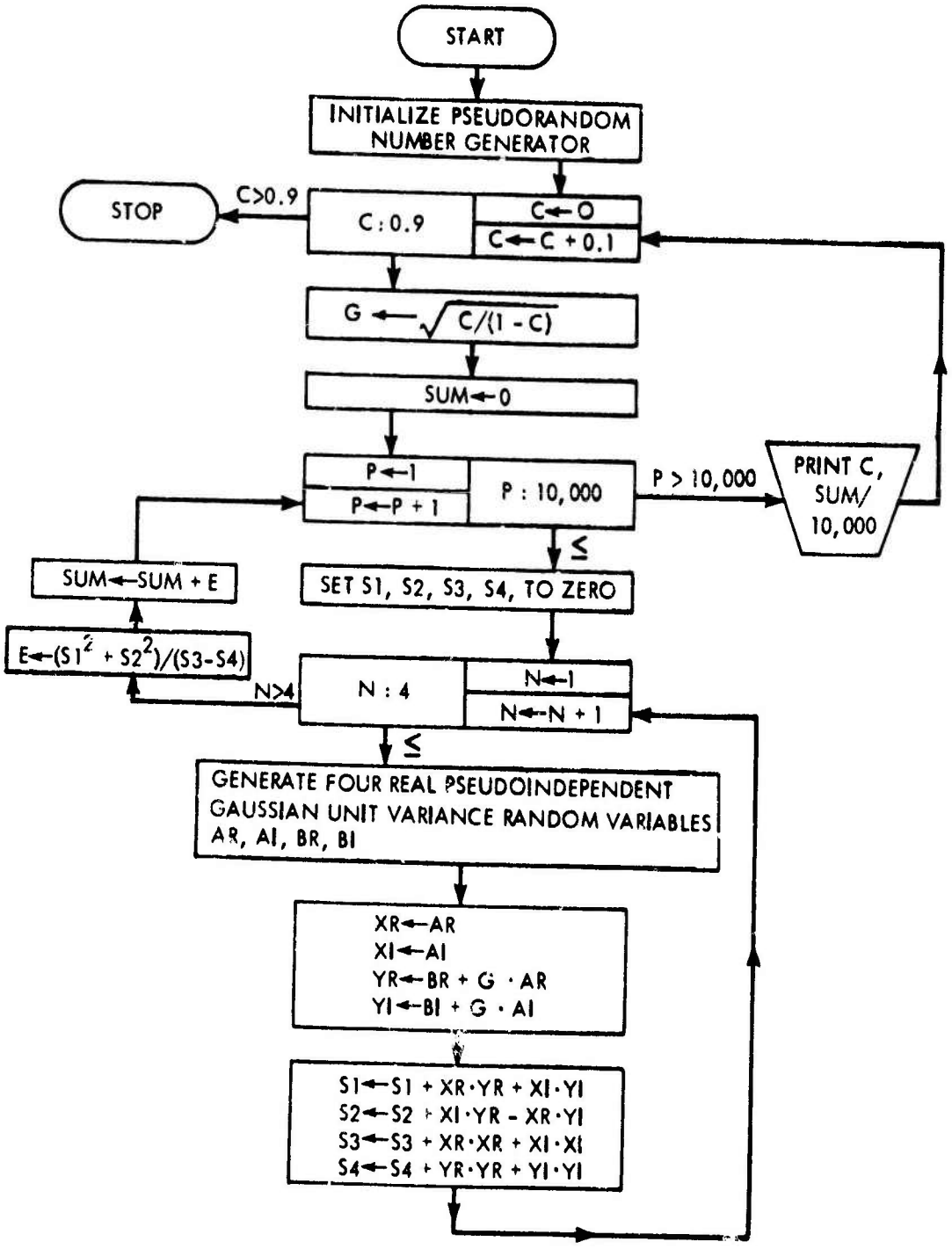

Figure B-6 Flow Diagram for Empirical Determination of Bias of $\hat{C}$; N=4; 10,000 Trials

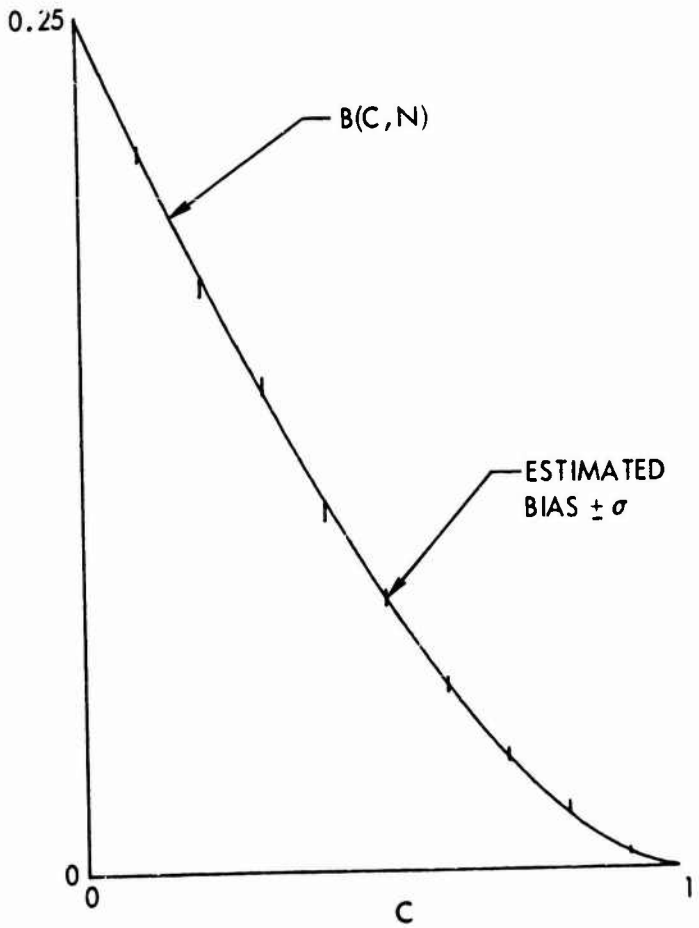

Figure B-7 Theoretical and Simulation Results for Bias of $\hat{C}$; N=4; 10,000 Trials

these tolerances is completely ruled out. Thus, the simulation confirms the theoretical result in (B-11) and rules out the approximation in (B-15).

Since we have a simulation technique which corroborates the theory so well, it is possible to employ it to investigate other more complicated functions of $\hat{C}$ which are very difficult (if not impossible) analytically. In particular, we use a bootstrap idea based upon that of Benignus (1969a) in an attempt to reduce the bias of the coherence estimate. Namely, we consider a modified estimate of MSC as

$$\hat{\hat{C}} = \max\left[0, \hat{C} - \frac{1}{N}(1-\hat{C})^2\left(1+\frac{2\hat{C}}{N}\right)\right], \qquad \text{(B-19)}$$

where we have estimated the bias by means of (B-13) and the initial estimate $\hat{C}$ of MSC. The reason for the 0 in (B-19) is that we are unwilling to accept negative estimates of coherence. (Without the 0 in (B-19) we can reduce the bias further at the expense of added variance.) The estimated bias and variance of $\hat{C}$ and $\hat{\hat{C}}$ are presented in Table B-1. It is observed that the bias of $\hat{C}$ is significantly reduced. However, the variance is increased. In fact, the estimated mean square error (MSE) (which equals the variance plus the square of the bias) is presented in Table B-1 and is greater for $\hat{\hat{C}}$ than for $\hat{C}$ when C is greater than 0.3; the opposite behavior holds when C is less than 0.3. (For N=4, C=0.3 is the crossover.) Thus, the choice

Table B-1

Estimated Bias, Variance and MSE of $\hat{C}$ and $\hat{\hat{C}}$ for N=4; 10,000 Trials

C	Bias ($\hat{C}$)	Bias ($\hat{\hat{C}}$)	Var ($\hat{C}$)	Var ($\hat{\hat{C}}$)	MSE ($\hat{C}$)	MSE ($\hat{\hat{C}}$)
0	.249	.146	.037	.040	.099	.062
.1	.210	.111	.045	.054	.090	.066
.2	.171	.076	.050	.064	.079	.070
.3	.142	.057	.053	.072	.073	.075
.4	.105	.030	.052	.073	.063	.074
.5	.080	.019	.048	.068	.054	.069
.6	.054	.008	.041	.059	.044	.059
.7	.033	.003	.030	.042	.031	.042
.8	.018	.0014	.018	.024	.019	.024
.9	.005	-.0006	.006	.008	.006	.008
1	0	0	0	0	0	0

between the two estimators, $\hat{C}$ and $\hat{\hat{C}}$, depends on whether one is bothered more by bias or MSE.

For larger N, the crossover value of C, at which $\hat{C}$ or $\hat{\hat{C}}$ has less MSE, decreases. For example, at N=8, it was observed to occur at C=0.2. Thus, for practical useful values of N (which are usually much larger than 1), the estimator $\hat{C}$ will have less MSE than $\hat{\hat{C}}$ over almost the whole range of C and will probably be preferred. Also, the bias is quite small for large N. The variance of $\hat{C}$ is discussed in the next section. Under the assumptions of smooth weighting functions and adequate frequency resolution, we will see variance is a more significant problem than bias. However, as seen in this section, when the assumptions are violated, the bias can be a significant source of estimation error.

B3. Variance of $\hat{C}$

An exact expression for the variance of C is Carter (1972a):

$$V = \frac{2(1-C)^N}{N(N+1)}\ {}_3F_2\left(3,\ N,\ N;N+2,\ 1;\ C\right) - \left[\frac{(1-C)^N}{N}\ {}_3F_2\left(2,N,N;N+1,\ 1;\ C\right)\right]^2 \quad \text{(B-20)}$$

(B-20) is plotted in Figure B-8. For the special case of C=0,

$$V = \frac{2}{N(N+1)} - \left(\frac{1}{N}\right)^2 = \frac{N-1}{N^2(N+1)}\ ,\ C=0\ , \quad \text{(B-21a)}$$

and

$$\cong \frac{1}{N^2}\ ,\ \text{for large N and C=0.} \quad \text{(B-21b)}$$

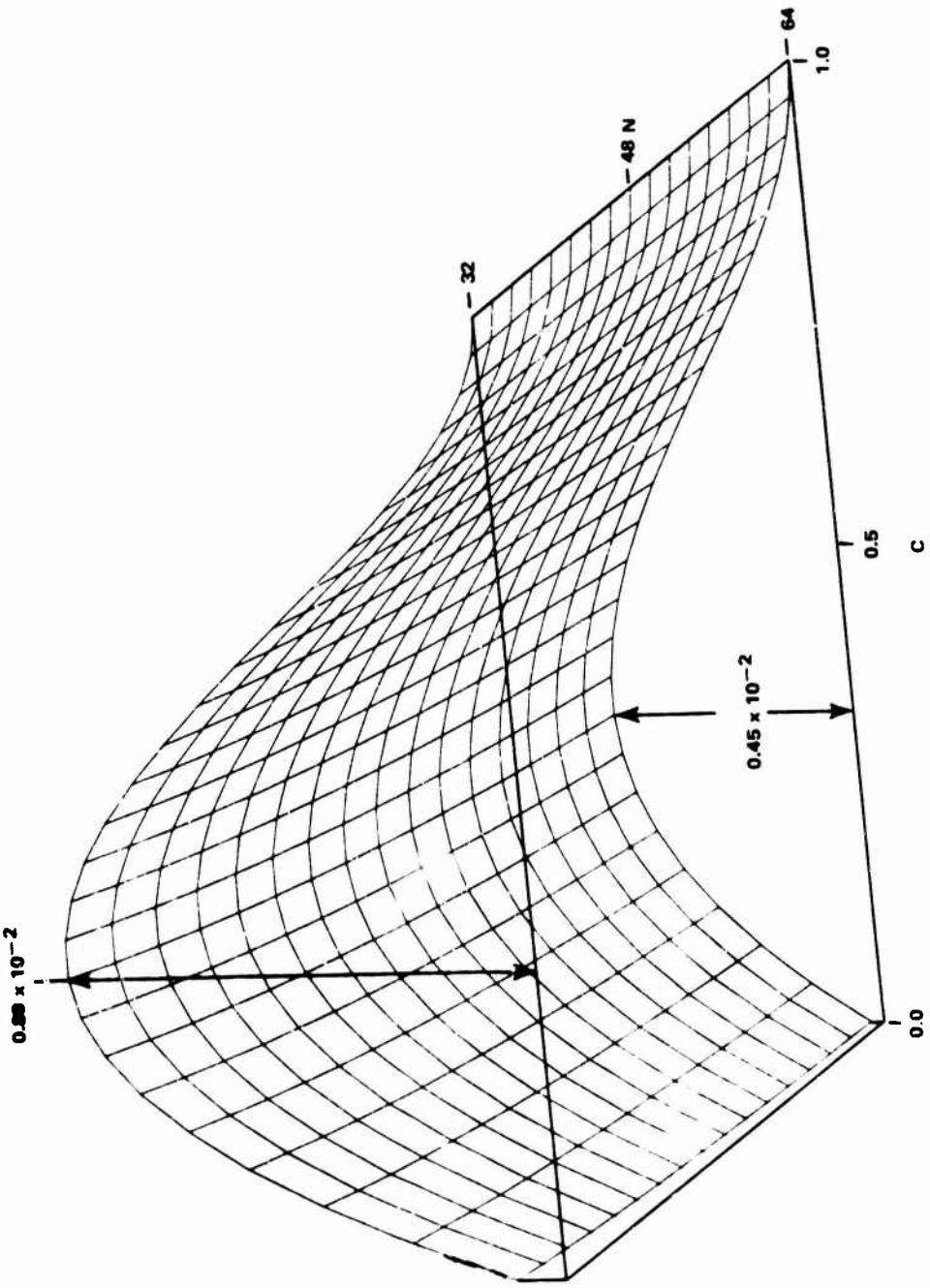

Figure B-8 Variance of $\hat{C}$ versus C and N

For large N and C≠0,

$$V \cong \frac{2}{N} C\left(1-C\right)^2 \quad , \tag{B-22}$$

which has a maximum value of $8/27N \cong 0.30/N$ at C=1/3. Thus the maximum variance is always less than 0.30/N regardless of the value of C. Hence, the variance of the estimator in the case where C is unknown (but nonzero) decreases inversely proportional to N. We note, by inspecting (B-20), that for larger and larger N, (B-22) becomes a better and better approximation.

Since, in general, we do not know the true value of MSC, we select N based on a worst case (maximum variance) analysis.

Provided we have used good weighting functions and good frequency resolution, the variance has a more serious effect than bias. For example, if C=1/3 and N=100, then the bias of $\hat{C}$ is less than 0.01, while the standard deviation (square root of the variance) is approximately equal to .05. Hence, even when 100 independent segments are processed, the MSC estimate still has significant variability.

B4. Receiver Operating Characteristics for a Linearly Thresholded Coherence Estimation Detector

An algorithm for computing the ROC, or the probability of detection, P_D, versus the probability of false alarm, P_F, for a linearly thresholded MSC estimation detector is presented together with an

example of a ROC table[1] (Carter (1976). A recent article (Gevins, Yeager, Diamond, Spire, Zeitlin, and Gevins (1975)) presents new results on using linearly thresholded MSC estimates to detect biomedical phenomena. The desire to establish a threshold below which MSC estimates are not presented to a human decision maker is an important issue in certain areas, such as brain wave analysis and sonar, where the volume of sensor data is large. For a fixed amount of averaging and a fixed threshold value, E, in the absence of a coherent source, there is still a certain probability, P_F, that an MSC estimate will exceed the threshold. Moreover, although the false alarm rate can be reduced by increasing E, to do so decreases P_D, when a coherent source is present. How much it decreases P_D will depend on the strength of the coherent source, that is, the true or underlying coherence that is being estimated. This section presents an algorithm for computing P_D versus P_F for a specified amount of averaging and underlying coherence. The pdf of $\hat{C}$, when C=0, is (from (B-3)):

$$p(\hat{C}|N,\ C=0) = (N-1)(1-\hat{C})^{(N-2)} \ . \qquad \text{(B-23)}$$

---

[1]The idea for computing ROC curves was suggested to the author by R. Trueblood, Naval Undersea Center, San Diego, California.

Hence, the probability of false alarm is

$$P_F = 1 - \int_0^E (N-1)(1-\hat{C})^{(N-2)} d\hat{C} \qquad \text{(B-24)}$$

or

$$E = 1 - \exp[\log(P_F)/(N-1)]; \qquad \text{(B-25)}$$

that is, for a specified P_F we establish a threshold according to (B-25). Now the computationally more complex question is: What probability of detection is achieved for this threshold value E? The answer, for a given value of C, is

$$P_D = \int_E^1 p(\hat{C}|N,C)\, d\hat{C} = 1 - P(\hat{C} \leq E|N,C) \ , \qquad \text{(B-26)}$$

where $P(\hat{C} \leq E|N,C)$ is the cdf. The cdf is given by (B-4), namely,

$$P(\hat{C} \leq E|N,C) = R \sum_{\ell=0}^{N-2} \left[\frac{1-E}{1-Z}\right]^{\ell} {}_2F_1(-\ell,\ 1-N;1;Z) \ , \qquad \text{(B-27a)}$$

where

$$Z = EC \qquad \text{(B-27b)}$$

$$R = E\left[\frac{(1-C)}{(1-Z)}\right]^N \qquad \text{(B-27c)}$$

${}_2F_1$ is the hypergeometric function.

The hypergeometric function is, in general, an infinite series; however, for negative integers, it is given by equation (15.4.1) of Abramowitz and Stegun (1964) as

$${}_2F_1(-\ell,1-N;1;Z) = \sum_{k=0}^{\ell} T_k \ , \qquad \text{(B-28a)}$$

where

$$T_k = \frac{(-\ell)_k (1-N)_k z^k}{(1)_k k!} \quad . \qquad \text{(B-28b)}$$

Pochhammer's Symbol $(z)_k$ (p. 256 of Abramowitz and Stegun (1964))

$$(z)_k = \frac{\Gamma(z+k)}{\Gamma(z)} \quad , \qquad \text{(B-28c)}$$

and where the Gamma function is given by Hankel's Contour integral (p. 255 of Abramowitz and Stegun (1964)) as

$$\Gamma(z) = \left[\frac{j}{2\pi} \oint (-t)^{-z} e^{-t} dt \right]^{-1}, \quad |z| < \infty \cdot \qquad \text{(B-28d)}$$

The path of integration starts at $+\infty$ on the real axis, circles the origin in the counterclockwise direction, and returns to the starting point. However, (B-27) can be computed without resort to complex integration methods (even when the real part of z=0) by noting for k an integer that Pochhammer's Symbol,

$$(z)_k = \begin{cases} z(z+1)(z+2)\ldots(z+k-1) \ , & k>0 \\ 1 & k=0 \ , \end{cases} \qquad \text{(B-29)}$$

is the product of k incrementally increasing terms. Now in (B-28b) when $Z=EC\neq 0$, the first term $T_0=1$ and the ratio of the k-th to the (k-1)-st term is

$$\frac{T_k}{T_{k-1}} = \frac{(k-1-\ell)(k-1+1-N)z}{k^2} \quad . \qquad \text{(B-30)}$$

Now each term in the sum can be computed from the previous term in a simple fashion. Indeed, the actual

computations can be implemented in BASIC on the Hewlett-Packard 9830A desk top calculator in less than 30 lines of code, Figure B-9. For models of the form

$$x(t) = s(t)+n_1(t) \tag{B-31a}$$

$$y(t) = s(t+D)+n_2(t) \ , \tag{B-31b}$$

where $s(t)$, $n_1(t)$, and $n_2(t)$ are mutually uncorrelated, and when $G_{n_1n_1}(f)=G_{n_2n_2}(f)=G_{nn}(f)$, the SNR is

$$\frac{G_{ss}(f)}{G_{nn}(f)} = \frac{\sqrt{C_{xy}(f)}}{1-\sqrt{C_{xy}(f)}} \ . \tag{B-32}$$

More generally, if

$$x(t) = z_1(t)+n_1(t) \tag{B-33a}$$

$$y(t) = z_2(t)+n_2(t) \ , \tag{B-33b}$$

where $z_i(t)$ is the output of a linear filter $H_i(f)$ excited by $s(t)$, i=1, 2 and the noises are mutually uncorrelated and uncorrelated with the signal, then it can be shown that (2-86)

$$C_{xy}(f)=C_{sx}(f)C_{sy}(f) \ ; \tag{B-34}$$

that is, the coherence between two receivers is the product of the coherence between the source and each of the individual receivers for the model (B-33). Substituting for the model in (B-33) results in

$$\frac{G_{z_1z_1}(f)}{G_{n_1n_1}(f)} \cdot \frac{G_{z_2z_2}(f)}{G_{n_2n_2}(f)} = \frac{C_{xy}(f)}{\left[1-C_{sx}(f)\right]\left[1-C_{sy}(f)\right]} \tag{B-35}$$

Now <u>if</u> $C_{sx}(f)=C_{sy}(f)=\left[C_{xy}(f)\right]^{1/2}$, then it follows

```
1Ø   N=8
2Ø   N1=N-1
3Ø   N2=N-2
4Ø   A=1-N
5Ø   C=Ø.25
6Ø   PRINT "THIS RUN IS FOR N="N" AND MSC="C
7Ø   FOR F1=Ø.Ø4 TO 1 STEP Ø.Ø4
8Ø   E=1-EXP(LOG(F1)/N1)
9Ø   Z=E*C
1ØØ  C4=(1-E)/(1-Z)
11Ø  C2=E*((1-C)/(1-Z))↑N
12Ø  S=Ø
13Ø  FOR L=Ø TO N2
14Ø  C3=C4↑L
15Ø  T=1
16Ø  F=1
17Ø  IF (L=Ø) THEN 23Ø
18Ø  FOR K=1 TO L
19Ø  K1=K-1
2ØØ  T=T*(A+K1)*(K1-L)*Z/(K*K)
21Ø  F=F+T
22Ø  NEXT K
23Ø  S=S+C3*F
24Ø  NEXT L
25Ø  P=C2*S
26Ø  FIXED 3
27Ø  PRINT E;F1;P,1-P
28Ø  NEXT F1
29Ø  END
```

Figure B-9 Computer Program to Compute ROC Tables

that SNR is

$$\left[\frac{G_{z_1z_1}(f)G_{z_2z_2}(f)}{G_{n_1n_1}(f)G_{n_2n_2}(f)}\right]^{1/2} = \frac{\sqrt{C_{xy}(f)}}{1-\sqrt{C_{xy}(f)}} \quad . \tag{B-36}$$

Hence, for models of the form of (B-31) or (B-33) if we want to look at the 0 dB (or equal SNR case), we must select

$$10 \log_{10}\left[\frac{\sqrt{C}}{1-\sqrt{C}}\right] = 0 \quad , \tag{B-37}$$

which implies C=0.25. Now suppose we average for only N=8 independent data segments. Then for P_F=0.04(0.04)1.00, the thresholds, P_F, cdf and P_D are given in Table B-2. If a sufficient amount of stationary data exists, effective performance can be improved by increasing N; if not, N can only be increased at the expense of degrading the frequency resolution with its inherent difficulties. For many problems, N=8 will be too small and P_F=0.04 will be too large or the performance will be desired for a different value (or family of values) of C. Example plots are given in Figures B-10 and B-11; more extensive results can be obtained by modifying the program, Figure B-9.

Table B-2. Threshold, P_F, cdf, and P_D for N=8 and C=0.25

THIS RUN IS FOR N=8 AND MSC=Ø.25

Ø.369	Ø.Ø4Ø	Ø.6Ø6	Ø.394
Ø.3Ø3	Ø.Ø8Ø	Ø.473	Ø.527
Ø.261	Ø.12Ø	Ø.389	Ø.611
Ø.23Ø	Ø.16Ø	Ø.327	Ø.673
Ø.2Ø5	Ø.2ØØ	Ø.279	Ø.721
Ø.184	Ø.24Ø	Ø.24Ø	Ø.76Ø
Ø.166	Ø.28Ø	Ø.2Ø8	Ø.792
Ø.15Ø	Ø.32Ø	Ø.181	Ø.819
Ø.136	Ø.36Ø	Ø.157	Ø.843
Ø.123	Ø.4ØØ	Ø.137	Ø.863
Ø.111	Ø.44Ø	Ø.119	Ø.881
Ø.1ØØ	Ø.48Ø	Ø.1Ø4	Ø.896
Ø.Ø89	Ø.52Ø	Ø.Ø9Ø	Ø.91Ø
Ø.Ø79	Ø.56Ø	Ø.Ø78	Ø.922
Ø.Ø7Ø	Ø.6ØØ	Ø.Ø66	Ø.934
Ø.Ø62	Ø.64Ø	Ø.Ø57	Ø.943
Ø.Ø54	Ø.68Ø	Ø.Ø48	Ø.952
Ø.Ø46	Ø.72Ø	Ø.Ø39	Ø.961
Ø.Ø38	Ø.76Ø	Ø.Ø32	Ø.968
Ø.Ø31	Ø.8ØØ	Ø.Ø25	Ø.975
Ø.Ø25	Ø.84Ø	Ø.Ø19	Ø.981
Ø.Ø18	Ø.88Ø	Ø.Ø14	Ø.986
Ø.Ø12	Ø.92Ø	Ø.ØØ9	Ø.991
Ø.ØØ6	Ø.96Ø	Ø.ØØ4	Ø.996
Ø.ØØØ	1.ØØØ	Ø.ØØØ	1.ØØØ

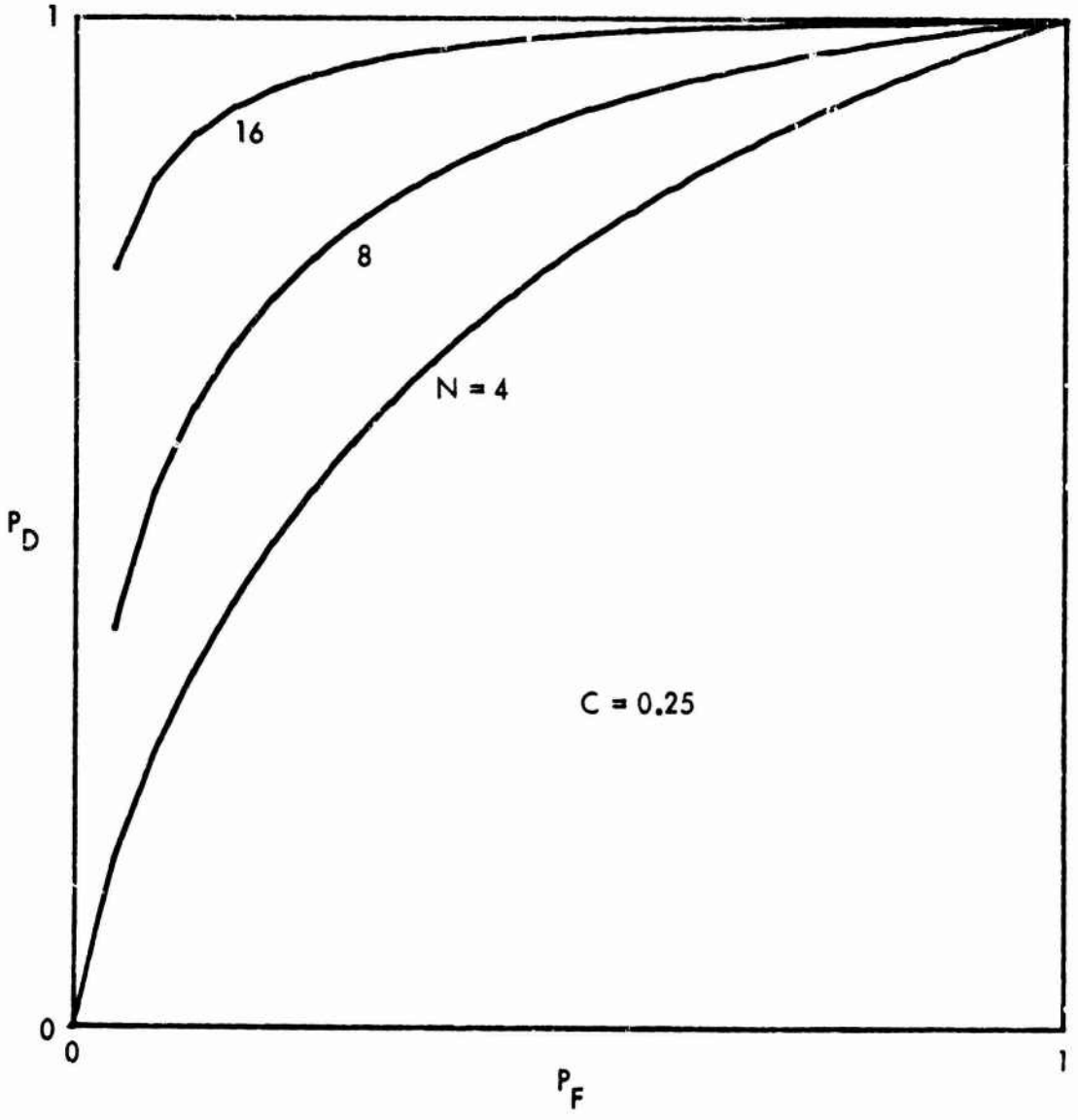

Figure B-10 ROC Curves for C=0.25; N=4, 8, 16

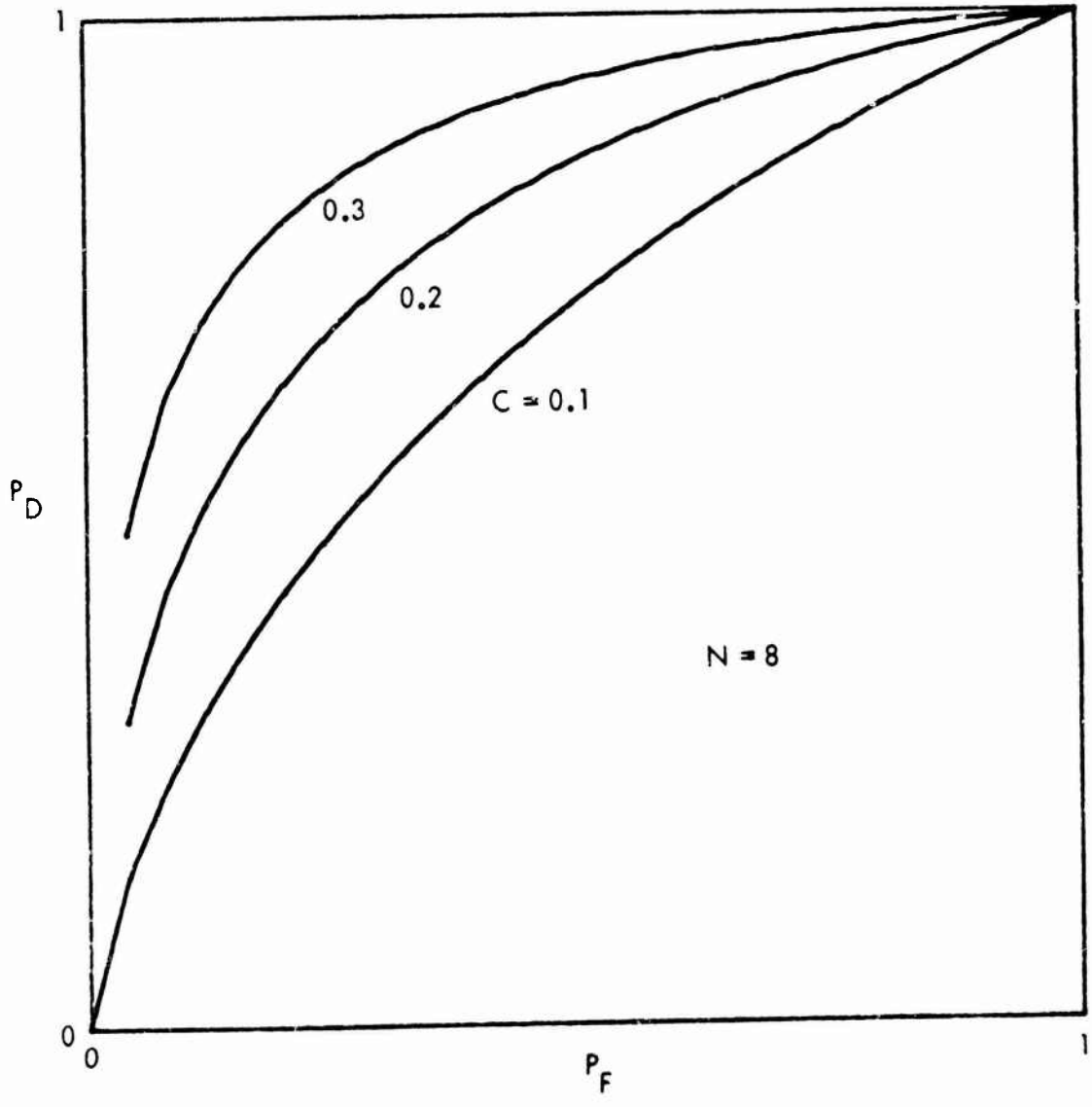

Figure B-11 ROC Curves for N=8; C=0.1, 0.2, 0.3

APPENDIX C

COMPUTER PROGRAM FOR SPECTRAL AND TIME DELAY ESTIMATION

This appendix is divided into two sections. The first section is a brief program description. The second section is a complete listing of the main program and subroutines necessary for program execution.

C1. Program Description

The main program estimates the auto and cross spectral density functions. These spectral estimates are used by the subroutine PRCES to estimate six different AML estimates for time delay (See Table 4-1 of the main text.) Facilities with spectral estimation programs can simply augment their computations with a call to PRCES. Facilities without spectral estimation algorithms will be able to use the programs listed in Section 2 of this appendix. The programs listed are intended to be general FORTRAN IV programs; they have been compiled and executed on the Univac 1108, the Control Data Corporation (CDC) 6600 and International Business Machine (IBM) 360. The spectral estimation programs have been used for research projects by: Williams (1971), Carter (1972a) and (1972b), Brady (1973), Carter, Knapp, and Nuttall (1973a), Carter, Nuttall, and Cable (1973), Santopietro (1973), Carter and Knapp (1975), and Appendix D

of this dissertation. These research projects were conducted entirely on the Univac 1108 and a significant program rewrite was undertaken to make the programs more transferable from one computer system to another.[1] The programs as a complete data processing system consist of input, computations and display. We have concentrated our rewrite efforts on the computations; both the input and display programs are expected to contain peculiarities of the particular computer being used. The input and display subroutines are modular so that only a minimum rewrite is required to transfer the program to another installation. The function of the input subroutine LOAD is to load the XX and YY arrays with NNN data points. If the data were stored on logical magnetic tape number 6 in binary format the call to LOAD could be replaced by the FORTRAN statement

"READ 6, XX(I), YY(I), I=1, NNN"

The subroutine LOAD listed in Section 2 is used to generate synthetic data for a suitable test case (though not the example for Appendix D). The display subroutine DPLOT is called either: (1) to initialize the plotter, (2) to plot the specified array, or (3) to terminate plotting. The subroutine listed in Section 2 is written for the Stromberg Carlson 4060 plot system. It must be rewritten for other systems. If a facility

---

[1]The programs originally written and documented by C.R.Arnold, G.C.Carter, and J.F.Ferrie, have been rewritten and tested by J.C.Sikorski,G.C.Carter and Dr. R.G.Williams.

has no plotting system, the subroutine should simply be a subroutine which returns; alternatively, the subroutine could print the XX array for I=ISTRT to ISTOP. Thus, for use at a new site, two subroutines (LOAD and DPLOT) need to be rewritten.

The main program also calls (in addition to DPLOT and LOAD): HICMP, FFT, LIST, LIST2, PRCES, and LREMV. The subroutine LREMV computes (and optionally removes) the linear trend and dc for the input time waveforms. These computations are performed for every time segment and are printed out by the main program as an aid to detecting nonstationarities or digitizing errors. The subroutines LIST and LIST2 are used to print out (list) results. The subroutine FFT computes the FFT (see, for example, Cooley-Tukey (1965)), coded and listed by Singleton (1969). Singleton's mixed radix algorithm has been shown by Ferrie and Nuttall (1971) to be significantly faster (though less accurate) than other proposed FFTs. Singleton's 600 line FORTRAN subroutine can be replaced with shorter programs (see, for example, p. 332 of Oppenheim and Schafer (1975)). Because of the availability of Singleton's listing in the literature, the FFT is not listed here. Note that the subroutine PRCES and the main program presume that the FFT output array is subscribed from 1 to NPFFT and <u>not</u> from 0 to (NPFFT-1). The subroutine PRCES implements the six AML processors given in Table 4-1. The subroutine PRCES calls on the

subroutines FFT and DPLOT (already discussed). Singleton's subroutine performs a mixed radix FFT; that is, the number of data points do not need to be integer powers of 2 such as 512, 1024, 2048 and 4096 but can have factors of 2's, 3's, and 5's, such as 1000, 1500, 2000 and 3000. Numbers which can be factored into 2's, 3's, and 5's only are called highly composite. Given the FORTRAN variable NNN, the subroutine HICMP finds the highly composite number closest to (but greater than or equal to) NNN. The output of HICMP is NEWNNN. For some applications, the program user will want NEWNNN to be twice as large as NNN; this is because the main program fills the data arrays with zero from NNN + 1 to NEWNNN. Such zero filling is (theoretically) required to inhibit the effect of circular convolution; in practice, though, (with stochastic data) zero filling does <u>not</u> warrant the added (doubled) computational cost. If it is desired, zero filling can simply be achieved by adding one line to HICMP: "NEWNNN = 2*NEWNNN".

In addition to calling several critical subroutines, the main program performs computations necessary to estimate the spectral characteristics of the two waveforms under investigation. The computations performed are briefly outlined in four major steps in appendix A. When the two input waveforms are complex, one FFT of each waveform segment is required as specified in

Appendix A. However, in most (though not all) practical data collection facilities, the input waveforms are real (not complex). When x(t) and y(t) are real, one FFT of the complex waveform x(t) + jy(t) can be computed and quickly be manipulated to form the FFT of x(t) and the FFT of y(t). (See p. 333-334 of Oppenheim and Schafer (1975); see also p. 271-293 of Rabiner and Rader (1972).) These observations, combined with (A-3) give rise to the FORTRAN statements used to estimate the spectral characteristics of x(t) and y(t). The application of this theory reduces the computation time for two real waveforms by a factor of two. The final comment necessary before presenting the computer listings is to describe the input FORTRAN variables. NNN is the number of data points per segment. ISR is the integer sampling rate (Hz). NDSJP is the number of disjoint segments in the total time waveform. SFX and SFY are scale factors used to adjust the (voltage) level of the input waveform to correct for frequency independent attenuations in the data collection and digitizing process. (When no correction is desired, the user sets SFX=SFY=1.0.) When the user desires the spectral estimates to appear 3 dB higher, he sets SFX=SFY=2.0.) With these five sample inputs, the input time data are processed. The next section gives a complete program and subroutine listing.

```
      C     FFT SPECTRUM ANALYSIS PROGRAM
      C
      C           SPECIFICATION AND TYPE STATEMENTS
      C
            DIMENSION XX(4098), YY(4098)
            DIMENSION GXX(2051), GYY(2051), GXYRE(2051), GXYIM(2051)
            DIMENSION WEGHT(4099), SCRCH(4099)
            EQUIVALENCE (WEGHT(1),SCRCH(1))
            DIMENSION PHI(4097)
      C
      C           SET INITIAL VALUES
      C
            IPRTR=4
            CALL DPLOT (XX,0,0,1)
      C
      C           READ INPUT CONTROL PARAMETERS FROM COMPUTER DATA CARD
      C
            READ 100, NNN,ISR,NDSJP,SFX,SFY
      C     NNN IS THE NUMBER OF DATA POINTS PER SEGMENT
      C     ISR IS THE SAMPLING RATE
      C     NDSJP IS THE NUMBER OF DISJOINT SEGMENTS
      C     SFX AND SFY ARE SCALE FACTORS FOR THE INPUT DATA
        100 FORMAT (3I5,2F10.5)
            NFFTS=NDSJP
      C
      C           PRINT INPUT CONTROL PARAMETERS
      C
            WRITE (IPRTR,105) NNN,ISR,NDSJP,SFX,SFY
        105 FORMAT (/1X,3I10,2E20.8/)
```

```
      C
      C            CALCULATE CONSTANTS
      C
           IF (NNN.GT.0.AND.NNN.LE.4096) GO TO 115
           WRITE (IPRTR,110)
  110 FORMAT (10X,'NNN ERROR')
           STOP
  115 CONTINUE
           VARX=0.0
           VARY=0.0
           DT=1.0/FLOAT(ISR)
           SF=SQRT(ABS(SFX*SFY))
      C
      C            PRINT OUT USER INFORMATION
      C
           IF (NFFTS.EQ.NDSJP) WRITE (IPRTR,120)
  120 FORMAT (//10X,'THE FOLLOWING DATA WAS NOT RUN WITH 50 PERCENT OVER
     1LAP')
           TIME=FLOAT(NDSJP*NNN)*DT
           WRITE (IPRTR,125) NDSJP,TIME
  125 FORMAT (18X,'THE',I4,' DISJOINT PIECES COMPRISE',F8.2,' SECONDS OF
     1 DATA')
      C
      C            COMPUTE NEW COMPOSITE NUMBER NNN AND INCREASE ARRAYS
      C
           CALL HICMP (NNN,NPFFT)
           IF (NPFFT.GT.4096) STOP
           WRITE (IPRTR,130) NPFFT
  130 FORMAT (18X,'NUMBER OF POINT FFT =',I5/)
```

```
C
C            CALCULATE CONSTANTS
C
      NP2=NPFFT+2
      ND2=NPFFT/2
      ND2P1=ND2+1
      ND2M1=ND2-1
      DF=1.0/(DT*FLOAT(NPFFT))
      FNYQ=FLOAT(ISR)/2.0
      CONST=0.25*DT/FLOAT(NNN)
      FLOW=0.0
      FHIGH=FNYQ
      ISTRT=IFIX(FLOW/DF)+1
      ISTOP=IFIX(FHIGH/DF)+1
C
C            COMPUTE AND SAVE WEIGHTING FUNCTION
C
      TPI=6.0*ATAN(1.0)
      TEMP=TPI/FLOAT(NNN)
      DO 135 I=1,NNN
      WEGHT(I)=0.816496581*(1.0-COS(TEMP*FLOAT(I-1)))
  135 CONTINUE
C
C            STORE ZEROS IN THE SUMMING ARRAYS
C
      DO 140 K=1,ND2P1
      GXX(K)=0.0
      GYY(K)=0.0
      GXYRE(K)=0.0
      GXYIM(K)=0.0
  140 CONTINUE
```

COPY AVAILABLE TO DDC DOES NOT PERMIT FULLY LEGIBLE PRODUCTION

```
      C
      C        COMPUTE AND SUM N FFT ESTIMATES
      C
           DO 195 KOUNT=1,NFFTS
      C
           DO 145 I=1,NPFFT
           XX(I)=0.0
      145  YY(I)=0.0
      C
      C             LOAD XX AND YY ARRAYS WITH NNN DATA POINTS
      C
           CALL LOAD (XX,YY,PHI,NNN,KOUNT,ISR)
      C
      C             PRINT OF FIRST 150 INPUT VALUES
      C
           IF (KOUNT.NE.1) GO TO 170
           WRITE (IPRTR,150)
      150  FORMAT (1H1,9X,'PRINTOUT OF FIRST 150 VALUES OF INPUT DATA',///)
           DO 160 I=1,50
           J=I+50
           K=I+100
           PRINT 155, (I,XX(I),YY(I),J,XX(J),YY(J),K,XX(K),YY(K))
      155  FORMAT (3(I7,1X,2F15.8,6X))
      160  CONTINUE
           WRITE (IPRTR,165)
      165  FORMAT (/1H1)
      170  CONTINUE
```

```
      C
      C            REMOVE THE LINEAR TREND AND COMPUTE THE VARIANCE
      C
            IS3=0
            CALL LREMV (XX,NNN,IS3,DX,SX)
            CALL LREMV (YY,NNN,IS3,DY,SY)
            VARXI=0.0
            VARYI=0.0
            DO 175 I=1,NNN
            VARXI=VARXI+XX(I)*XX(I)
        175 VARYI=VARYI+YY(I)*YY(I)
            VARXI=VARXI/FLOAT(NNN-1)
            VARYI=VARYI/FLOAT(NNN-1)
            WRITE (IPRTR,180) KOUNT,DX,DY,SX,SY,VARXI,VARYI,IS3
        180 FORMAT (5X,I5,' DX=',E12.6,' DY='E12.6,' SX=',E12.6,' SY=',E12.6,'
           1 VX=',E12.6,' VY=',E12.6,I5)
            VARX=VARX+VARXI
            VARY=VARY+VARYI
      C
      C            WEIGHT THE INPUT DATA WITH COSINE WINDOW
      C
            DO 185 I=1,NNN
            XX(I)=XX(I)*WEGHT(I)
            YY(I)=YY(I)*WEGHT(I)
        185 CONTINUE
      C
      C            COMPUTE FAST FOURIER TRANSFORM
      C
            CALL FFT (XX,YY,NPFFT,NPFFT,NPFFT,-1)
```

```
      C
      C              COMPUTE SPECTRA
      C
            GXX(1)=GXX(1)+4.0*XX(1)**2
            DO 190 K=2,ND2P1
            J=NP2-K
            GXX(K)=GXX(K)+(XX(K)+XX(J))**2+(YY(K)-YY(J))**2
            GYY(K)=GYY(K)+(YY(K)+YY(J))**2+(XX(J)-XX(K))**2
            GXYRE(K)=GXYRE(K)+XX(K)*YY(J)+XX(J)*YY(K)
            GXYIM(K)=GXYIM(K)+XX(J)**2+YY(J)**2-XX(K)**2-YY(K)**2
        190 CONTINUE
            GYY(1)=GYY(1)+4.0*YY(1)**2
            GXYRE(1)=GXYRE(1)+2.0*(XX(1)*YY(1))
            GXYIM(1)=0.0
      C
      C        GO BACK FOR NEXT SEGMENT
      C
        195 CONTINUE
      C
      C              NORMALIZE ESTIMATES
      C
            FNSG=FLOAT(NFFTS)
            OFNSG=1.0/FNSG
            VARX=VARX*OFNSG
            CONST=CONST*OFNSG
            CNSTC=2.0*CONST
            DO 200 K=1,ND2P1
            GXX(K)=GXX(K)*CONST*SFX
            GYY(K)=GYY(K)*CONST*SFY
            GXYRE(K)=GXYRE(K)*CNSTC*SF
            GXYIM(K)=GXYIM(K)*CONST*SF
            SCRCH(K)=DF*FLOAT(K-1)
        200 CONTINUE
            VARY=VARY*OFNSG
```

```
C
C            PRINT OUT VARIANCES
C
      WRITE (IPRTR,205) VARX,VARY
  205 FORMAT (/10X,'AVERAGE VARIANCES ARE, VX=',E12.6,' VY=',E12.6//)
      VARX=0.0
      VARY=0.0
      DO 210 K=1,ND2P1
      VARX=VARX+GXX(K)
      VARY=VARY+GYY(K)
  210 CONTINUE
      VARX=VARX*DF*2.0/SFX
      VARY=VARY*DF*2.0/SFY
      WRITE (IPRTR,215) VARX,VARY
  215 FORMAT (/10X,'INTEGRATED VARIANCES ARE, VX=',E12.6,' VY=',E12.6//)
C
C            CONVERT GXX  TO DB AND PLOT
C
      DO 220 I=1,ND2P1
      XX(I)=GXX(I)
      PHI(I)=10.0*ALOG10(MAX(GXX(I),1.0E-30))
  220 CONTINUE
      CALL DPLOT (PHI,ISTRT,ISTOP,2)
      WRITE (IPRTR,225)
  225 FORMAT (1H1,/10X,'DUMP OF XX PSD')
      CALL LIST (PHI,SCRCH,ISTRT,ISTOP,IPRTR)
```

COPY AVAILABLE TO DDC DOES NOT PERMIT FULLY LEGIBLE PRODUCTION

```
206       C
207       C            COMPUTE AND DISPLAY AUTOCORRELATION FUNCTION OF INPUT SIGNAL
208       C
209             DO 230 I=1,NPFFT
210             YY(I)=0.0
211         230 CONTINUE
212             DO 235 K=2,ND2P1
213             J=NP2-K
214             XX(J)=XX(K)
215         235 CONTINUE
216             CALL FFT (XX,YY,NPFFT,NPFFT,NPFFT,+1)
217             RO=XX(1)*DF
218             WRITE (IPRTR,240) RO
219         240 FORMAT (//9X,'RO FOR INPUT SIGNAL XX =',E15.8,//)
220             ONDRO=1.0/XX(1)
221             DO 245 I=1,ND2P1
222             XX(I)=XX(I)*ONDRO
223         245 CONTINUE
224             XMIN=0.0
225             CALL DPLOT (XX,1,ND2P1,2)
226             WRITE (IPRTR,250)
227         250 FORMAT (1H1,10X,'DUMP OF X DATA AUTO CORRELATION')
228             CALL LIST2 (XX,XMIN,1,ND2P1,IPRTR,DT)
229       C
230       C            CONVERT GYY  TO Db AND PLOT
231       C
232             DO 255 I=1,ND2P1
233             XX(I)=GYY(I)
234             PHI(I)=10.0*ALOG10(MAX(GYY(I),1.0E-30))
235         255 CONTINUE
236             CALL DPLOT (PHI,ISTRT,ISTOP,2)
237             WRITE (IPRTR,260)
238         260 FORMAT (1H1,//10X,'DUMP OF YY PSD')
239             CALL LIST (PHI,SCRCH,ISTRT,ISTOP,IPRTR)
```

```
C
C            COMPUTE AND DISPLAY AUTOCORRELATION FUNCTION OF INPUT SIGNAL
C
      DO 265 I=1,NPFFT
      YY(I)=0.0
  265 CONTINUE
      DO 270 K=2,ND2P1
      J=NP2-K
      XX(J)=XX(K)
  270 CONTINUE
      CALL FFT (XX,YY,NPFFT,NPFFT,NPFFT,+1)
      RO=XX(1)*DF
      WRITE (IPRTR,275) RO
  275 FORMAT (//9X,'RO FOR INPUT SIGNAL YY =',E15.8,//)
      ONDRO=1.0/XX(1)
      DO 280 I=1,ND2P1
      XX(I)=XX(I)*ONDRO
  280 CONTINUE
      CALL DPLOT (XX,1,ND2P1,2)
      WRITE (IPRTR,285)
  285 FORMAT (1H1,10X,'DUMP OF Y DATA AUTO CORRELATION')
      CALL LIST2 (XX,XMIN,1,ND2P1,IPRTR,DT)
C
C            COMPUTE AND DISPLAY PHASE FROM AVERAGED GXYRE AND GXYIM SPEC
C
      DO 305 K=1,ND2P1
      XXK=GXYRE(K)
      IF (XXK) 300,290,300
  290 IF (GXYIM(K)) 300,295,300
  295 XXK=1.0
  300 PHI(K)=57.29577971*ATAN2(GXYIM(K),XXK)
  305 CONTINUE
```

COPY AVAILABLE TO DDC DOES NOT
PERMIT FULLY LEGIBLE PRODUCTION

```
272       C
273       C            PLOT PHASE FROM -PHLIM TO PHLIM
274       C
275             PHLIM=1800.0
276             XX(1)=0.0
277             DO 310 K=2,ND2P1
278             XX(K)=DF*FLOAT(K-1)
279             X=PHI(K)-PHI(K-1)
280             PHI(K)=PHI(K)-SIGN(360.,X)*AINT(0.5+ABS(X)/360.0)
281             IF (PHI(K).GT.PHLIM) PHI(K)=PHI(K)-PHLIM
282             IF (PHI(K).LT.-PHLIM) PHI(K)=PHI(K)+PHLIM
283           310 CONTINUE
284             CALL DPLOT (PHI,ISTRT,ISTOP,2)
285             WRITE (IPRTR,315)
286           315 FORMAT (1H1,10X,'DUMP OF CONTINUOUS PHASE VALUES')
287             CALL LIST (PHI,SCRCH,ISTRT,ISTOP,IPRTR)
288       C
289       C            COMPUTE CROSS SPECTRUM AND SQUARED COHERENCY
290       C
291             DO 320 K=1,ND2P1
292             PHI(K)=GXYRE(K)**2+GXYIM(K)**2
293             XX(K)=PHI(K)/(GXX(K)*GYY(K))
294           320 CONTINUE
295             CALL DPLOT (XX,1,ND2P1,2)
296             WRITE (IPRTR,325)
297           325 FORMAT (1H1,10X,'DUMP OF THE SQUARED COHERENCE')
298             CALL LIST (XX,SCRCH,ISTRT,ISTOP,IPRTR)
```

```
C
C            CONVERT GXY TO DB AND PLOT
C
      DO 330 I=1,ND2P1
      PHI(I)=5.0*ALOG10(MAX(PHI(I),1.0E-30))
  330 CONTINUE
      CALL DPLOT (PHI,ISTRT,ISTOP,2)
      WRITE (IPRTR,335)
  335 FORMAT (1H1,10X,'DUMP OF THE CROSS SPECTRUM')
      CALL LIST (PHI,SCRCH,ISTRT,ISTOP,IPRTR)
C
C            COMPUTE SIX TIME FUNCTIONS
C
      CALL PROCES (GXX,GYY,GXYRE,GXYIM,NPFFT,XX,YY,IPRTR,DT)
C
C            COMPUTE MODULUS OF TRANSFER FUNCTION IN DB AND PLOT
C
      DO 340 K=1,ND2P1
      TEMP=(GXYRE(K)**2+GXYIM(K)**2)/GXX(K)**2
      PHI(K)=10.0*ALOG10(MAX(TEMP,1.0E-30))
  340 CONTINUE
      WRITE (IPRTR,345)
  345 FORMAT (1H1,10X,'DUMP OF THE TRANSFER FUNCTION')
      CALL LIST (PHI,SCRCH,ISTRT,ISTOP,IPRTR)
      CALL DPLOT (PHI,ISTRT,ISTOP,2)
C
C            TERMINATE PROGRAM
C
      CALL DPLOT (XX,0,0,3)
      STOP
C
      END
```

```
      SUBROUTINE DPLOT (XX,ISTART,ISTOP,INTSW)
C
C******** INTSW=1-INITIALIZE PLOTTER
C                2-PLOT DATA
C                3-CLOSE OUT PLOTTER
C
      DIMENSION Z(200), XX(1)
C
      IF (INTSW.EQ.2) GO TO 100
      IF (INTSW.EQ.3) GO TO 115
C
C        INITIALIZE PLOTTER
C
      CALL MODESG (Z,0)
      GO TO 120
C
  100 CALL SETSMG (Z,19,11.0)
      CALL SETSMG (Z,20,8.25)
C
C        DRAW GRIDS
C
      CALL OBJCTG (Z,0.5,0.5,10.5,7.5)
      CALL SUBJEG (Z,0.0,0.0,10.0,7.0)
      DX=7.0/7.0
      DY=10.0/10.0
      CALL GRIDG (Z,DX,DY,0.,0.)
C
C        SEARCH FOR MAXIMUM DATA VALUE
C
      TEMP=1.0E-20
      DO 105 I=ISTART,ISTOP
      TEMP=AMAX(ABS(XX(I)),TEMP)
  105 CONTINUE
```

```
      C
      C        WRITE MAXIMUM VALUE ON THE PLOTTER
      C
            CALL OBJCTG (Z,0.0,0.0,11.0,8.25)
            CALL SUBJEG (Z,0.0,0.0,11.0,8.25)
            CALL LEGNDG (Z,1.0,7.75,15,'MAXIMUM VALUE =')
            CALL NUMBRG (Z,2.5,7.75,-12.5,TEMP)
      C
      C        PLOT NORMALIZED DATA
      C
            CALL OBJCTG (Z,0.5,0.5,10.5,7.5)
            CALL SUBJEG (Z,0.0,-1.0,10.0,1.0)
      C
            NXIVLS=ISTOP-ISTART
            DLTAX=10.0/FLOAT(NXIVLS)
            XCORD=0.0
            IBEGIN=ISTART+1
            TEMP2=XX(ISTART)/TEMP
            CALL LINESG (Z,0,XCORD,TEMP2)
            DO 110 I=IBEGIN,ISTOP
            XCORD=XCORD+DLTAX
            TEMP2=XX(I)/TEMP
            CALL LINESG (Z,1,XCORD,TEMP2)
        110 CONTINUE
            CALL PAGEG (Z,0,1,1)
      C
      C        CLOSE OUT PLOTTER
      C
        115 IF (INTSW.EQ.3) CALL EXITG (Z)
        120 CONTINUE
            RETURN
      C
            END
```

```
      SUBROUTINE HICMP (NNN,NEWNN)
C
      DIMENSION NFACT(7)
C
      DATA (NFACT(I),I=1,7) /512,500,128,100,5,3,2/
      NUMBR=7
      NUP=NNN
      IF (NUP.LE.1) NUP=2
C
  100 CONTINUE
      NEWNN=NUP
C
      DO 115 L=1,NUMBR
C
  105 M=MOD(NEWNN,NFACT(L))
      IF (M.NE.0) GO TO 110
      NEWNN=NEWNN/NFACT(L)
      GO TO 105
  110 IF (NEWNN.EQ.1) GO TO 120
C
  115 CONTINUE
C
      NUP=NUP+1
      GO TO 100
C
  120 NEWNN=NUP
      RETURN
C
      END
```

```
      SUBROUTINE LIST (DATA,FREQ,ISTRT,ISTOP,IPRNT)
      DIMENSION DATA(1), FREQ(1)
C
      WRITE (IPRNT,100)
  100 FORMAT (5X,'FREQUENCY')
C
      DO 110 I=ISTRT,ISTOP,10
      J=I+9
      IF (J.GT.ISTOP) J=ISTOP
      WRITE (IPRNT,105) FREQ(I),(DATA(K),K=I,J)
  105 FORMAT (2X,F8.3,10(2X,F10.4))
  110 CONTINUE
C
      RETURN
C
      END
```

```
      SUBROUTINE LIST2 (DATA,XMIN,ISTRT,ISTOP,IPRNT,DT)
C
      DIMENSION DATA(1)
C
      WRITE (IPRNT,100)
  100 FORMAT (5X,'TIME')
C
      TIME=XMIN
C
      DO 110 I=ISTRT,ISTOP,10
      J=I+9
      IF (J.GT.ISTOP) J=ISTOP
      WRITE (IPRNT,105) TIME,(DATA(K),K=I,J)
  105 FORMAT (2X,F8.4,10(2X,F10.4))
      TIME=TIME+(10.0*DT)
  110 CONTINUE
C
      RETURN
C
      END
```

```
      SUBROUTINE LOAD (XX,YY,PHI,NNN,KOUNT,ISR)
C
      DIMENSION XX(1), YY(1), PHI(1)
      DIMENSION PHASE(5), FREQ(5)
C
      DT=1.0/FLOAT(ISR)
      TPI=8.0*ATAN(1.00)
      FREQ(1)=10.0
      FREQ(2)=27.0
      FREQ(3)=43.9
      FREQ(4)=71.8
      FREQ(5)=108.31
      TPID=TPI/10.0
      DO 100 K=1,5
      PHASE(K)=K*TPI/5.0
  100 FREQ(K)=TPI*FREQ(K)
C
      DO 110 I=1,NNN
      TIME=((KOUNT-1)*NNN+I)*DT
      SUM=0.0
      DO 105 K=1,5
  105 SUM=SUM+SIN(FREQ(K)*TIME+PHASE(K))
      XX(I)=SUM
      IF (XX(I).GT.1.0) XX(I)=1.0
      IF (XX(I).LT.-1.0) XX(I)=-1.0
      YY(I)=XX(I)+3.0*XX(I)**2
  110 CONTINUE
C
      RETURN
C
      END
```

```
1               SUBROUTINE LREMV (XX,NNN,ISWCH,DC,SLOPE)
2       C
3       C               DIMENSION ARRAY AND ESTABLISH CONSTANTS
4       C
5               DIMENSION XX(1)
6       C
7               FLN=FLOAT(NNN)
8               DC=0.0
9               SLOPE=0.0
10      C
11              DO 100 I=1,NNN
12              DC=DC+XX(I)
13              SLOPE=SLOPE+XX(I)*FLOAT(I)
14        100 CONTINUE
15      C
16      C               COMPUTE STATISTICS
17      C
18              DC=DC/FLN
19              SLOPE=12.0*SLOPE/(FLN*(FLN*FLN-1.0))-6.0*DC/(FLN-1.0)
```

```
C
C            PRINT OUT CHECK OUT INFORMATION
C
      IF (ISWCH-1) 125,115,105
C
C            REMOVE TREND (MEAN AND SLOPE) AND REPORT REMOVAL
C
  105 CONTINUE
      FLN=DC-0.5*(FLN+1.0)*SLOPE
      DO 110 I=1,NNN
      XX(I)=XX(I)-FLOAT(I)*SLOPE-FLN
  110 CONTINUE
      GO TO 125
C
C            REMOVE THE DC COMPONENT
C
  115 CONTINUE
      DO 120 I=1,NNN
      XX(I)=XX(I)-DC
  120 CONTINUE
C
  125 RETURN
C
      END
```

```
      SUBROUTINE PRCES (GXX,GYY,GXYRE,GXYIM,NPFFT,XX,YY,IPRTR,LT)
C
      DIMENSION GXX(1), GYY(1), GXYRE(1), GXYIM(1), XX(1), YY(1)
      DO 100 NTIME=1,6
C
      NP2=NPFFT+2
      ND2P1=(NPFFT/2)+1
      ND2=NPFFT/2
      ND2M1=ND2-1
      DO 100 K=1,ND2P1
C
      IF (NTIME.EQ.1) TEMP=1.0/SQRT(GXX(K)*GYY(K))
      IF (NTIME.EQ.2) TEMP=1.0/SQRT(GXYRE(K)**2+GXYIM(K)**2)
      IF (NTIME.EQ.3) TEMP=1.0
      IF (NTIME.EQ.4) TEMP=1.0/GXX(K)
      GXYMG=SQRT(GXYRE(K)**2+GXYIM(K)**2)
      COHR2=GXYMG**2/(GXX(K)*GYY(K))
      COHR2=MIN(COHR2,.9999999)
      IF (NTIME.EQ.5) TEMP=COHR2/((1.-COHR2)*GXYMG)
      TEMP1=GXX(K)-GXYMG
      H=1.0
      IF (ABS(TEMP1).LT.0.0000001) TEMP1=0.0000001*SIGN(H,TEMP1)
      IF (NTIME.EQ.6) TEMP=GXYMG/(TEMP1**2)
      IF (NTIME.EQ.7) TEMP=1./(TEMP1**2)
      IF (NTIME.EQ.8) TEMP=1./TEMP1
C
      XX(K)=GXYRE(K)*TEMP
      YY(K)=GXYIM(K)*TEMP
C
  100 CONTINUE
C
```

```
      DO 105 K=2,ND2P1
      J=NP2-K
      XX(J)=XX(K)
      YY(J)=-YY(K)
  105 CONTINUE
      YY(ND2P1)=0.0
C
      CALL FFT (XX,YY,NPFFT,NPFFT,NPFFT,1)
C
      TEMP=0.0
      DO 110 K=1,NPFFT
      IF (TEMP.GE.ABS(XX(K))) GO TO 110
      KOFMX=K
      TEMP=ABS(XX(K))
  110 CONTINUE
C
      WRITE (IPRTR,115) NTIME
  115 FORMAT ('1','  RESULTS OF PROCESSOR',I5//)
      WRITE (IPRTR,120) TEMP,KOFMX
  120 FORMAT (' MAX OF',E20.8,' AT DELAY',I5/)
      TEMP=1.0/TEMP
      DO 125 K=1,NPFFT
      XX(K)=XX(K)*TEMP
  125 CONTINUE
      DO 135 K=1,40
      J=NP2-K
      TEMP1=XX(K)*100.0
      TEMP2=XX(J)*100.0
      WRITE (IPRTR,130) NTIME,K,TEMP1,TEMP2
  130 FORMAT (5X,2I10,2F10.4)
  135 CONTINUE
C
```

```
64              DO 140 I=1,ND2P1
65              YY(I+ND2M1)=XX(I)
66          140 CONTINUE
67              DO 145 I=1,ND2M1
68              YY(I)=XX(ND2P1+I)
69          145 CONTINUE
70              NLAG=100
71              ITMP1=ND2-NLAG
72              ITMP2=ND2+NLAG
73              XMIN=-DT*FLOAT(1-NLAG)
74              XMAX=DT*FLOAT(1+NLAG)
75        C
76              IF (NTIME.EQ.1) WRITE (IPRTR,150)
77          150 FORMAT (1H1,10X,'DUMP OF SCOT FUNCTION')
78              IF (NTIME.EQ.2) WRITE (IPRTR,155)
79          155 FORMAT (1H1,10X,'DUMP OF PHAT FUNCTION')
80              IF (NTIME.EQ.3) WRITE (IPRTR,160)
81          160 FORMAT (1H1,10X,'DUMP OF CROSS CORRELATION')
82              IF (NTIME.EQ.4) WRITE (IPRTR,165)
83          165 FORMAT (1H1,10X,'DUMP OF IMPULSE RESPONSE')
84              IF (NTIME.EQ.5) WRITE (IPRTR,170)
85          170 FORMAT (1H1,10X,'DUMP OF H-T(I) FUNCTION')
86              IF (NTIME.EQ.6) WRITE (IPRTR,175)
87          175 FORMAT (1H1,10X,'DUMP OF ECKART FUNCTION')
88              CALL LIST2 (YY,XMIN,ITMP1,ITMP2,IPRTR,DT)
89        C
90              CALL DPLOT (YY,ITMP1,ITMP2,2)
91          180 CONTINUE
92              RETURN
93        C
94              END
```

APPENDIX D

EXAMPLE COMPUTER RUN FOR SPECTRAL AND TIME DELAY ESTIMATION

Theoretical equations have been derived in Chapter 3 for ML estimation of time delay. A computer program to achieve an AML estimate of delay is given in Appendix C. The purpose of this chapter is to describe four example cases which were run to substantiate the theory and validate the computer program. One computer run was made for each of the cases. Only one of the runs will be explicitly reported here. In all of the four cases studied, the true delay was set equal to zero (without loss of generality). Further, the signal attenuation was set equal to unity so that (3-1) becomes

$$x_1(t) = s(t)+n_1(t) \qquad \text{(D-1a)}$$

$$x_2(t) = s(t+D)+n_2(t) \qquad \text{(D-1b)}$$

$$D = 0 \ . \qquad \text{(D-1c)}$$

Our desire is to see whether (and "how well") we can estimate the (assumed unknown) parameter D, given a T second observation of $x_1(t)$ and $x_2(t)$. The variance of the ML processor (as discussed after (3-34)) depends on the particular signal and noise spectral characteristics (in particular, $C_{12}(f)$). Moreover, the variance of the

delay estimate can only be empirically determined by resort to numerous (expensive) computer runs. We have not done that here (but have suggested further work in this area (Chapter 6)). We have, however, made four computer runs for the data cases synthesized by Figure D-1. As shown in the figure, the signal spectrum has two nonzero frequency bands. The bands are 10 Hz wide centered at 5 and 50 Hz. Each of the five filters represented in Figure D-1 is the cascade of two sections, each with a 48 dB/octave roll off. The noise generators generate white noise. Details of the hardware are the same as described on pages 71-72 of Carter (1972a). The actual data generation required less hardware than shown in Figure D-1, but the simulation is easier to visualize by studying Figure D-1 and is closer to what would be done in a real time simulation of the type suggested in Chapter 6. In our experiment, we adjust the SNR by adjusting the gain in Figure D-1.

The digital outputs of the data synthesized are stored on magnetic tape for use by the computer program (Appendix C). Longer observation time is achieved by reading more data from the magnetic tape. In the four example cases, the ML processor output was examined for two different signal levels and two different averaging times T. Expect for absolute SNR level all four example cases had the same signal and the same noise spectral densities. As expected, when the SNR

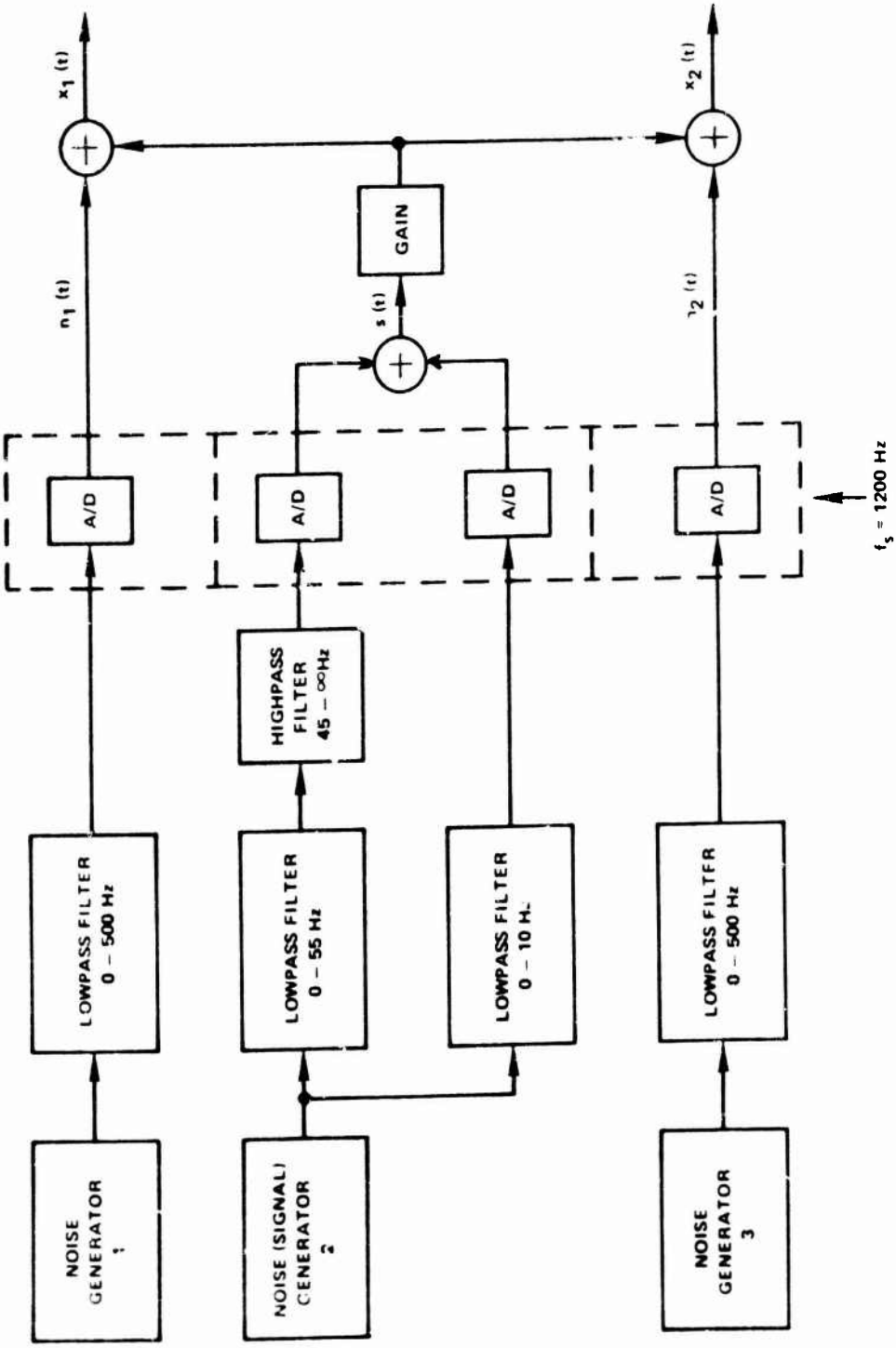

Figure D-1 Data Synthesis for Example Case

was low, more averaging time was required to extract a "good" delay estimate; this behavior is predicted by (3-34). In particular, of our four cases, the low SNR and short averaging case resulted in unusable delay estimates. The reason for this was apparent upon inspecting the coherence estimates used to approximate the true coherence. As predicted in appendix B with short averaging times (that is, small N), we were unable to detect a low coherent source.

This happened to our one trial at low SNR and short averaging; however, by increasing the averaging time, an acceptable time delay estimate was obtained. We were able to increase the averaging time (essentially without bound) since the example cases were using laboratory data.

The case which we will report in detail is the high-coherence, short-averaging case. In particular, the gain in Figure D-1 is adjusted so that $C \cong 0.6$ in the frequency bands with signal power and $C \cong 0$ in the other bands. The characteristics of $x_1(t)$ and $x_2(t)$ were estimated from 8 seconds of data with 16 independent segments (each of 1/2 second duration, that is, 2 Hz resolution). FFTs of 600 samples (1/2 sec times 1200 samples/sec) can be performed using the fast mixed radix FFT of Singleton (1969).

The characteristics of the noise generators in Figure D-1 were essentially identical. Thus, for the

model (D-1), $G_{x_1x_1}(f)=G_{x_2x_2}(f),\forall f$. The estimates of $G_{x_1x_1}(f)$ are depicted in Figure D-2. The estimates of $G_{x_2x_2}(f)$ were extremely similar and are not repeated. The extent to which $x_1(t)$ and $x_2(t)$ are similar is measured by the MSC estimate in Figure D-3. Since the CC and delay D depend upon the phase, the phase estimates are depicted in Figure D-4. The slope of the phase estimates is an important indicator of delay[1] in those frequency bands where the MSC is strong (namely, 0-10 Hz and 45-55 Hz). Using the algorithm discussed in Chapter 3 and the estimation techniques of appendix A implemented in appendix C, we have obtained the delay estimate given in Figure D-5. From Figure D-5 we see that the GCC with ML weighting peaks very close to the true value of delay, namely, D=0. A blowup of Figure D-5 given in Figure D-6 shows that the peak is within 10 msec of the true value. Clearly, the estimation technique proposed is a viable method for estimating time delay.

---

[1] Dimensionally the slope is the phase angle in radians divided by the frequency in radians per sec. Thus the slope of the phase is measured in seconds.

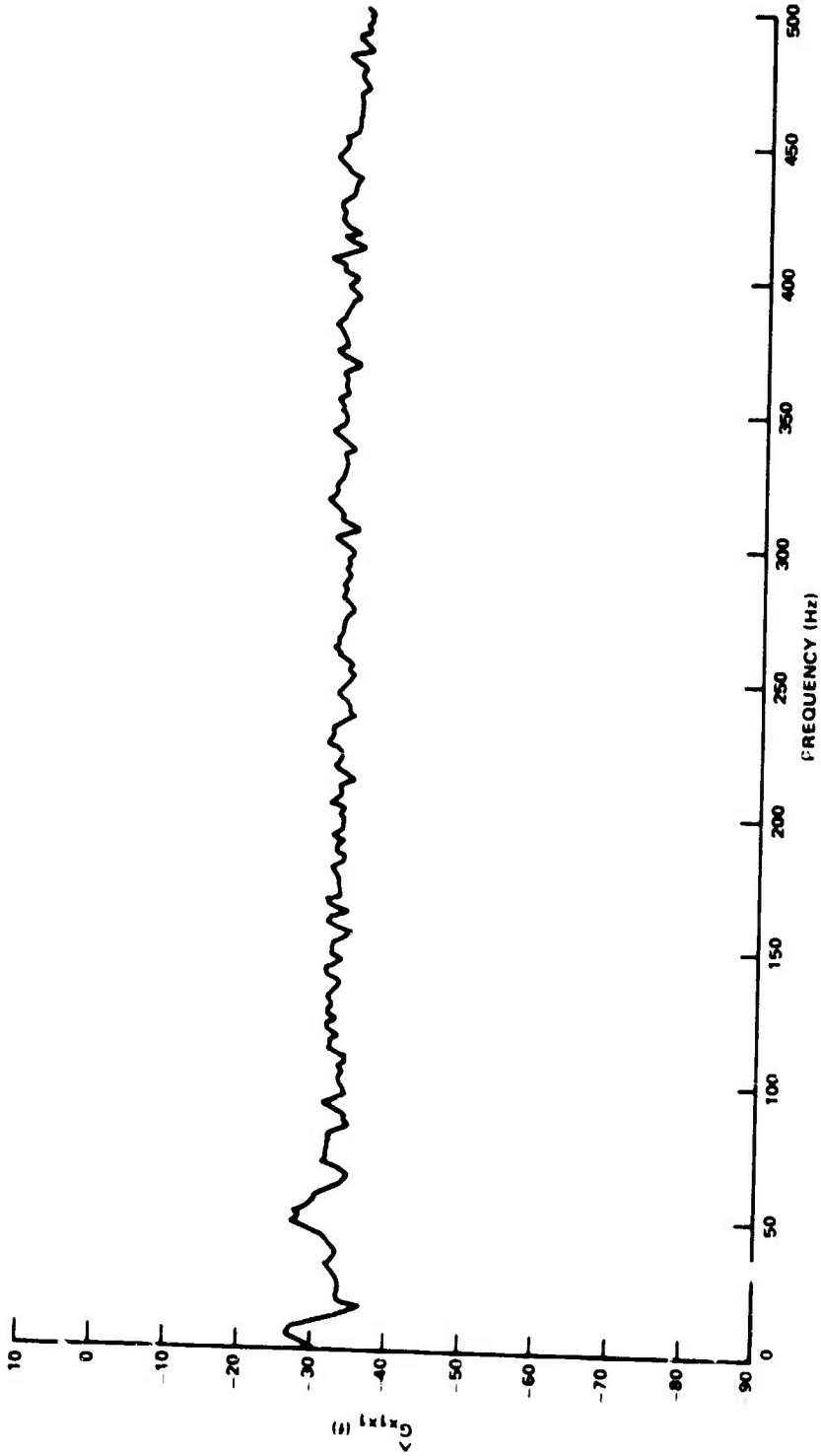

Figure D-2 Estimates of $G_{x_1x_1}(f)$ for Example Case

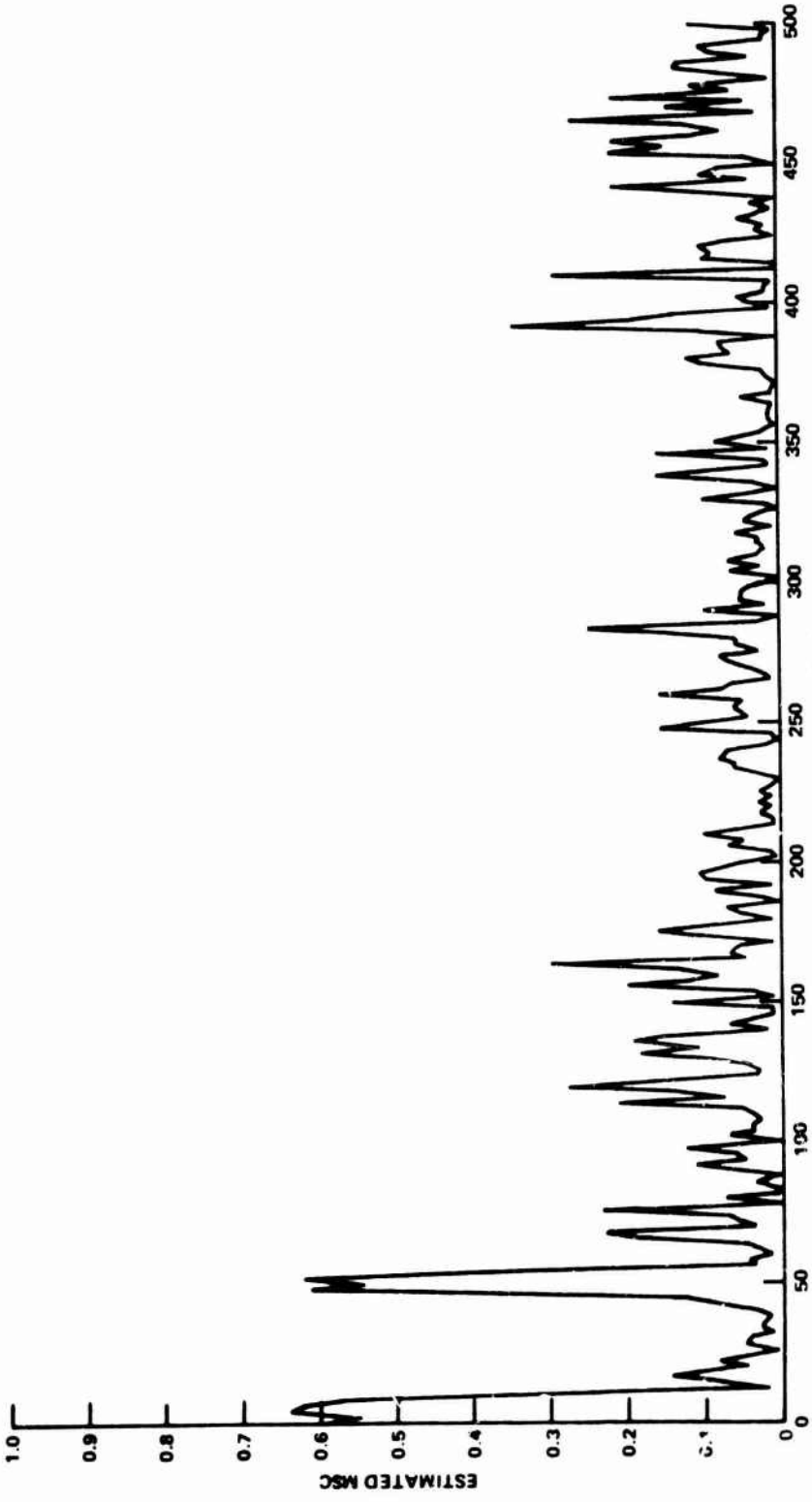

Figure D-3 Estimates of $C_{x_1x_2}(f)$ for Example Case

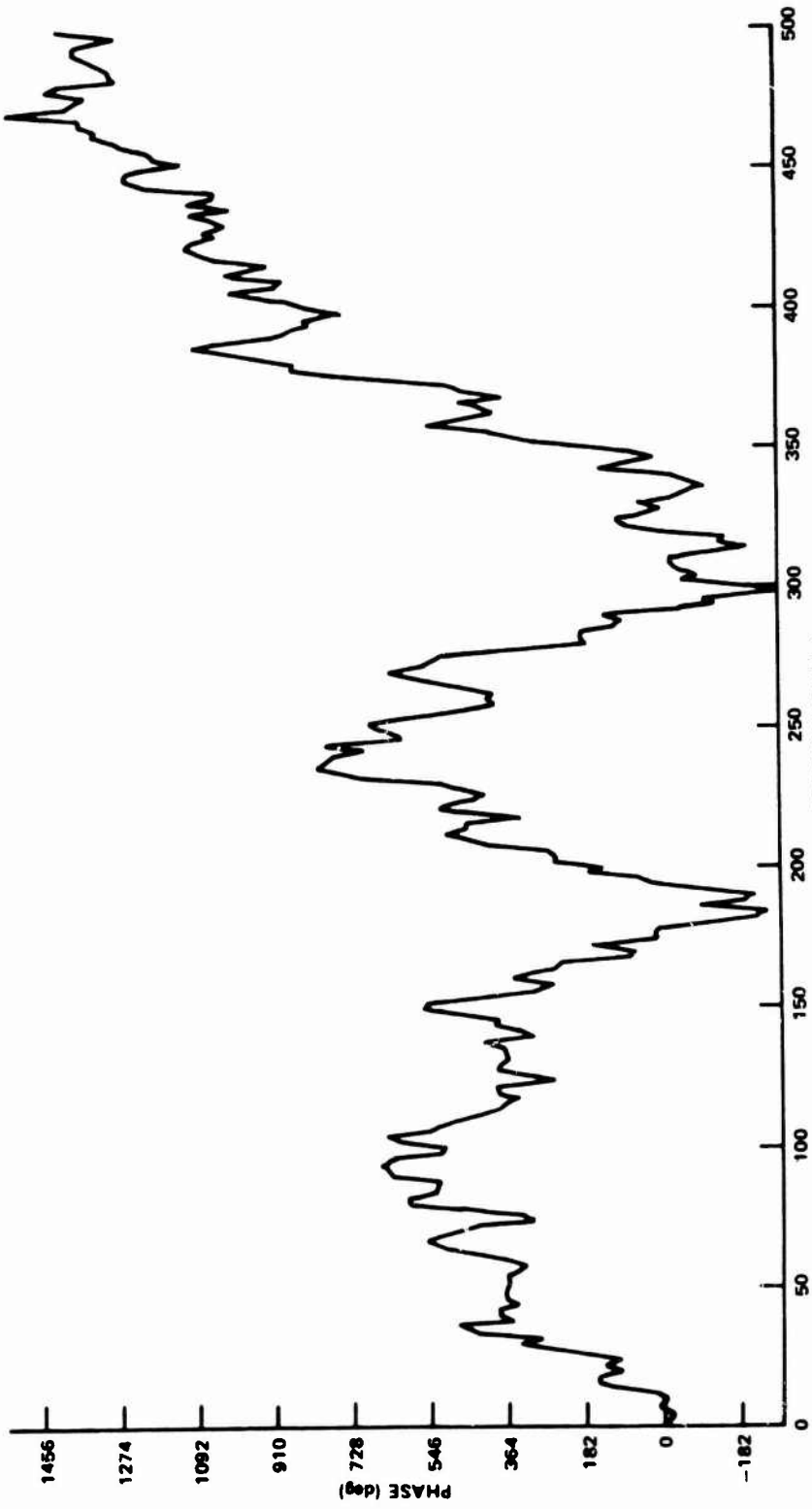

Figure D-4 Estimates of $\phi_{x_1 x_2}(f)$ for Example Case

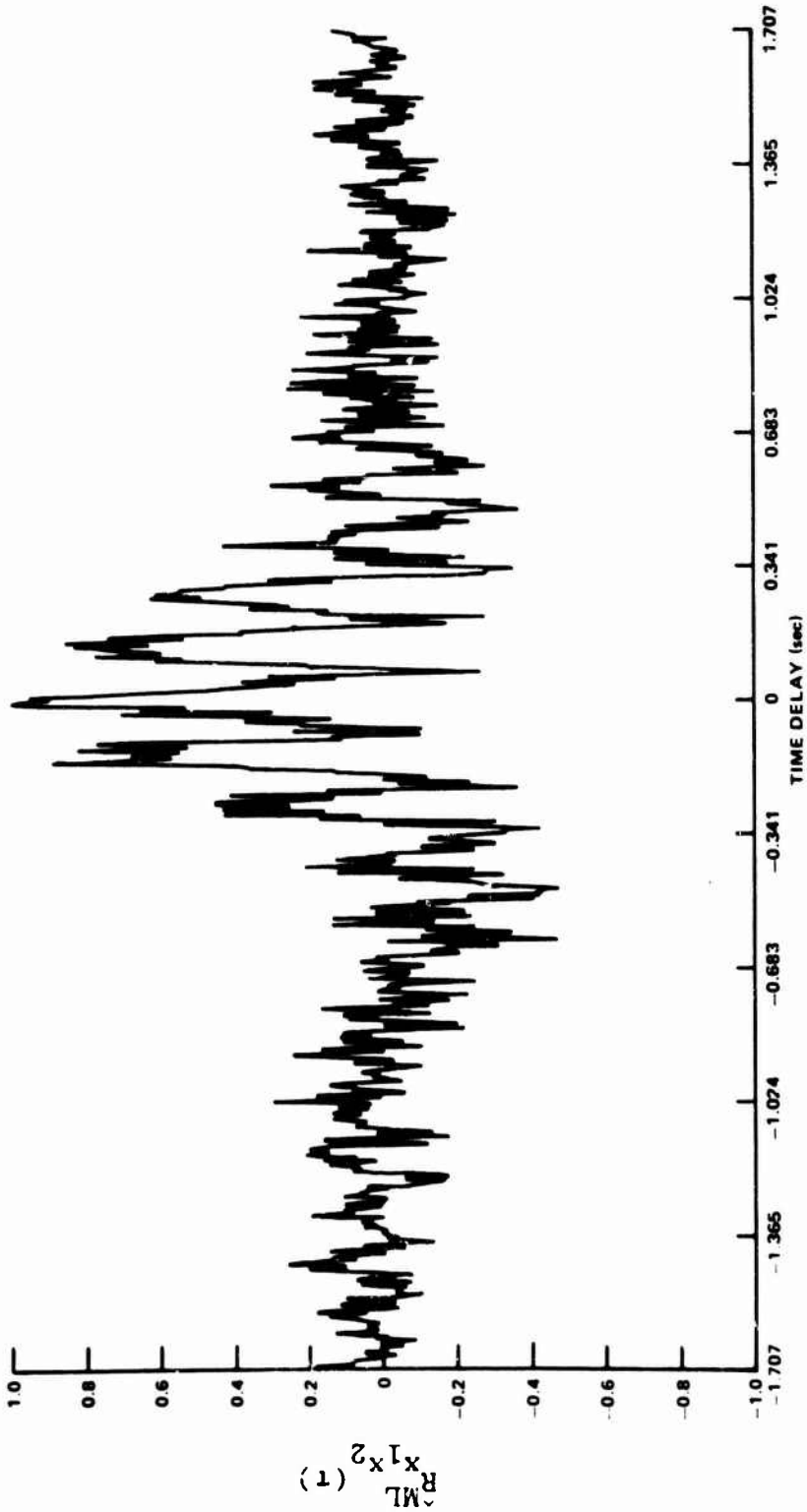

Figure D-5 Estimates of Time Delay Using ML Weighting with GCC Processing

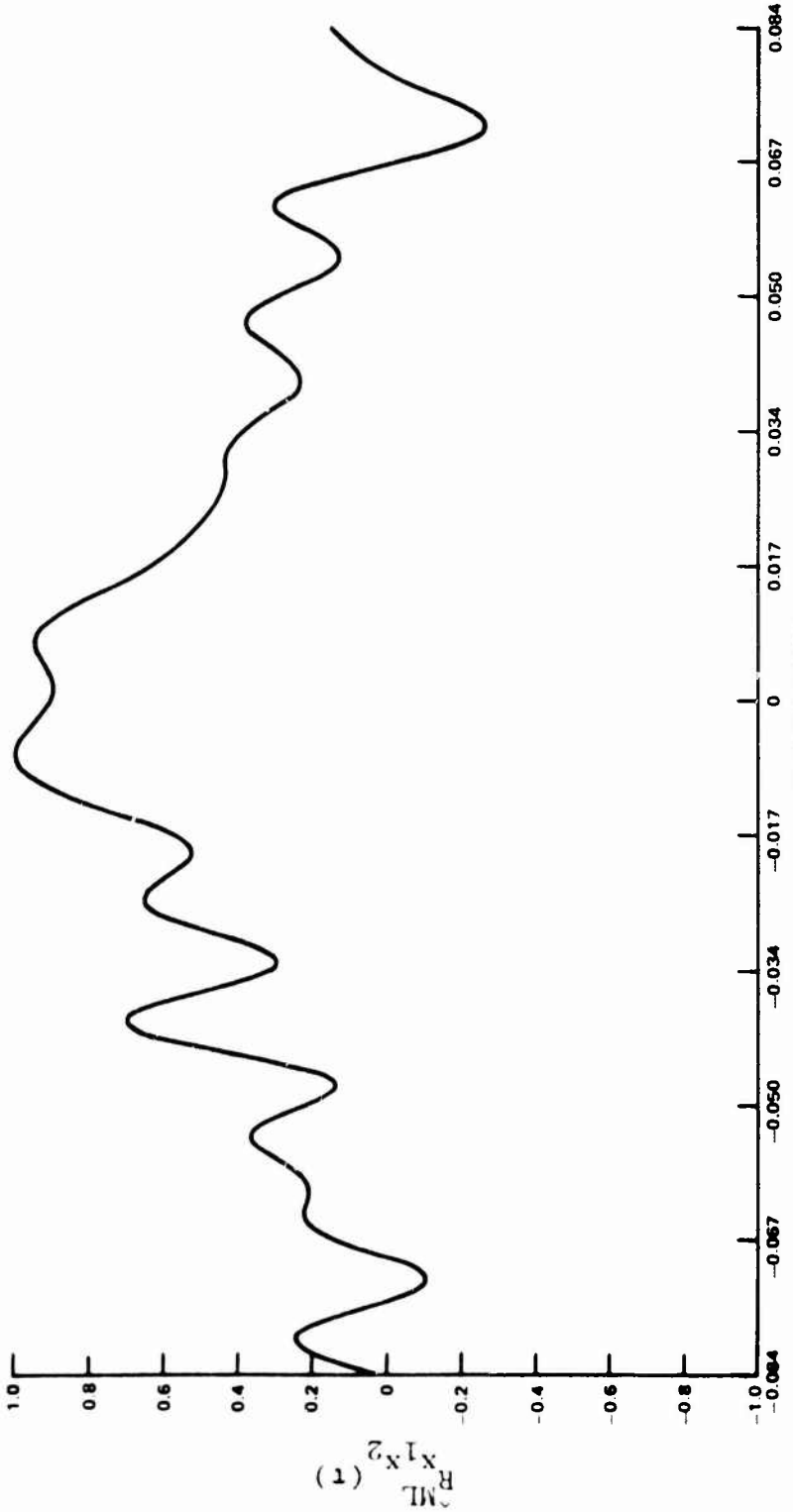

Figure D-6 Expanded Figure D-5 Time Delay Estimates

BIBLIOGRAPHY

Abramowitz and Stegun, I.A., (ed.), (1964), Handbook of Mathematical Functions with Formulas, Graphs, and Mathematical Tables, U. S. Government Printing Office, Washington, D.C.

Akaike, H. and Yamanouchi, Y., (1963), "On the statistical estimation of frequency response function," Ann. of Inst. Statist. Math., 14, 23-56.

Alexander, M. J. and Vok, C. A., (1963), Tables of the Cumulative Distribution of Sample Multiple Coherence, Rocketdyne Division, North American Aviation, Inc., Research Report 63-67.

Alsup, J. M., Means, R. W., and Whitehouse, H. J., (1973), "Real Time Discrete Fourier Transforms Using Surface Acoustic Wave Devices," Proc. IEEE International Specialist Seminar on Component Performance and System Applications of Surface Acoustic Wave Devices, Aviemore, Scotland, U.K.

Amos, D. E. and Koopmans, L. H., (1963), Tables of the Distribution of the Coefficient of Coherence for Stationary Bivariate Gaussian Processes, Sandia Corp. Monograph SCR-483.

Anderson, T. W., (1958), An Introduction to Multivariate Statistical Analysis, New York, John Wiley and Sons, Inc.

Bangs, W. J., III, (1971), Array Processing with Generalized Beam-Formers, Yale Ph.D. Thesis, New Haven, CT.

Bendat, J. S. and Piersol, A. G., (1971), Random Data: Analysis and Measurement Procedures, New York, John Wiley and Sons, Inc.

Benignus, V. A., (1969a), "Estimation of the Coherence Spectrum and its Confidence Interval Using the Fast Fourier Transform," IEEE Trans. Audio Electroacoustics, AU-17, No. 2, 145-150.

Benignus, V. A., (1969b), "Estimation of Coherence Spectrum of Non Gaussian Time Series Populations," IEEE Trans. Audio Electroacoustics, AU-17, No. 3, 198-201.

Bingham, C., Godfrey, M. D., and Tukey, J. W., (1967), "Modern Techniques of Power Spectrum Estimation," IEEE Trans. Audio Electroacoustics, AU-15, No. 2, 56-66.

Blackman, R. B. and Tukey, J. W., (1958), The Measurement of Power Spectra, New York, Dover Publications, Inc.

Box, G. E. and Jenkins, G. M., (1970), Time Series Analysis: Forecasting and Control, San Francisco, CA, Holden-Day, Inc.

Brady, J. F., (1973), An Experimental Study of Vibration Noise, and Drag of a Cylinder Rotating in Water and Certain Polymer Solutions, University of Rhode Island Ph.D. Thesis, Kingston, R.I.

Brillinger, D. R., (1975), Time Series, Data Analysis and Theory, New York, Holt, Rinehart and Winston.

Buss, D. D., Collins, D. R., Bailey, W. H. and Reeves, C.R., (1973), "Transversal Filtering Using Charge-Transfer Devices," IEEE Journal of Solid State Circuits, SC-8, No. 2, 138-146.

Cannon, M., (1974), "Blind Image Deblurring with Phase Reversals," presented at IEEE Arden House Workshop, Harriman, N.Y. (See also Stockham, T. G., Jr., Cannon, T. M., and Ingeretsen, R. B.,(1965),"Blind Deconvolution Through Digital Signal Processing," Proc. IEEE, Vol. 63, No. 4 , 678-692.)

Carter, G. C., (1972a), Estimation of the Magnitude-Squared Coherence Function (Spectrum), University of Connecticut MSEE Thesis, Storrs, CT. (See also Naval Underwater Systems Center, TR 4343, New London, CT.)

Carter, G. C., (1972b), Coherence Estimation as Affected by Weighting Functions and Fast Fourier Transform Size, Naval Underwater Systems Center TR 4423, New London, CT.

Carter, G. C., (1976), "Receiver Operating Characteristics for a Linearly Threshold Coherence Estimator Detector," submitted to IEEE Trans. Acoust. Speech, Signal Processing.

Carter, G. C. and Knapp, C. H., (1975), "Coherence and Its Estimation via the Partitioned Modified Chirp-Z Transform," IEEE Trans. Acoust., Speech, Signal Processing, ASSP-23, No. 3, 257-264.

Carter, G. C. and Knapp, C. H., (1976a), "Time Delay Estimation," accepted for publication in Proc. of the First International Conference on Acoustic, Speech, and Signal Processing, Philadelphia, PA.

Carter, G. C. and Knapp, C. H., (1976b), "Time Compression Estimation," Manuscript Draft.

Carter, G. C., Knapp, C. H. and Nuttall, A. H., (1973a), "Estimation of the Magnitude-Squared Coherence Function via Overlapped Fast Fourier Transform Processing," IEEE Trans. on Audio Electroacoustics, AU-21, 337-344.

Carter, G. C., Knapp, C. H. and Nuttall, A. H., (1973b), "Statistics of the Estimate of the Magnitude-Coherence Function," IEEE Trans. on Audio Electro-acoustics, AU-21, 388-389.

Carter, G. C. and Nuttall, A. H., (1972), "Statistics of the Estimate of Coherence," Proc. IEEE, 60, No. 4, 465-466.

Carter, G. C., Nuttall, A. H. and Cable, P. G., (1973), "The Smoothed Coherence Transform," Proc. IEEE, 61, 1497-1498.

Clay, C. S., Hinich, M. J. and Shaman, P., (1973), "Error Analysis of Velocity and Direction Measurements of Plane Waves Using Thick Large-Aperture Arrays," J. Acoustic Soc. Am., 53, No. 4, 1161-1166.

Cooley, J. W. and Tukey, J. W., (1965), "An Algorithm for the Machine Calculation of Complex Fourier Series," Mathematics of Computation, 19, 297-301.

Davenport, W. B., Jr., (1970), Probability and Random Processes, New York, McGraw-Hill Book Company.

Dubes, R. C., (1968), The Theory of Applied Probability, Englewood Cliffs, New Jersey, Prentice-Hall, Inc.

Eckart, C., (1952), Optimal Rectifier Systems for the Detection of Steady Signals, University of California, Scripps Institution of Oceanography, Marine Physical Laboratory Rep. SIO 12692, SIO Ref. 52-11.

Enochson, L. D. and Goodman, N. R., (1965), Gaussian Approximations to the Distribution of Sample Coherence, Air Force Flight Dynamics Laboratory, Research and Tech. Division, AF Systems Command, Wright-Patterson AFB, OH, Bull. AFFDL-TR-65-67.

Ferrie, J. F., Nawrocki, C. W. and Carter, G. C., (1973), "The PAM-Chirp-Z Transform," Proc. of the 1973 IEEE International Conference on the Ocean Environment, Seattle, WA.

Ferrie, J. F., Nawrocki, C. W. and Carter, G. C., (1975), "Applications of the Partitioned and Modified Chirp-Z Transform to Oceanographic Measurements," IEEE Trans. on Acoustic, Speech, Signal Processing, 243-244.

Ferrie, J. F. and Nuttall, A. H., (1971), Comparison of Four Fast Fourier Transform Algorithms, Naval Underwater Systems Center, TR 4113, New London, CT.

Fisher, R. A., (1950), Contributions to Mathematical Statistics, New York, John Wiley and Sons, Inc., (Chapter 14 originally published as "The General Sampling Distribution of the Multiple Correlation Coefficient," Proc. of the Royal Society, Series A, 121, (1928), 654-673.)

Gelfand, I. M. and Yaglom, A. M., (1959), "Calculation of the Amount of Information about a Random Function Contained in Another Such Function," Amer. Math. Soc. Transl., 12 Series 2, 199-246.

Gevins, A. S., Yeager, C. L., Diamond, S. L., Spire, J. P., Zeitlin, G. M. and Gevins, A. H., (1975), "Automated Analysis of the Electrical Activity of the Human Brain (EEG): A Progress Report," Proc. IEEE, 63, No. 10, 1382-1399.

Gold, B. and Rader, C. M., (1969), Digital Processing of Signals, New York, McGraw-Hill Book Company.

Goodman, N. R., (1957), On the Joint Estimation of the Spectra, Cospectrum, and Quadrature Spectrum of a Two-Dimensional Stationary Gaussian Process, Scientific Paper 10, New York University, New York.

Gradshteyn, I. S. and Ryzhik, I. M., (1965), Table of Integrals, Series, and Products, New York, Academic Press.

Halvorsen, W. G. and Bendat, J. S., (1975), "Noise Source Identification Using Coherent Output Power Spectra," Sound and Vibration, 15-24.

Hamon, B. V. and Hannan, E. G., (1974), "Spectral Estimation of Time Delay for Dispersive and Non-Dispersive Systems," J. Royal Sta. Soc. Ser. C. (Appl. Statist.), 23, 134-142.

Hannan, E. J., (1970), Multiple Time Series, New York, John Wiley and Sons, Inc.

Hannan, E. J. and Robinson, P. M., (1973), "Lagged Regression with Unknown Lags," J. Royal Statist. Soc., Ser. B, 35, No. 2, 252-267.

Hannan, E. J. and Thomson, P. J., (1971), "The Estimation of Coherence and Group Delay," Biometrika, 58, 469-481.

Hannan, E. J. and Thomson, P. J., (1973), "Estimating Group Delay," Biometrika, 60, 241-253.

Haubrich, R. A., (1965), "Earth Noise, 5 to 500 Millicycles per Second, 1. Spectral Stationarity, Normality, and Non Linearity," J. Geophysical, Res., 70, No. 6, 1415-1427.

James, D. V., (1974), "Quantization Errors in the Fast Fourier Transform," presented at IEEE Arden House Workshop, Harriman, N.Y. (See also, James, D. V., (1975), "Quantization Errors in the Fast Fourier Transform", IEEE Trans. on Acoustic, Speech, Signal Processing, ASSP-23, No. 3, 277-282.)

Jenkins, G. M. and Watts, D. G., (1968), Spectral Analysis and Its Applications, San Francisco, Holden-Day, Inc.

Jury, E. I., (1964), Theory and Application of the Z Transform Method, New York, John Wiley and Sons, Inc.

Kennedy, R. S., (1969), Fading Dispersive Communications Channels, New York, Wiley-Interscience.

Knapp, C. H., (1966), Optimum Linear Filtering for Multi-Element Arrays, General Dynamics/Electric Boat Division, Rep. U417-66-031, Groton, CT.

Knapp, C. H. and Carter, G. C., (1976), "The Generalized Correlation Method for Estimation of Time Delay," accepted for publication in IEEE Trans. on Acoustic, Speech, Signal Processing.

Kochenburger, R. J. (1972), Computer Simulation of Dynamic Systems, Englewood Cliffs, N. J., Prentice-Hall, Inc.

Koopmans, L. H., (1964), "On the Coefficient of Coherence for Weakly Stationary Stochastic Processes," Ann. Math. Statist., 35, 532-549.

Koopmans, L. H. (1974), The Spectral Analysis of Time Series, New York, Academic Press.

Lee, Y. W., (1960), Statistical Theory of Communications, New York, John Wiley and Sons, Inc.

Lindorff, D. P., (1965), Theory of Sampled Data Control Systems, New York, John Wiley and Sons, Inc.

MacDonald, V. H. and Schultheiss, P. M., (1969), "Optimum Passive Bearing Estimation," J. Acoust. Soc. Am., 46, 37-43.

Nettheim, N., (1966), The Estimation of Coherence, Stanford University Department of Stat. TR No. 5, Stanford, CA.

Nuttall, A. H., (1958), Theory and Application of the Separable Class of Random Processes, MIT Ph.D. Thesis. (Also published as Research Laboratory of Electronics Report 343, Cambridge, MA.)

Nuttall, A. H., (1971), Spectral Estimation by Means of Overlapped FFT Processing of Windowed Data, Naval Underwater Systems Center Report No. 4169, New London, CT. (and supplement NUSC TR-4169S).

Nuttall, A. H. and Carter, G. C., (1976a), Approximations for Statistics of Coherence Estimators, Naval Underwater Systems Center TR 5291, New London, CT.

Nuttall, A. H. and Carter, G. C., (1976b), "Bias of the Estimate of Magnitude-Squared Coherence," submitted to IEEE Trans. on Acoustic, Speech, Signal Processing.

Nuttall, A. H. and Carter, G. C. and Montavon, E. M., (1974), "Estimation of the Two-Dimensional Spectrum of the Space-Time Noise Field for a Sparse Line Array," J. Acoust. Soc. Am., 55, 1034-1041.

Nuttall, A. H. and Hyde, D. W., (1969), A Unified Approach to Optimum and Sub-Optimum Processing for Arrays, Naval Underwater Systems Center, TR 992, New London, CT.

Oppenheim, A. V. and Schafer, R. W., (1975), Digital Signal Processing, Englewood Cliffs, N.J., Prentice-Hall, Inc.

Otnes, R. K. and Enochson, L., (1972), Digital Time Series Analysis, New York, Wiley-Interscience.

Papoulis, A., (1965), Probability, Random Variables and Stochastic Processes, New York, McGraw-Hill Book Company.

Rabiner, L. R. and Rader, C. M. (ed.), (1972), Digital Signal Processing, New York, IEEE Press.

Rabiner, L. R., Schafer, R. W. and Rader, C. M., (1969), "The Chirp-Z Transform Algorithm and Its Application," The Bell System Technical Journal, 48, No. 5, 1249-1292, and (1969), "The Chirp-Z Transform Algorithm," IEEE Transactions Audio Electroacoustics, AU-17, No. 2, 86-92.

Roth, P. R., (1971), "Effective Measurements Using Digital Signal Analysis," IEEE Spectrum, 8, 62-70.

Sage, A. P. and Melsa, J. L., (1971), Estimation Theory with Applications to Communications and Control, New York, McGraw-Hill Book Company.

Santopietro, R. F., (1973), Measurement, Analysis and Reduction of Noise in the High Frequency, University of Pennsylvania, Ph.D. Thesis, Philadelphia, PA.

Schilling, S. A., (1972), A Study of the Chirp-Z Transform and Its Applications, MSEE Thesis, University of Kansas, Manhattan, KS.

Schultheiss, P. M., (1968), "Passive Sonar Detection in the Presence of Interference," J. Acoust. Soc. Am., 43, No. 3, 418-425.

Shannon, C. E. and Weaver, W., (1949), The Mathematical Theory of Communication, Urbana, IL., University of Illinois Press.

Singleton, R. C., (1969), "An Algorithm for Computing the Mixed Radix Fast Fourier Transform," IEEE Transactions on Audio Electroacoustics, AU-17, No. 2., 93-102.

Silverman, R. A., (1957), "Locally Stationary Random Processes," IRE Trans. on Info. Th., 182-187.

Tick, L. J., (1967), "Spectral Analysis of Time Series, ed. by B. Harris, New York, John Wiley and Sons, Inc., 133-152.

Urick, R. J., (1967), Principles of Underwater Sound for Engineers, New York, McGraw-Hill Book Company. (Also second edition, 1975, Principles of Underwater Sound, same publisher.)

Van Trees, H. L., (1968), Detection, Estimation and Modulation Theory, Part I., Detection Estimation and Linear Modulation Theory, New York, John Wiley and Sons, Inc.

Van Trees, H. L., (1971), Detection, Estimation and Modulation Theory, Part III, Radar/Sonar Signal Processing and Gaussian Signals in Noise, New York, John Wiley and Sons, Inc.

Wahba, G., (1966), Cross Spectral Distribution Theory for Mixed Spectra and Estimation of Prediction Filter Coefficients, Stanford University Department of Stat. TR No. 15, Stanford, CA.

Weiner, N., (1930), "Generalized Harmonic Analysis," Acta. Math., 55, 117-258.

Weinstein, C. and Oppenheim, A., (1969), "A Comparison of Round-Off Noise in Floating Point and Fixed Digital Filter Realizations," Proc. IEEE, 57, 1181-1183, (see also 429-431 of Rabiner and Rader (1972)).

Welch, P. D., (1967), "The Use of Fast Fourier Transform for the Estimation of Power Spectra: A Method Based on Time Averaging Over Short, Modified Periodograms," IEEE Transactions on Audio Electroacoustics, AU-15, No. 2, 70-73.

Whalen, A. D., (1971), Detection of Signals in Noise, New York, Academic Press.

Williams, R. G., (1971), Estimating Ocean Wind Wave Spectra by Means of Underwater Sound, Ph.D. Dissertation, New York University, N.Y., (Also published as Naval Underwater Systems Center TR 4097, New London, CT., and in a condensed form in J. Acoust. Soc. Am., 53, No. 3, 910-920, (1973).)

Wozencraft, J. M. and Jacobs, I. M., (1967), Principles of Communication Engineering, New York, John Wiley and Sons, Inc.

INITIAL DISTRIBUTION LIST

Addressee	No. of Copies
CNM (MAT-03, -03L4, -035)	3
ASN (R&D)	1
NRL	1
NAVELEX, PME-124	2
NAVSEA, SEA-09G3	4
NADC	1
NWC	1
DTNSRDC	1
NCSL	1
NCEL	1
NSWC	1
NELC	1
NUC	1
NAVSEC, SEC-6034	1
NAVPGSCOL	1
Woods Hole Oceanographic Institution	1
SACLANT Research Centre	1
DDC, Alexandria	12
DIA, Code DT-2C	1